September 2019

Coupled Landscape and Channel Dynamics Across the Ganges-Brahmaputra Tidal-Fluvial Continuum, Southwest Bangladesh

Edwin Jefferson Bomer IV
Louisiana State University and Agricultural and Mechanical College

COUPLED LANDSCAPE AND CHANNEL DYNAMICS ACROSS THE GANGES-BRAHMAPUTRA TIDAL-FLUVIAL CONTINUUM, SOUTHWEST BANGLADESH

A Dissertation

Submitted to the Graduate Faculty of the
Louisiana State University and
Agricultural and Mechanical College
in partial fulfillment of the
requirements for the degree of
Doctor of Philosophy

in

The Department of Geology and Geophysics

by
Edwin Jefferson Bomer IV
B.A. Washington University in St. Louis, 2014
M.S. Louisiana State University, 2016
December 2019

ACKNOWLEDGEMENTS

This dissertation would not have been possible without the support and guidance of many individuals. First and foremost, I'd like to thank my advisor, Dr. Carol Wilson, for technical support and for allowing me the freedom to pursue my personal research interests, which resulted in the third component (Chapter 4) of this dissertation. I was Carol's first Ph.D. student, but from the beginning she provided thoughtful advice as well as a contagious enthusiasm for her work. Carol also helped compose the National Science Foundation (NSF) proposal that funded my dissertation, and for that I am deeply appreciative. I am also grateful to the rest of my dissertation committee, including Dr. Samuel Bentley, Dr. Sophie Warny, and my Dean's Representative, Dr. Eurico D'Sa. Special thanks are extended to Sam for his assistance with countless revisions of my MS manuscript. Much gratitude is expressed to Dr. Tracy Quirk (LSU Department of Oceanography and Coastal Sciences) for helpful discussions on how to calculate and represent carbon storage results in Chapter 3.

Several people outside LSU also contributed to the development of my academic and professional career. I wish to thank the entire NSF-Coastal SEES research consortium, especially Rip Hale, Steve Goodbred, and Liz Chamberlain, for constructive feedback and collaboration that substantially improved the quality of my manuscripts, abstracts, and presentations. Thanks are given to John Martin, Aitor Ichaso, Vanessa Kertznus, among many others at Shell E&P who offered career advice, especially with regard to leveraging my academic research skills to industry-related projects.

The five field campaigns I made to Bangladesh over the course of my Ph.D. were memorable and rewarding experiences that would not have been successful without the assistance of many Bangladeshi colleagues. Students from Dhaka University, including Arif

Rahman, Sourov Bijoy Datta, Abdullah Al Nahian, Nithy Khair, and Md. Saddam Hossain, were instrumental in carrying out field work, handling logistics on the ground, and translating between English and Bengali with local villagers. Dr. Dilip Datta and Zahid Shawon from Khulna University were tremendous assets to our coring efforts along the Gorai River. Dilip generously made space for us in his lab while Zahid assisted in the field and helped navigate village roads in remote areas of the country. Finally, special thanks go out to Md. Nazrul "Bachchu" Islam and the entire Pugmark Tour crew. Bachchu's team made field work in the backwoods of Bangladesh nicer and more comfortable for us than it ever should have been – everything from carrying heavy scientific equipment hundreds of meters through dense mangrove foliage to preparing copious amounts of incredible Bengali food for us every night.

The projects in this dissertation were supported by an NSF-Coastal SEES grant, which not only funded field and lab work for the projects but also provided me with a generous research assistantship throughout my Ph.D. Additional funding from the American Association of Petroleum Geologists (AAPG), the Geological Society of America (GSA), and the Society for Sedimentary Geology (SEPM) made field work possible for Chapter 4. I also offer my thanks to the New Orleans Geological Society, American Petroleum Institute, Chevron Corporation, and Houston Energy Corporation for generous academic scholarships.

A final acknowledgement goes to all the friends I made at LSU over the past five years, and to my family and fiancée, Caroline, for patience and moral support throughout this process.

TABLE OF CONTENTS

LIST OF TABLES

LIST OF FIGURES

ABSTRACT

The Ganges-Brahmaputra (G-B) Delta of Bangladesh and India is widely considered to be one of the most vulnerable coastal systems in the world, owing to locally-accelerated sea level rise and landscape modification by human activities. Recent research efforts have identified pronounced elevation differences between natural and embanked areas in the G-B tidal delta plain, suggesting that natural landscapes are keeping pace with sea-level rise while anthropogenic locations are actively subsiding. However, this observation represents a singular point in time, and longitudinal trends of surface elevation in these regions are presently unknown. For communities residing in upstream regions of G-B delta plain, river bank stability is a primary concern, yet no scientifically-grounded assessments of channel dynamics exist for these areas. To address these knowledge deficits, this dissertation aims to: (1) compare rates of surface elevation change in the natural G-B tidal delta plain to those of current and projected trends of sea-level rise; (2) identify subsurface processes that influence elevation change, constrain their relative importance, and place findings within the context of carbon storage; and (3) develop a process-based framework for predicting riparian substrate composition across the tidal-fluvial transition zone of the G-B delta plain. Taken together, it is hoped that understanding the controls on elevation change and substrate erodibility will contribute to more effective management and adaptation strategies in these regions and in other deltaic systems worldwide.

The results of the studies indicate that: (1) natural areas of the G-B tidal delta plain are currently maintaining surface equilibrium with accelerated sea-level rise, though questions remain about the long-term future of this region, especially with regard to the continued supply of upstream sediments; (2) both physical and biotic parameters govern subsurface dynamics and elevation change in the G-B tidal delta plain, and the soils of this region host larger amounts of

terrestrial carbon than expected; and (3) a shift from uniform to non-uniform flow conditions influences the stratigraphic architecture of river banks across the G-B tidal-fluvial transition zone. This change in stratigraphy, in turn, controls river channel mobility and thus susceptibility to fluvial erosion.

CHAPTER 1. INTRODUCTION

River deltas, situated at the interface of land and sea, are among the most dynamic yet vulnerable environments on Earth. Deltaic landscapes are generally characterized by low elevation and topographic gradient, rendering these areas susceptible to inundation from sea-level rise, river flooding, and storms (e.g., Day et al., 2007; Jankowski et al., 2017; Tessler et al., 2015). In spite of these hazards, approximately 500 million people worldwide live within or near deltas (Syvitski et al., 2009), largely because of the abundant natural resources (e.g., fertile soil, groundwater, hydrocarbons) and ecosystem services (e.g., storm protection, fisheries, fluvial transportation networks) that they provide. Recent trends indicate that the world's population is becoming increasingly concentrated along coasts (McGranahan et al., 2007; Small and Nicholls, 2003), despite general recognition that sea level will continue to rise, or even accelerate, in the 21st century (Church et al., 2013; IPCC, 2013; Jevrejeva et al., 2008; Nicholls and Cazenave, 2010). As coastal resource stakeholders begin to develop management strategies for the future (Peyronnin et al., 2013; World Bank, 2015), a pressing need exists for interdisciplinary, science-based studies of deltaic morphodynamics (Goodbred et al., 2016; Rogers et al., 2017). Paramount to such research initiatives is an understanding of how deltaic landscapes, both above and below the ground surface, change over time in response to natural processes and human-induced modification of the environment. This dissertation seeks to explore these process-response relationships in one of the largest and most vulnerable deltas on Earth – the Ganges-Brahmaputra (G-B) Delta of Bangladesh and India (Figs. 1.1, 1.2).

Although deltaic systems share general commonalities in physical processes (e.g. river and coastal hydrodynamics), each is subjected to a different magnitude of anthropogenic conditioning (Goodbred and Saito, 2012; Tessler et al., 2015; Vörösmarty et al., 2009). The

expansive “mega-deltas” of South and Southeast Asia (Fig. 1.1), with their dense population centers and burgeoning infrastructure development, have been heavily altered by human settlement (Brown and Nicholls, 2015; Goodbred and Saito, 2012; Seto, 2011; Small et al., 2018; Woodroffe et al., 2006). Indeed, six of the Asian mega-deltas, including the G-B delta, are ranked among the top ten deltas most influenced by human activity (Tessler et al., 2015). In the case of the G-B system, natural subsidence from tectonics and sediment loading has been augmented by groundwater extraction (Higgins et al., 2014) and reduced floodplain aggradation from embankment-induced sediment exclusion (Auerbach et al., 2015a). The latter human alteration is particularly evident in the G-B tidal delta plain (Fig. 1.2), where the widespread development of embanked (“poldered”) agrarian land since the 1960s has modified the tidal channel network, resulting in tide range amplification (Pethick and Orford, 2013) and channel siltation (Wilson et al., 2017). These adverse effects directly impact >30 million people living in the G-B tidal delta plain (BBS, 2011), underscoring the dynamic nature of deltas and the far-reaching impacts such morphologic changes can have on human livelihoods.

Fig. 1.1. Geographical context of the Ganges-Brahmaputra Delta with respect to other human-impacted mega-deltas in South and Southeast Asia.

It has long been observed that deltas are prone to land loss, with notable accounts from the Mississippi (Blum and Roberts, 2009; Day et al., 2000; Gagliano et al., 1981), Nile (Stanley, 1996), and Yellow (Murray et al., 2014) river deltas, among others. Recently, however, it has been argued that the vulnerability of coastal landscapes is overstated in the literature (Kirwan et al., 2016), and that such ecosystems have the potential to keep pace with sea-level rise through biophysical feedback mechanisms (e.g., enhanced below-ground organic productivity from elevated levels of CO_2; Langley et al., 2009). To properly assess the current state and future response of deltaic landscapes to sea-level rise, it is crucial to quantify the vertical movement of the ground surface relative to local rates of sea-level rise. Several techniques have been utilized for this purpose, including: satellite altimetry (e.g., Farr et al., 2007), airborne LiDAR (e.g., Gesch, 2009), real time kinematic-global positioning surveys (RTK-GPS; e.g., Renschler et al., 2002), and the surface elevation table-marker horizon (SET-MH; e.g., Cahoon et al., 2002) method. The first two components of this dissertation (Chapters 2 and 3) investigate elevation dynamics using the SET-MH technique, which benefits from high measurement accuracy (~1 mm) and replicability (Cahoon et al., 2002), as well as a global network of SET studies (Webb et al., 2013).

The specific purpose of Chapter 2 is to compare longitudinal rates of surface elevation change to those of local ("effective") sea-level rise (Pethick and Orford, 2013) in the G-B tidal delta plain (Fig. 1.2). Contrary to previous notions that deltaic landscapes passively submerge to sea-level rise (the "bathtub" model; e.g., Houghton, 2005), we find that the natural G-B tidal delta plain exhibits robust adaptability by maintaining surface equilibrium in the face of human-induced tidal amplification. The empirical findings of this study not only demonstrate the current sustainability of the Sundarbans mangrove system, but also ground-truth input parameters for

numerical forward models of floodplain accretionary dynamics (Day et al., 1999; Rogers and Overeem, 2017). The second component of the dissertation (Chapter 3) builds on this work by identifying the subsurface processes that govern landscape evolution in the natural G-B tidal delta plain (Fig. 1.2). Belowground influences on elevation change are known to be highly site-specific (Cahoon et al., 2006), and in the G-B system, we find that both physical (e.g., seasonal changes in pore-water content) and biotic processes (e.g., organic matter decomposition) influence elevation change, despite its status as a mineral-rich delta where physical processes are expected to supersede biotic processes.

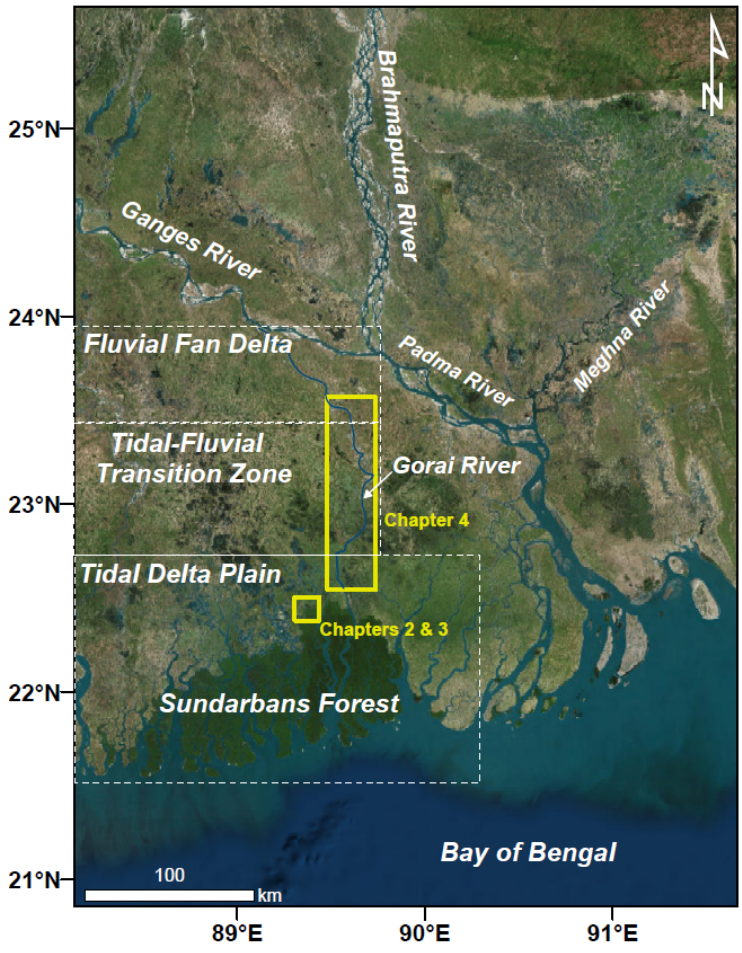

Fig. 1.2. Overview map of the G-B Delta, with major rivers and hydrodynamic zones labeled in white, and the study areas for respective dissertation chapters indicated in yellow. Hydrodynamic boundaries are based on observations in the Gorai River (Chapter 4), and the associated terminology follows that of Wilson and Goodbred (2015).

Upstream of the coastal zone, communities may be less vulnerable to inundation from sea-level rise but are nonetheless impacted by fluvio-deltaic hazards, namely the migration of river channels (e.g., Das et al., 2014; Haque and Zaman, 1989; Hunter, 2005; Mutton and Haque, 2004; RMMRU, 2007; Zaman, 1991). In Bangladesh alone, tens of thousands of people are displaced by river erosion every year (RMMRU, 2007), leading to disputes over property and the proliferation of impoverished squatter settlements (Mutton and Haque, 2004; Zaman, 1991). It is well established that riparian substrate architecture is a primary control on river channel mobility (e.g., (Fernandes et al., 2016; Fisk, 1952; Ikeda, 1989). However, little information presently exists on upstream-to-downstream changes in river bank composition in the G-B delta that can be used to forecast locations susceptible to future channel migration. Chapter 4 fills this knowledge gap by integrating sedimentological, stratigraphic, and geomorphic data across the fluvial to tidal continuum in the Gorai River, a distributary of the Ganges in southwest Bangladesh (Fig. 1.2). The results of this study indicate a fundamental shift in channel mobility in the Gorai that is spatially coincident with a transition from predominantly cohesive to non-cohesive strata; both transitions may in turn be influenced by the vertical position of the channel bed relative to mean sea level (i.e., the backwater effect, see Paola and Mohrig, 1996). Such findings are significant not only for characterizing modern channel morphodynamics across the fluvial to tidal transition zone but also for the prediction of reservoir-quality (i.e., sand-rich) rock in ancient, hydrocarbon-bearing fluvial-tidal formations (Feldman and Demko, 2015; Ichaso and Dalrymple, 2014).

CHAPTER 2. SURFACE ELEVATION AND SEDIMENTATION DYNAMICS IN THE GANGES-BRAHMAPUTRA TIDAL DELTA PLAIN, BANGLADESH: EVIDENCE FOR MANGROVE ADAPTATION TO HUMAN-INDUCED HYDROLOGICAL DISTURBANCES

2.1. Introduction

The unhindered deposition of detrital and organic material is crucial for maintaining surface equilibrium in low-lying coastal margins (Nicholls et al., 2007; Syvitski et al., 2009; Vörösmarty et al., 2009), especially given the prospect of accelerated eustatic sea-level rise (Church and White, 2006; Jevrejeva et al., 2008). However, recent research in a variety of delta systems, including the Mississippi (Meade and Moody, 2009), Ganges-Brahmaputra (Auerbach et al., 2015a), Nile (McManus, 2002) and Yellow (Wang et al., 2007), has provided numerous examples of how man-made river control structures stagnate, or in some cases, completely prevent sediment delivery to the floodplain. These anthropogenic modifications to the landscape also alter river channel hydrodynamics, leading to deleterious effects like channel siltation (C. Wilson et al., 2017; Wolanski et al., 2001) and tide range amplification (Pethick and Orford, 2013). While restorative techniques are currently being developed and implemented in some coastal communities (e.g., Mississippi River Delta, Peyronnin et al., 2013), it is well accepted that the interplay of hydrodynamics, sediment deposition, and landscape evolution can differ substantially among deltaic systems (Orton and Reading, 1993; Syvitski and Saito, 2007). Thus, site-specific consideration of these geomorphic processes, in addition to understanding the degree of human-induced modification, is critical for properly assessing the sustainability of the system and for formulating restoration initiatives that balance environmental, economic, and humanitarian interests.

Among delta systems worldwide, the Ganges-Brahmaputra (G-B) delta is considered to be one of the most vulnerable to the effects of climate change, owing in large part to anthropogenic stressors (Higgins et al., 2018; Syvitski et al., 2009; Tessler et al., 2015). Indeed, the G-B delta, with a burgeoning population of ~144 million, is the most populated delta on Earth (Higgins, 2016). In Bangladesh, which occupies roughly 70% of the G-B delta, a significant proportion of the population lives at or near sea level, placing millions of inhabitants at risk of inundation from rising sea levels as well as cyclone-induced storm surges. In an effort to mitigate these environmental hazards, the Bangladesh government began constructing earthen embankments along channel margins in low-lying agrarian regions of the country in the 1960s (Alam, 1996; Allison, 1998; Islam, 2006). Cultivated land within these embankments, hereafter referred to by the Dutch term "polder," also benefitted from augmented rice production due to prevention of saline water intrusion during the dry season. However, it is now widely recognized that polderization has contributed to a variety of deleterious outcomes that affect communities both in the vicinity and far from their construction.

For instance, Pethick and Orford (2013) compared long-term tide gauge records from three stations located in the Passur Estuary (see Fig. 2.1A for location) and found that the rate of change of mean high water level exceeded that of mean sea level between 1968 and 2011, indicating that an increase in tidal range had occurred over this time span (e.g., from ~1.4 to ~2.3 m at Khulna). The timing of tidal range amplification and observation that the magnitude of change was particularly high near poldered regions suggested that embankment construction and resultant reduction of the tidal prism were the causal mechanisms. A subsequent study found the closure of 1500 km of tidal channels reroutes 1.4 km^3 of water (C. Wilson et al., 2017). Accordingly, if the effects of human alteration are not considered (e.g., tidal amplification in this

case), rates of sea-level rise can be substantially underestimated (Kirwan and Megonigal, 2013; Pethick and Orford, 2013). These findings underscore the notion that eustatic sea-level rise and subsidence are not the only processes affecting the surface equilibrium of coastal systems, as delta floodplains aggrade to mean flood elevation (Tornqvist and Bridge, 2002) and tidal landscapes build to approximately mean high water (MHW, Kirwan and Guntenspergen, 2010).

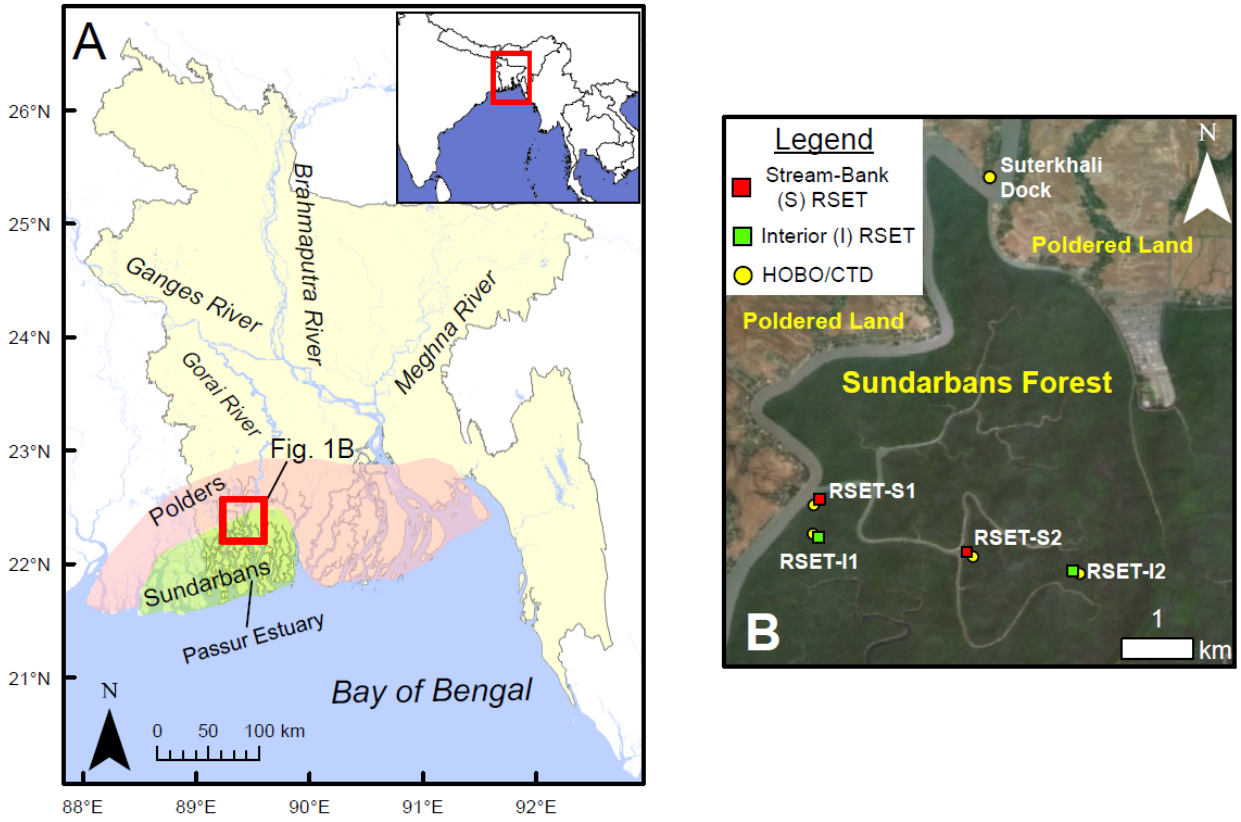

Fig. 2.1. (A) Physiographic map of greater Bangladesh with the Sundarbans mangrove forest and poldered areas outlined in green and pink, respectively; (B) rod surface elevation table (RSET) and hydrologic instrument coverage in the field area.

Situated adjacent to the poldered landscape is the Sundarbans National Park (hereafter referred to as the Sundarbans), a pristine and expansive mangrove forest that spans ~10,000 km^2 (Fig. 2.1A). The Sundarbans holds importance for coastal populations as the mangrove ecosystem offers a wide range of ecological resources (e.g., fish, crabs, timber, and honey) and provides a natural buffer from storm surges and tidal bores (e.g., Van Coppenolle et al., 2018).

Although it is recognized that poldered regions exist at an elevation deficit relative to the surrounding natural tidal platforms (Auerbach et al., 2015a; Rogers and Overeem, 2017), the vulnerability of the natural G-B tidal delta plain and Sundarbans forest to inundation from sea-level rise is presently unclear. Loucks et al. (2010) indicate progressive submergence of the Sundarbans with increasing sea level ("bathtub model"), particularly in excess of 20 cm of sea-level rise and in low-lying areas of the forest interior. Conversely, other researchers contend that the Sundarbans is geomorphically stable based on observed sediment accretion rates that approximate the local rate of relative sea-level rise (~1 cm yr^{-1}, Allison and Kepple, 2001; Rogers et al., 2013). Ultimately, however, the fate of coastal wetlands is controlled by the maintenance of surface elevation, and numerous studies have shown that shallow subsidence and RSLR can outpace gains from accretion (e.g., Cahoon et al., 2006; Krauss et al., 2010; Lovelock et al., 2011; Rogers et al., 2006). Rates of surface elevation change, in conjunction with the forcing components (e.g., tidal hydroperiod, sedimentation dynamics), are therefore critical to accurately assess the sustainability of the G-B tidal delta plain and other coastal systems worldwide.

This study reports the first longitudinal data (i.e., seasonal measurements over a time span of 5 years) on elevation and sedimentation dynamics in the natural G-B tidal delta plain, using a modified version of the widely applied surface elevation table-marker horizon methodology (e.g., Cahoon et al., 2002). Understanding seasonal and inter-annual changes in surface elevation is vital for informed decisions on land management (World Bank, 2015), a topic that remains a matter of debate in coastal Bangladesh (Auerbach et al., 2015b; Hossain et al., 2015). Thus, the specific objectives of this study are to: (1) document surface elevation and sediment accretion change in different hydro-geomorphic landscapes of the natural G-B tidal

delta plain, (2) ascertain the importance of seasonal processes on elevation and accretion dynamics, (3) identify surficial and below-ground processes that govern these changes, and (4) determine whether the landscapes are sustainable with respect to sea-level rise.

2.2. Study area

Originating in the greater Himalaya, the Ganges and Brahmaputra rivers flow south through India and coalesce in central Bangladesh. Water discharge and sediment load of these rivers are strongly regulated by climatic conditions, the most notable of which being the South Asian monsoon (e.g., Coleman, 1969). From June through September, southwest winds blow onshore from the Bay of Bengal, triggering persistent rainfall and flooding throughout the Indian subcontinent. The annual deluge is largely responsible for the 1060 Mt of sediment and 1270 km^3 of water delivered to the G-B delta and Indian Ocean each year (Milliman and Farnsworth, 2011 and references therein). Integrated satellite imagery analyses and field observations on the inner continental shelf indicate that the direction of the residual current and sediment transport is landward and to the west (Barua et al., 1994). Nearshore waves and tides then advect these turbid waters inland through a dense network of tidal channels, dispersing sediments throughout the lower tidal delta plain (Hale et al., 2019). This sediment conveyance pathway allows areas that are no longer directly connected with fluvial point sources to maintain vertical accretion in accordance with rising sea level (Rogers et al., 2013).

Within the greater G-B delta system, the present study is focused on the tide-dominated, lower delta plain (Fig. 2.1A). Located ~150 km west of the river mouth, the G-B tidal delta plain was the active lobe of the delta prior to periodic, eastward avulsions of the main-stem Ganges and Brahmaputra rivers during the late Holocene (Allison et al., 2003). Today, the tidal delta plain is less connected to fluvial input: the Gorai River is the only source of fresh water to the

region and has decreased in mean discharge by 95% over the past ~50 years partly due to the construction of the Farakka barrage (EGIS, 2000; Mirza, 1998; Shaha and Cho, 2016) and partly due to natural infilling of the Ganges-Gorai distributary off-take (Pethick, 2012; Winterwerp and Giardino, 2012). Like much of Bangladesh, the lower delta plain experiences a tropical monsoonal climate, which is characterized by mean high and low temperatures of 31 and 22 °C, respectively, and mean annual precipitation in excess of 180 cm. Areas that have not been cleared for agricultural purposes are dominated by an assemblage of mangroves that includes Sundari (*Heritiera fomes*), Gewa (*Excoecaria agallocha*), Kankra (*Bruguiera decandra*), and Bain (*Avicennia marina*) species (Giri et al., 2014). Sediment cores taken across the lower delta plain to ~5 m depth reveal that the shallow subsurface typically consists of fining-upward successions of mud-rich sand to rooted silts and clays (Allison et al., 2003).

2.3. Methods

2.3.1. Surface elevation change

Inter-annual surface elevation change was recorded using an array of rod surface elevation table (RSET) instruments (Figs. 2.1B, 2.2, see also Appendix A for installation details and measurement dates). During RSET installation, stainless steel rods (15 mm in diameter, 1.22 m in length) were driven into the substrate until refusal and cemented within 10-cm diameter PVC pipes for stability. The depth of the benchmark ranged from 12.2 to 18.3 m, depending on the local depth of the incompressible substrate (i.e., consolidated sand). Following the procedures of Cahoon et al. (2002), nine measurements of surface elevation were taken at eight different positions for a total of 72 measurements at each site. During data collection, any natural obstructions (e.g., tree roots, pneumatophores) or bioturbation features (e.g., crab mounds, footprints) that interfered with the true ground surface were noted, and the associated

measurements were omitted during analysis. RSET stations were established in two hydro-geomorphic settings in the Sundarbans mangrove forest: 1) within close proximity (~10 m) of a tidal channel and typically slightly higher elevation, termed "stream-bank (S)," and 2) distal (>100 m) from any tidal channel and typically at lower platform elevation, termed "interior (I)" (Fig. 2.1B; Table 2.1). RSET instruments were deployed in two phases: RSET-S1 and I1 were installed in May 2014, while RSET-S2 and I2 were installed in October 2015. Baseline measurements were taken at least a month after deployment to allow for any disturbance during installation to have recovered. Due to differences in deployment periods, RSET results reported by hydro-geomorphic setting were averaged when instrument deployment periods coincided (e.g., RSET-S1 and S2 between October 2015 and March 2019) and were reported individually when they did not coincide (e.g., RSET-S1 between May 2014 and October 2015).

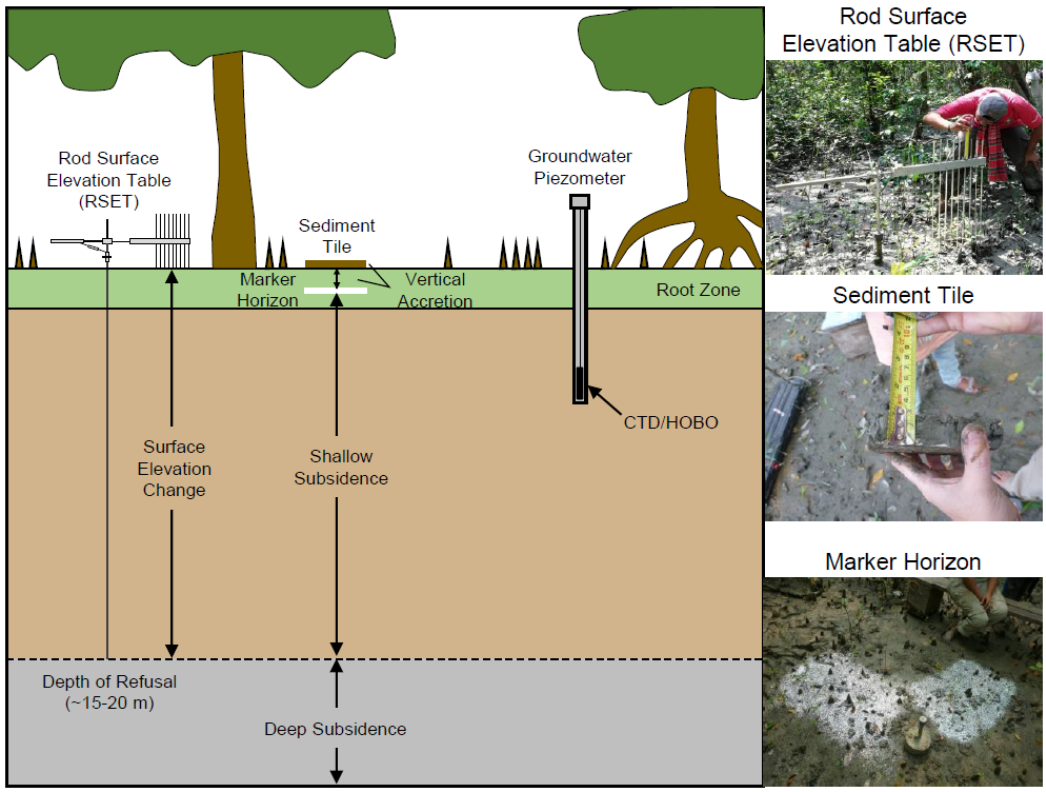

Fig. 2.2. Schematic diagram (not to scale) of methods employed in this study (modified from Cahoon et al., 2002). RSETs, marker horizons (either brick dust or plastic glitter), sediment tiles, and piezometers were deployed within the Sundarbans forest.

2.3.2. Vertical accretion

Seasonal sediment vertical accretion was directly measured using two methods: sediment tiles and marker horizons (Fig. 2.2). As recommended by Steiger et al. (2003), these two techniques were used together to provide quality control in this dynamic depositional setting. Following the approach of Rogers et al. (2013), four ceramic sediment tiles (area = 100 cm^2), were placed on the ground surface in the vicinity of each RSET station (Fig. 2.2). Following a deployment period of ~6 months, tiles were excavated and vertical accretion was measured at two points on each side of the tile for a total of eight measurements per tile (Fig. 2.2). The average of all measurements (n = 32, when all tiles were found) was calculated to obtain the amount of seasonal accretion. During data collection, any evidence of faunal disturbance (e.g., broken tile, crab mounding) was noted and associated measurements were omitted during analysis. Tiles were cleared of sediments following each sampling period and re-deployed in the same location for consistency and to facilitate identification in subsequent data collection periods.

Sediment accretion as recorded by tiles was supplemented with artificial marker horizons (Cahoon and Turner, 1989; Fig. 2.2). Brick dust or plastic glitter was dispersed on the ground surface in two plots (area ≈ 1 m^2) situated on different sides of the RSET receiver (Fig. 2.2, Appendix A). During subsequent field excursions, small cubic cores (~4 cm^2) were excavated in undisturbed locations to locate marker horizons and quantify sediment accretion. The distance from the ground surface to the marker horizon was calculated as the amount of vertical accretion that had occurred during the deployment period. Additionally, the vertical distribution and order of markers in the subsurface was noted and used to assess the degree of bioturbation.

2.3.3. Shallow subsidence

Comparisons of surface elevation and vertical accretion trends can be used to quantify shallow subsidence, adapted from Cahoon et al. (1995) as:

$$SS = VA - SEC \quad (1)$$

where SS is calculated shallow subsidence, VA is measured vertical accretion, and SEC is measured surface elevation change. Positive values of SS indicate that shallow subsidence occurred at depth between the ground surface and the depth of refusal for the RSET rods (see Fig. 2.2, Appendix A), whereas negative values indicate shallow subsurface expansion has occurred. SS values close to zero indicate that surface elevation change is occurring primarily as a function of sediment accretion, with negligible shallow subsidence or expansion (see Cahoon, 2015).

2.3.4. Platform flooding

Local surface and groundwater hydrodynamic data were obtained from Schlumberger Diver CTD (conductivity, temperature, and pressure) and Onset U20L-01 HOBO (water pressure) instruments attached to a dock piling in a nearby tidal channel (n = 1; surface water) and emplaced in piezometers on the platforms near the RSET instruments (n = 4; groundwater piezometers screened from the surface to a depth of 2 m) (Figs. 2.1B, 2.2). The instruments logged data every 10 minutes to document water level, water temperature, and electrical conductivity (a proxy for salinity) changes over tidal and seasonal time scales. Mangrove platform flooding events were identified in the hydrograph data by a rapid increase in water pressure followed by a gradual decline in pressure as waters receded from the platform. Seasonal duration of platform inundation (i.e., hydroperiod) was quantified at two locations (RSET-S1 and RSET-I1) by tabulating time periods when water levels met or exceeded the level of the ground

surface, as established by (Auerbach et al., 2015a) in the EGM96 datum. Other locations (RSET-I2 and RSET-S2) were excluded from hydroperiod analysis due to: (i) short time periods of deployment, and (ii) missing or compromised data from instrument vandalism.

2.3.5. Statistical analyses and parameter comparisons

To evaluate whether seasonal conditions (e.g., monsoonal flooding) significantly impacted surface elevation change and sediment accretion, we compared seasonal changes in these parameters using two-tailed *t*-tests assuming equal variances. In addition, relationships between: (1) hydroperiod and sediment accretion; (2) groundwater level and surface elevation change; and (3) groundwater level and shallow subsidence were assessed for significance using regression analysis. In all cases, a significance level of $\alpha = 0.05$ was used to reject the null hypothesis. Linear trends of surface elevation change were directly compared to local rates of relative sea-level rise (0.9 cm yr^{-1}) to assess whether the investigated landscapes are keeping pace with sea-level change. Relative sea-level rise combines the effects of eustatic sea-level rise at the northern Bay of Bengal (0.3 cm yr^{-1}, Cazenave et al., 2008) and total subsidence (i.e., shallow and deep components, 0.6 cm yr^{-1}, Grall et al., 2018; Hanebuth et al., 2013; Khan and Islam, 2008). No statistical methods were applied to these comparisons as rates of surface elevation change must simply meet or exceed those of sea-level rise to be considered sustainable (e.g., Morris et al., 2002).

2.4. Results

2.4.1. Surface elevation change

Among the two hydro-geomorphic settings, the highest rates of surface elevation change were observed at stream-bank sites, where elevation increased over time at a rate of 2.16 ± 0.26 cm yr^{-1} (Fig. 2.3A; Table 2.1) and greatly exceeded the rate of relative sea-level rise (0.9 cm yr^{-}

^{1}). Surface elevation increased at these locations during both the monsoon and dry season, though positive elevation increments were significantly higher during the monsoon season (Fig. 2.3A; Table 2.2). Sundarbans interior sites displayed a slightly lower rate of surface elevation gain, collectively increasing at a rate of 1.32 ± 0.17 cm yr^{-1} (Fig. 2.3A; Table 2.1), which also exceeded the rate of relative sea-level rise (0.9 cm yr^{-1}). A strong seasonal signal was apparent in this hydro-geomorphic zone: surface elevation change was positive during the monsoon season but often negative during the dry season (Fig. 2.3A; Table 2.2). Over time, however, elevation gain during the monsoon season exceeded elevation loss during the dry season, resulting in an overall positive trend (Fig. 2.3A).

2.4.2. Vertical accretion

Rates of vertical accretion as determined by the sediment tile method varied considerably depending on the hydro-geomorphic setting (Fig. 2.3B). For instance, accretion rates at stream-bank sites (3.29 ± 0.24 cm yr^{-1}) were approximately 55% higher than those at interior sites (2.12 ± 0.20 cm yr^{-1}) (Table 2.1). This discrepancy was almost exclusively derived from differences in monsoon season accretion as dry season accretion was similar at stream-bank (1.00 ± 0.27 cm) and interior (0.91 ± 0.26 cm) settings (Table 2.2). Seasonal differences in vertical accretion were significant at Sundarbans stream-bank settings, but not at Sundarbans interior locations (Table 2.2). Rates of vertical accretion as measured by the marker horizon method were generally higher than those measured by sediment tiles (Table 2.1). However the horizons, differentiated by color, were often found out of sequence in the subsurface, indicating error associated with bioturbation.

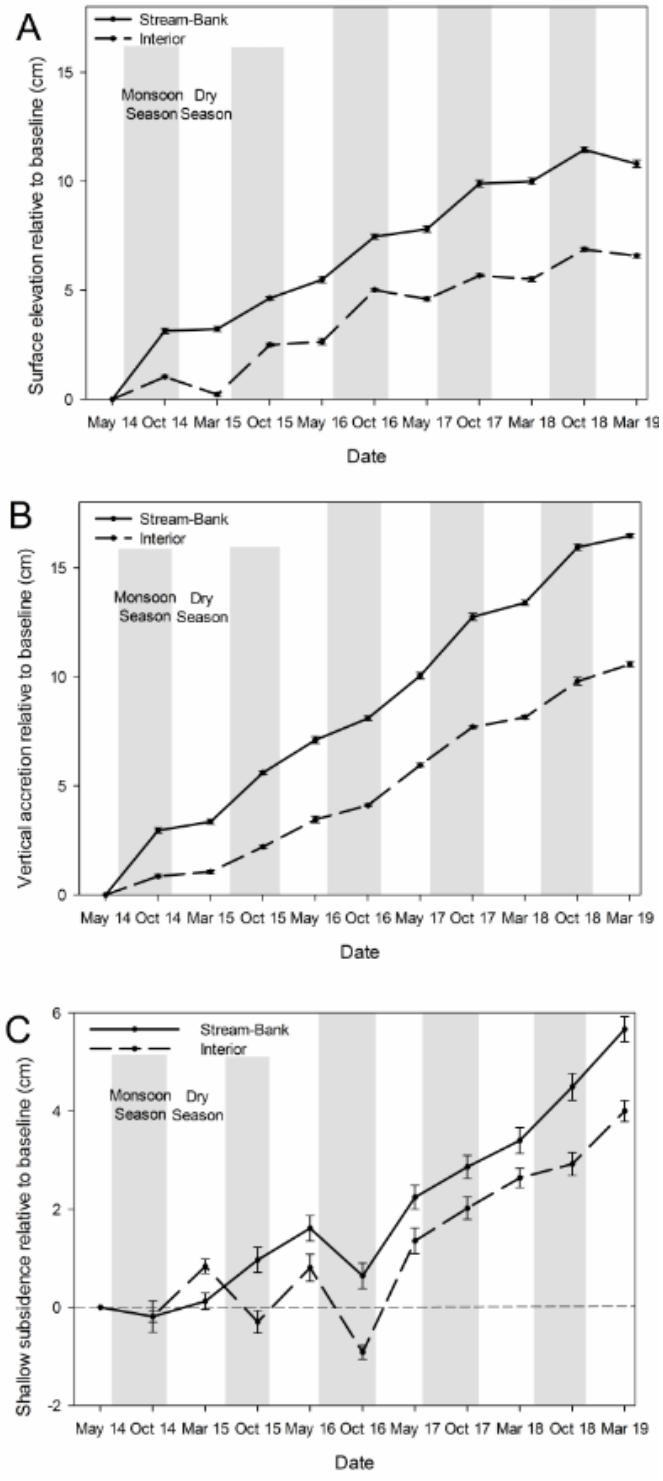

Fig. 2.3. Inter-annual change in (A) surface elevation, (B) vertical accretion, and (C) shallow subsidence grouped by hydro-geomorphic setting. Note the change in scale for (C) and that values of negative shallow subsidence represent expansion in the shallow subsurface (i.e., clay expansion, belowground biomass production, etc.). Values are the average of two sites and represent longitudinal change relative to the baseline measurement. Error bars are the standard error for all measurements.

Table 2.1. Mean annual rates (± standard error) of surface elevation, vertical accretion measured by sediment tiles (ST) and marker horizons (MH), and shallow subsidence among study sites. Shallow subsidence values are based on the difference between surface elevation change and vertical accretion from the sediment tile method, when available. Shallow subsidence errors are propagated from the surface elevation and vertical accretion error component pools.

Station	**Landscape**	**Record Duration (yr)**	**Surface Elevation Change (cm yr^{-1})**	**Vertical Accretion – ST (cm yr^{-1})**	**Vertical Accretion – MH (cm yr^{-1})**	**Shallow Subsidence (cm yr^{-1})**
RSET-S1	Stream-Bank	5.0	2.59 ± 0.17	3.29 ± 0.29	3.64 ± 1.18	0.70 ± 0.46
RSET-I1	Interior	5.0	1.40 ± 0.14	2.62 ± 0.28	2.78 ± 1.01	1.22 ± 0.42
RSET-I2	Interior	3.5	1.05 ± 0.22	1.76 ± 0.29	2.32 ± 0.73	0.71 ± 0.51
RSET-S2	Stream-Bank	3.5	1.16 ± 0.37	3.00 ± 0.31	3.00 ± 0.57	1.84 ± 0.68
Average	Stream-Bank	5.0	2.16 ± 0.26	3.29 ± 0.24	3.32 ± 0.88	1.13 ± 0.50
Average	Interior	5.0	1.32 ± 0.17	2.12 ± 0.20	2.55 ± 0.87	0.80 ± 0.37

Table 2.2. Mean seasonal values (± standard error) of surface elevation change (SEC), vertical accretion using sediment tiles (VA-ST), and shallow subsidence (SS) for the two hydro-geomorphic settings. The presence or absence of significant seasonal differences for the various parameters was established using independent two-tailed *t*-tests (see methods section 2.3.5 for more details).

Landscape	**Monsoon Season SEC (cm)**	**Dry Season SEC (cm)**	**Seasonal Difference in SEC?**	**Monsoon Season VA (cm)**	**Dry Season VA (cm)**	**Seasonal Difference in VA-ST?**	**Monsoon Season SS (cm)**	**Dry Season SS (cm)**	**Seasonal Difference in SS?**
Stream-bank	2.01 ± 0.28	0.15 ± 0.22	Yes (t-ratio = 4.69, P = 0.0016)	2.29 ± 0.31	1.00 ± 0.27	Yes (t-ratio = 2.80, P = 0.0231)	0.28 ± 0.34	0.85 ± 0.21	No (t-ratio = 1.29, P > 0.05)
Interior	1.63 ± 0.26	-0.31 ± 0.14	Yes (t-ratio = 5.84, P = 0.0004)	1.21 ± 0.19	0.91 ± 0.26	No (t-ratio = 0.83, P > 0.05)	-0.42 ± 0.40	1.22 ± 0.25	Yes (t-ratio = 3.13, P = 0.0141)

2.4.3 Shallow subsidence

Over the entire dataset, vertical accretion exceeded surface elevation gain at both stream-bank and interior settings, indicating that shallow subsidence occurred between the ground surface and RSET benchmark (Fig. 2.3C; Table 2.1). Rates of shallow subsidence at stream-bank sites (1.13 ± 0.50 cm yr^{-1}) were ~34% higher than those of interior sites (0.80 ± 0.37 cm yr^{-1}, Table 2.1). Seasonal patterns of shallow subsidence were similar for both hydro-geomorphic settings, exhibiting greater subsidence during the dry season than during the monsoon season (Fig. 2.3C). There were, however, a couple instances during the monsoon season when surface elevation gain exceeded vertical accretion, indicating shallow subsurface expansion (e.g., between May and October 2016, Fig. 2.3C).

2.4.4. Platform flooding

Surface hydrologic data recorded within the tidal channel at Suterkhali dock (see Fig. 2.1B for location) reveal that the local area is characterized by a semidiurnal tidal regime with a tide range of ~3 to 5 m (Fig. 2.4A). A water level setup of ~0.5 to 0.7 m is observed during the monsoon season (Fig. 2.4A), as documented in other coastal regions of the G-B delta (Barua, 1990). GPS and theodolite surveys undertaken by Auerbach et al. (2015a) determined the average elevation of the Sundarbans relative to pertinent tidal frame constituents, including mean high water (MHW), mean sea level (MSL), and mean low water (MLW), within the EGM96 datum (Fig. 2.4A). Comparing the average elevation of the Sundarbans, +2.6 m relative to EGM96, to the Suterkhali tide data suggests that during the monsoon season, flooding of the mangrove platform should occur during every spring high tide up to ~0.5 m depth and during a few isolated neap high tides (Fig. 2.4A). This approach also suggests that platform inundation

during the dry season should occur during new moon spring tides, with little flooding otherwise (Fig. 2.4A).

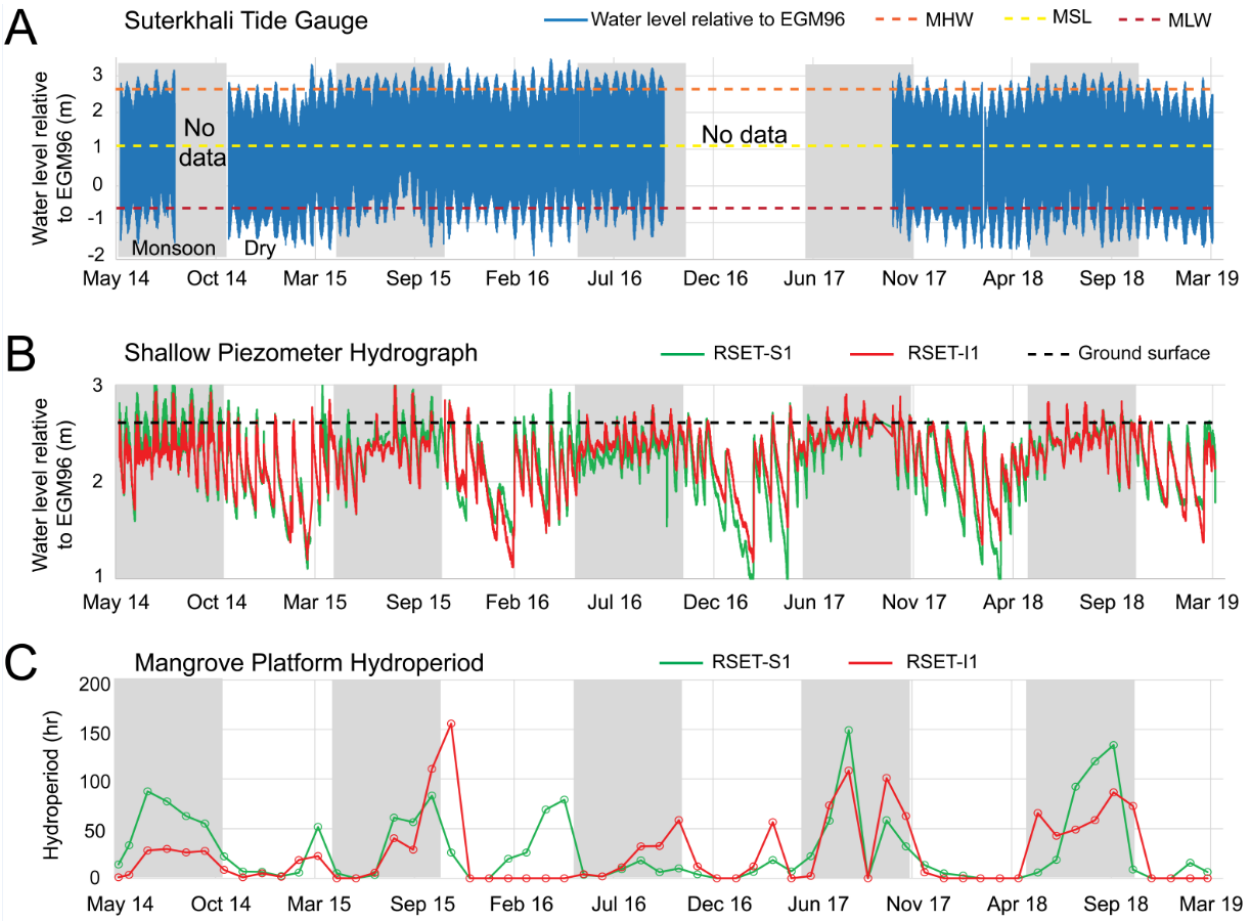

Fig. 2.4. (A) Water level measurements at Suterkhali dock (see Fig. 2.1B) including local tidal frame constituents. Note that during the monsoon season (time periods shaded in grey) there is a coastal set-up of water regionally (after Barua, 1990), which raises mean water level by ~50-70 cm. Abbreviations: MHW- mean high water; MSL - mean sea level; MLW - mean low water (after Auerbach et al., 2015a). (B) Hydrographs for shallow piezometers near RSET-S1 and RSET-I1, located within the Sundarbans (see Fig. 2.1B), illustrating fluctuations in water level related to neap-spring cycles during the dry (white) and monsoon (grey) seasons. The dashed line represents the overbank flooding threshold (i.e., mangrove platform elevation), which is only surpassed ~ every 2 weeks during the monsoon season spring tides. Note that during neap tides, groundwater levels lower as much as ~1.25 m, exacerbated during the dry season when the platform hydroperiod is reduced by ~62% (see also Fig. 2.5). (C) Monthly tidal hydroperiod of the mangrove platform at RSET-S1 and RSET-I1 locations.

The hydrodynamics from piezometers located on the Sundarbans mangrove platform display weekly, large-scale fluctuations in water level due to neap-spring tidal cycles (Fig. 2.4B). When placed within the context of the mangrove platform ground surface, this data indicates

when the platform is inundated and the depth of inundation, as well as the shallow groundwater table dynamics (Figs. 2.4B, 2.4C). Piezometer results generally substantiate tide gauge approximations of inundation and indicate that during the monsoon season platform inundation occurs during the majority of spring high tides and occasionally during neap high tides (Fig. 2.4B). In contrast, platform flooding during the dry season is relatively scarce, occurring only during some new moon spring tides and exhibiting evidence of negligible inundation for several weeks to months at a time (e.g., between Dec 16 and Feb 17, Figs. 2.4B, 2.4C). Shallow groundwater table dynamics are controlled by neap-spring cyclicity and seasonal conditions (Fig. 2.4B). During the monsoon season, the groundwater table typically lowers 0.3 to 0.5 m relative to the platform surface (Fig. 2.4B). Groundwater fluctuations are more dramatic during the dry season, when lowering of the groundwater table in excess of 1 m was documented on multiple occasions (e.g., between Jan and Feb 17, Fig. 2.4B). Over the cumulative dataset, stream-bank site RSET-S1 documented greater hydroperiod in comparison to interior site RSET-I1, though there were multiple months when the hydroperiod of RSET-I1 exceeded that of RSET-S1 (e.g., Nov 15, Fig. 2.4C).

2.5. Discussion

2.5.1. Surface controls on landscape dynamics

Rates of surface elevation change and sediment accretion from this study, which represent the first coordinated measurements in the G-B tidal delta plain, were in general much greater than those reported in other mangrove systems. In a review of mangrove settings across the worldwide RSET network, Sasmito et al. (2016) found that for pristine mangrove sites with >1 year of data (n = 45), surface elevation and vertical accretion rates averaged 0.07 and 0.55 cm yr^{-1}, respectively. Corresponding measurements from this study, averaging 1.74 and 2.71 cm yr^{-1}

for our study sites in the natural Sundarbans mangrove forest (Table 2.1), are up to an order of magnitude greater than the worldwide average, which underscores the amount of sediment discharged from the G-B river mouth, as well as the efficiency of the system to redistribute these sediments to the tidal delta plain (~150-200 km from the river mouth, *sensu* Rogers et al., 2013; Wilson and Goodbred, 2015). To our knowledge, the only location with comparably high rates of surface elevation change is at Sanjiang in Dongzhaiguang Bay, China, where elevation increased at an average rate of 1.75 cm yr^{-1} (Fu et al., 2018). The mangrove forests of the Sundarbans and Sanjiang share commonality as mineral-rich, riverine systems that are situated in the vicinity of large population centers (Fu et al., 2018; Rogers et al., 2013). Owing to a general lack of organic matter accumulation in this type of environment (e.g., Rovai et al., 2018), mineral-rich, riverine mangrove systems are heavily reliant on the continued supply of upstream sediments in order to maintain positive surface elevation change over time.

Vertical accretion measurements using the marker horizon method in this study generally yielded higher values than analogous measurements using sediment tiles (Table 2.1). Based on the observation that marker horizons were often found out of sequence in the subsurface, we attribute this difference to the presence of post-depositional mixing (i.e., bioturbation). Mangrove crabs (*Scylla serrata*) are abundant in the Sundarbans forest and commonly burrow during low tide (Alberts-Hubatsch et al., 2016), likely altering the subsurface particle distribution. In contrast to the marker horizons, sediment tiles provide a physical barrier that prevent mixing of older sediments, and as such, justify this should be the preferred proxy for establishing vertical accretion and shallow subsidence rates in this area (Table 2.1). Nevertheless, the sediment accretion rates derived from both techniques in this study may be overestimated as short-term additive measurements typically yield higher values than a single

long-term measurement that incorporates sediment dewatering and compaction (e.g., Steiger et al., 2003). Therefore, the rates of shallow subsidence reported here (Fig. 2.3C, Table 2.1) should be viewed as upper estimates for this region. Additionally, we acknowledge that due to the relatively short duration of this study (5 years), our rates of sediment accretion will naturally be higher than those obtained using techniques that investigate longer time scales (e.g., decadal to centennial sedimentation rates from short-lived radioisotopes, e.g., Allison and Kepple, 2001), and thus should not be directly compared.

In the G-B tidal delta plain, we find that the patterns of surface elevation change reflect hydrodynamic processes that are in turn governed by seasonal climatic conditions. During the summer monsoon, elevated suspended sediment concentrations in the tidal channels (Barua, 1990; Hale et al., 2019; Hale et al., *in press*) combined with increased frequency of platform inundation (from an average of 85.2 ± 42.9 hr to 229.2 ± 95.9 hr; Figs. 2.4C, 2.5) promote surface elevation gain, principally through the accumulation of newly deposited sediment (*sensu* Marion et al., 2009). Indeed, we found that the duration of inundation of the platform (i.e., hydroperiod) strongly controls the magnitude of sediment accretion as presented earlier: a significant positive relationship exists between these two parameters ($r^2 = 0.70$, $P < 0.0001$; Fig. 2.5). Accordingly, elevation gains were significantly greater during the monsoon season as compared to during the dry season at all hydro-geomorphic settings (Table 2.2). We note however, similar to other wetland settings, seasonal differences in sediment accretion were site-specific (Table 2.2). Sundarbans stream-bank locations exhibited seasonal differences in accretion, likely reflecting greater access to the sediment-rich waters of the monsoon season (Hale et al., *in press*). On the other hand, Sundarbans interior sites did not exhibit seasonal differences in sediment accretion, suggesting that part of the monsoon sediment load was

sequestered on or near the channel banks and did not reach the interior of the mangrove platform (*sensu* Rogers and Goodbred, 2014).

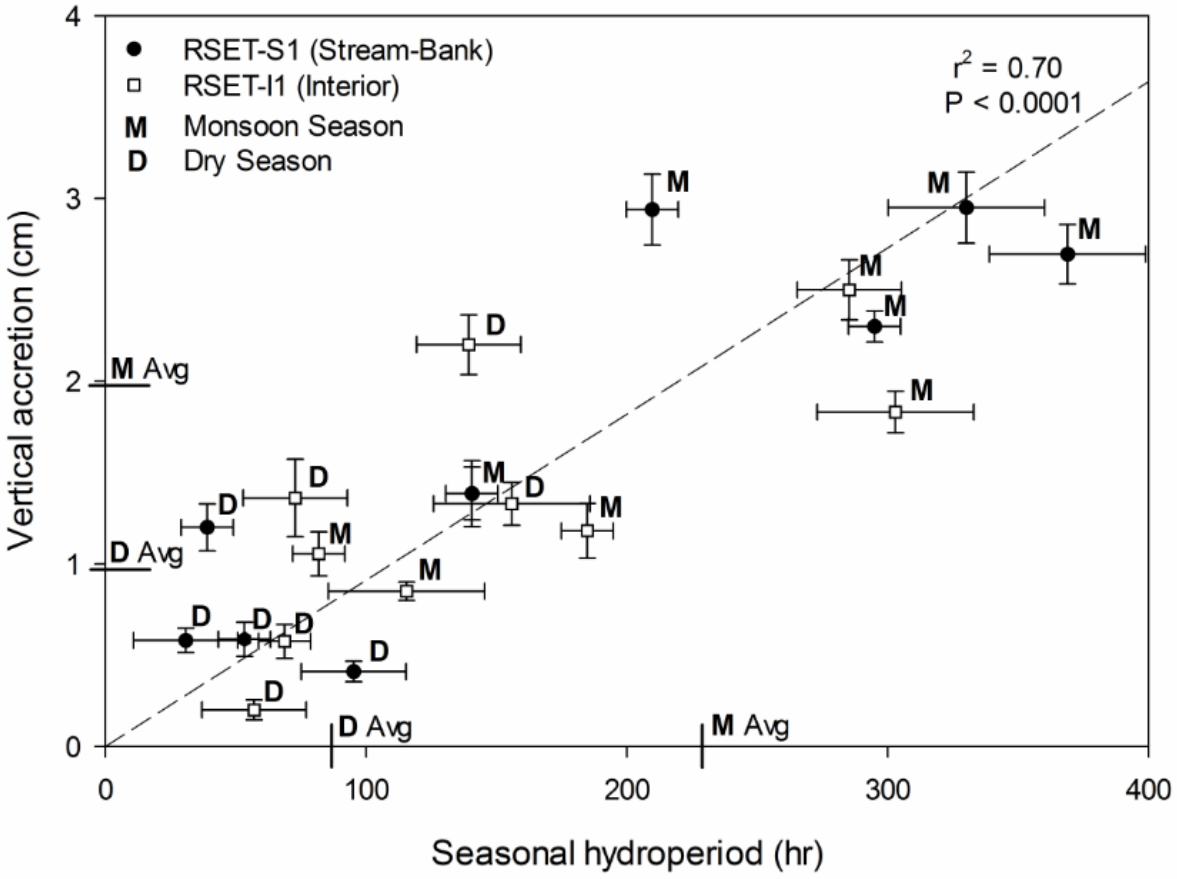

Fig. 2.5. Relationship between observed vertical accretion on tiles and calculated seasonal inundation for RSET-S1 and RSET-I1 locations in the Sundarbans mangrove forest.

Mangrove vegetation density likely also plays a role in the capture and deposition of sediments carried in suspension by tidal waters. Hydrodynamic field and modeling studies in Australian mangrove forests indicate that the interaction between tidal currents and subaerial vegetation (e.g., pneumatophores) produces zones of stagnant water in which suspended sediments preferentially settle (Furukawa et al., 1997; Furukawa and Wolanski, 1996). Correspondingly, it is possible that a portion of the total sediment load carried by flood tides is deposited within close proximity of the channel, effectively diluting the tidal water as it propagates towards the interior of the platform (e.g., Furukawa and Wolanski, 1996). Hale et al.

(*in press*) documented a 15% reduction in peak suspended sediment concentration from stream-bank (RSET-S2 in this study) to interior sites (RSET-I2 in this study) in the monsoon season, corroborating the notion of progressive sediment extraction from tidal waters. Generally higher than expected rates of sediment accretion at Sundarbans sites during the dry season could be attributed to the facilitated deposition of silt- and clay-size particles via electrochemical flocculation (e.g., Winterwerp and Kesteren, 2004) when waters are relatively saline during this time of the year (up to 25 ppt, Shaha and Cho, 2016). Silt and clay are the dominant grain sizes in the Sundarbans mangrove forest, together accounting for >85% of the near-surface sediments (depth = 10-50 cm) in the study area (Allison et al., 2003).

2.5.2. Subsurface controls on landscape dynamics

It is well established that vertical accretion is a strong influence on surface elevation change in wetlands and deltaic settings (e.g., Neubauer, 2008; Nyman et al., 2006), however it is not the only parameter that controls displacement of the land surface through time. As seen by differences in surface elevation and vertical accretion (cf., Figs. 2.3A, 2.3B, Table 2.1), a portion of the absolute elevation gain can be lost to below-ground processes and resultant shallow subsidence. In general, a variety of subsurface processes in wetlands contribute to shallow subsidence, including groundwater flux (Cahoon et al., 1995; Rogers and Saintilan, 2008; Whelan et al., 2005), sediment compaction (Day et al., 1999; Knott et al., 1987; Lovelock et al., 2011), clay abundance and mineralogy (Karathanasis and Hajek, 1985; Nelson and Miller, 1997; Schafer and Singer, 1976), and organic matter production and decomposition (Cahoon et al., 2003; McKee et al., 2007). These studies show that the relative importance of these factors is highly location-specific; therefore, careful consideration of each of these processes is critical when characterizing landscape evolution.

The presence of both subsidence and expansion of the substrate in this study area using RSET methods (Fig. 2.3C) coupled with groundwater piezometer data (Fig. 2.4B) suggest that seasonal fluctuations in shallow groundwater level (<2 m depth) influence landscape dynamics in the natural G-B tidal delta plain. This is demonstrated through a positive and significant relationship between deviations in groundwater level and surface elevation change ($r^2 = 0.76$, $P < 0.0001$; Fig. 2.6A). Similarly, a negative and significant relationship is observed between deviations in groundwater level and shallow subsidence and expansion ($r^2 = 0.33$, $P = 0.0077$; Fig. 2.6B). These seasonal relationships among groundwater level, surface elevation change, and shallow subsidence suggest that more frequent flooding during the monsoon promotes groundwater recharge and soil swelling (e.g., Harvey et al., 2006), contributing to surface elevation gain (Fig. 2.6A) and substrate expansion (Fig. 2.6B). Conversely, less frequent flooding coupled with enhanced evapotranspiration rates during the dry season (e.g., Brammer, 2004) leads to soil desiccation, shallow subsidence (Figs. 2.3C, 2.6B), and surface elevation loss (Fig. 2.6A). The swelling and shrinking of near-surface sediments in response to volumetric changes in pore-water is a well-documented phenomenon (e.g., Nuttle et al., 1990; Nuttle and Hemand, 1988; Whelan et al., 2005) that has been reported in other locations with seasonal climates. For instance, work in the mangrove forests of Everglades National Park, Florida, USA demonstrated that monthly changes in surface elevation were strongly correlated with coincident variations in groundwater level (Whelan et al., 2005).

It is also well recognized that clay mineralogy is a primary control on the shrink and swell potential of sediments and soils (e.g., Karathanasis and Hajek, 1985; Schafer and Singer, 1976). Sediments in southwest Bangladesh contain a clay mineral assemblage that is primarily composed of illite (~60%), with lesser amounts of smectite, chlorite, and kaolinite (~10-15%

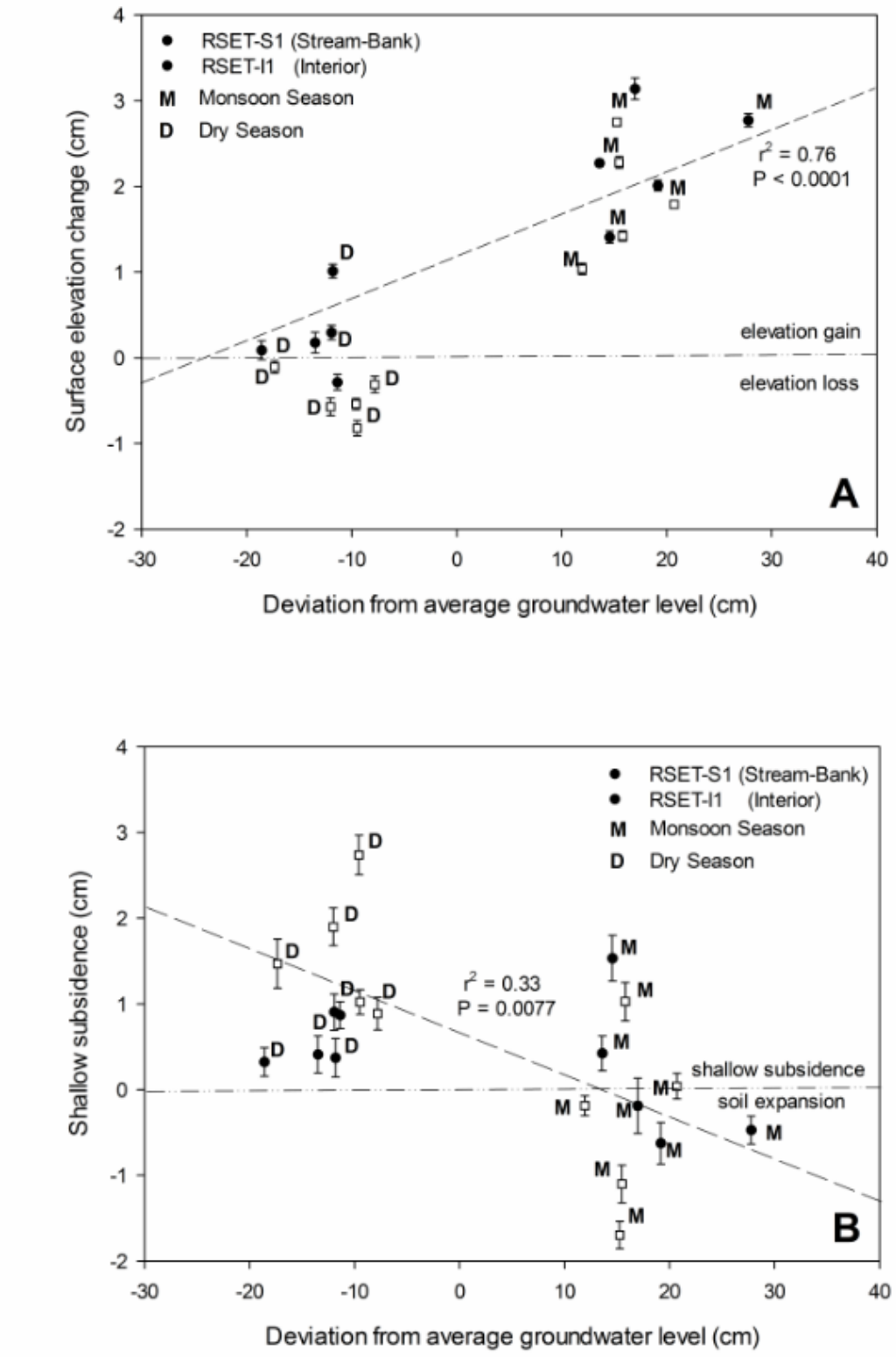

Fig. 2.6. Seasonal relationships between (A) surface elevation change and (B) shallow subsidence with normalized differences in groundwater level from RSET and piezometers located within the Sundarbans mangrove forest.

each, Allison et al., 2003). Among clay mineral suites, those with high illite and minor smectite components have a "moderate to high" shrink and swell potential (Nelson and Miller, 1997), which along with lowering of the groundwater table documented here (Figs. 2.4B, 2.6), may explain the pronounced seasonal differences of elevation change and sediment accretion within the Sundarbans (Figs. 2.3A, 2.3B, Table 2.2).

Previous laboratory and field studies in salt marshes of the Atlantic Coast, USA suggest that substrate compaction is strongly controlled by sediment organic content, wherein organic-rich sediments like peat are more compressible than inorganic sediments like detrital sand and silt (e.g., Knott et al., 1987; van Asselen et al., 2009). The surface sediments (i.e., 0-2 cm depth) of the Sundarbans mangrove forest are very low in organic content, ranging between 2.9 and 3.8% by mass (Rogers et al., 2013), and this trend continues to >1 m depth (Allison et al., 2003; Bomer et al., 2019). Based on these observations it follows that organic compaction should not compose a large proportion of the shallow subsidence. We thus postulate that in the case of the mineral-rich G-B tidal delta plain, bulk grain size and water and clay content of the shallow stratigraphy are more likely to control the magnitude of compaction. We also note it is likely that compaction-induced subsidence also occurs below the RSET benchmark where overburden pressure is greater (i.e., "deep subsidence," Cahoon et al., 1995), however, due to the depth limitations of RSET investigations, the relative contribution of deep subsidence is not quantified here (requires other methods such as GPS or stratigraphic age control, see Grall et al., 2018; Steckler et al., 2010). Recent geodetic reports have provided insights on total subsidence (i.e., shallow plus deep components) in the eastern part of the G-B delta, demonstrating that rates of

total subsidence range from 0 to 1.8 cm yr^{-1} (Higgins et al., 2014). In this study, rates of shallow subsidence across all locations ranged from 0.70 to 1.84 cm yr^{-1} (Table 2.1), which when compared to the rates of total subsidence from Higgins et al. (2014), suggests that the majority of compaction in this delta occurs in the uppermost ~10 to 20 m of the subsurface. This notion is consistent with the findings of Törnqvist et al. (2008), who show that in the Mississippi River Delta much of the subsidence results from the compaction of relatively shallow (~15 m depth), Holocene-age sediments.

2.5.3. Sea-level rise and landscape vulnerability

The long-term sustainability of mangrove forests and other low-lying coastal landscapes requires that gains in surface elevation must meet or exceed rates of sea-level rise (e.g., Woodroffe et al., 2016). Our data indicate that the natural G-B tidal delta plain is much less vulnerable to sea level-induced submergence than previously thought (e.g., Houghton, 2005; Loucks et al., 2010). We document that surface elevation gain at stream-bank (2.16 ± 0.26 cm yr^{-1}) *and* interior sites (1.32 ± 0.17 cm yr^{-1}) in the Sundarbans greatly outpaces the rate of relative sea-level rise (0.9 cm yr^{-1}) (Fig. 2.7). Furthermore, it seems apparent that relative sea-level rise plus the effects of tidal amplification (which combined = 1.2-1.6 cm yr^{-1}, hereafter referred to as "effective sea-level rise," *sensu* Pethick and Orford, 2013) is a more dominant control on the mangrove surface geomorphic evolution. The results of this study indicate that the surface elevation of the Sundarbans mangrove platform (both stream-bank and interior settings) is increasing in response to changes in the level of mean high water (MHW) instead of eustatic sea-level rise (Fig. 2.7). This finding highlights the resilience and adaptability of mangrove ecosystems to local environmental disturbances (e.g., Alongi, 2008), in this case to tidal amplification and associated increase in platform flooding from embankment-induced channel

constriction (Pethick and Orford, 2013). This adaptability mechanism is reflected in the geomorphic stability of the Sundarbans mangrove forest.

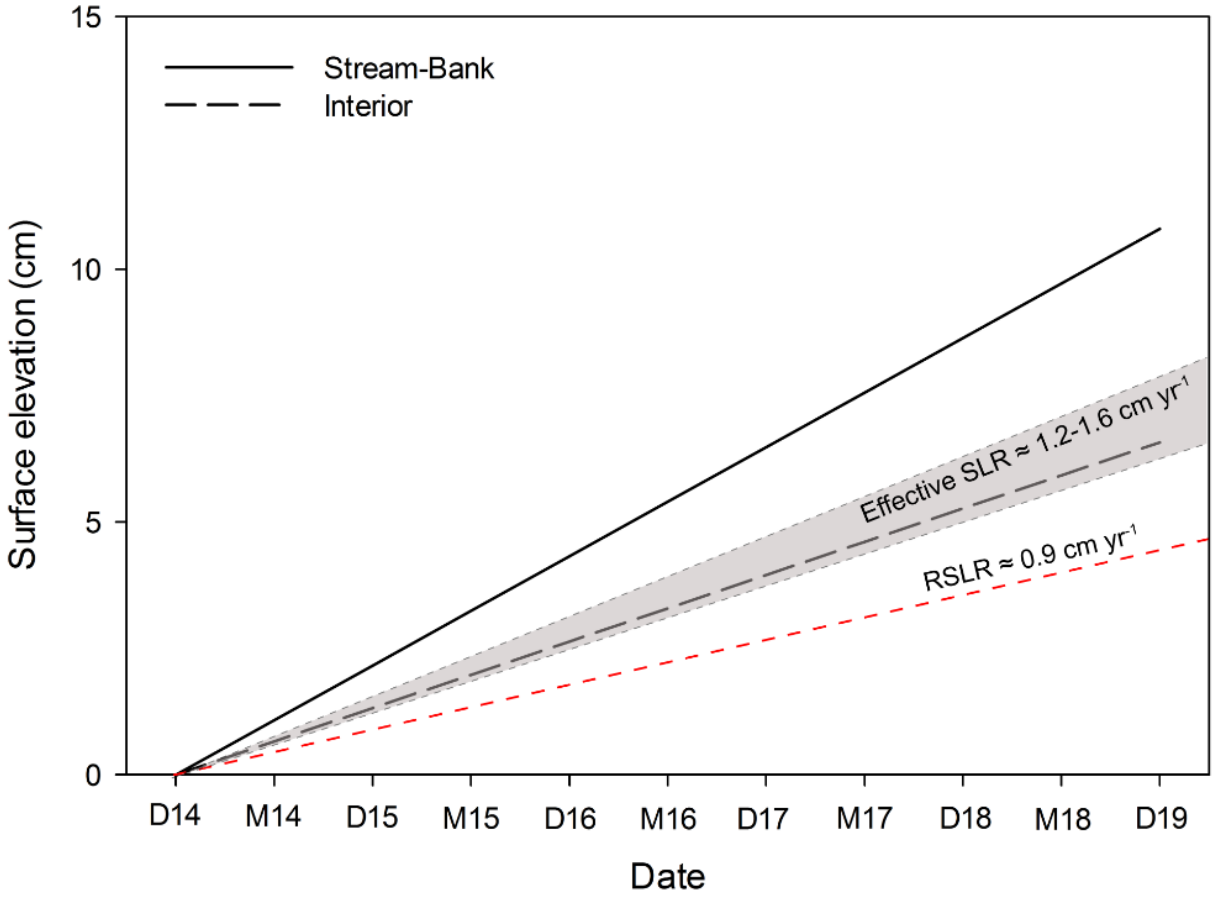

Fig. 2.7. Linear trajectories for surface elevation change at hydro-geomorphic settings compared to upper and lower estimates of sea-level rise: relative sea-level rise (RSLR) integrates the effects of eustatic sea-level rise and subsidence (Cazenave et al., 2008; Khan and Islam, 2008; Hanebuth et al., 2013; Grall et al., 2018) whereas effective sea-level rise includes the effects of RSLR plus tidal range amplification from embankment construction (Pethick and Orford, 2013). "D" and "M" refer to dry and monsoon seasons while the numbers correspond to the year (e.g., D14 = dry season of 2014).

For instance, remote sensing research across the Sundarbans indicates little conversion of interior mangrove platforms to open water over the past 30 years (Giri et al., 2007), most likely a result of effective sediment distribution through the interior of the tidal delta plain by smaller-order tidal creeks (Hale et al., *in press*; Rogers et al., 2013). These large-scale observations, along with

findings from the present study, contradict oversimplified models of land loss which put forth the notion that low elevation areas, such as the Sundarbans interior sites, passively submerge in response to rising sea levels (Houghton, 2005; Loucks et al., 2010).

Although the proceedings of this study represent an important first step in quantifying elevation and sedimentation dynamics in the Sundarbans and G-B tidal delta plain, we acknowledge that our results may not be representative of the entire Sundarbans mangrove forest. For example, changes in surface elevation near the Bay of Bengal may be less influenced by tidal amplification (quantified as 0.3 cm yr^{-1} in this area by Pethick and Orford, 2013) and more influenced by higher subsidence rates as a result of thicker sediment loading (quantified as 0.5 cm yr^{-1} in this area by Grall et al., 2018). Similarly, the western portion of the Sundarbans forest likely experiences less deposition as a result of the increased distance from the G-B river mouth (Flood et al., 2018). We stress that further research is necessary to constrain the spectrum of these parameters, and the resulting geomorphic expression, across the greater Sundarbans.

Although natural, unmodified areas of the G-B delta appear to be currently sustainable as presented here, major concerns for the long-term future of the delta are still present, particularly with respect to reductions in sediment supply from upstream sources. Over the next 30 years, India's National River Linking Project is expected to add 43 dams and 29 link canals to the country's infrastructure, leading to substantial downstream reductions in suspended sediment load for the Ganges and Brahmaputra rivers, estimated at 39-75% and 9-25%, respectively (Higgins et al., 2018). If such upstream blockages and associated reductions in sediment load are realized, aggradation rates would decrease delta-wide (Higgins et al., 2018), weakening the natural defense of the system to relative and effective sea-level rise, and ultimately render the G-B delta more vulnerable to the effects of global climate change. Additionally, the rate of eustatic

sea-level rise is expected to increase throughout the 21st century (IPCC, 2013), further compromising the adaptability of mangroves in the Sundarbans. Finally, it should be stressed that in the G-B tidal delta plain and possibly other coastal systems, *effective sea-level rise* is the main hydrodynamic parameter that places human livelihood at risk, given that the land surface relative to MHW is ultimately what dictates flood risk and associated damage to crops and infrastructure. Future studies should consider the range of anthropogenic practices involved and constrain the magnitude of their influence on depositional conditions to properly evaluate landscape evolution.

2.6. Conclusions

In the G-B tidal delta plain, surface elevation change is controlled by a variety of factors that occur both at the surface (e.g., sediment deposition, tidal flooding) and in the shallow subsurface (e.g., seasonal groundwater fluctuations, hydro-expansion and contraction of clay minerals, sediment compaction). Newly available inter-annual records of surface elevation, vertical accretion, and shallow subsidence in the G-B tidal delta plain reveal much needed insights on the sustainability of this region. In this study, we document that in the natural stream-bank and interior settings of the Sundarbans mangrove forest, which remain hydrologically connected to sediment-laden tidal waters, elevation gain is occurring at rates of 2.16 ± 0.26 cm yr^{-1} and 1.32 ± 0.17 cm yr^{-1}, respectively. These rates of elevation gain exceed that of relative sea-level rise (0.9 cm yr^{-1}) and more closely follow the range of effective sea-level rise (1.2-1.6 cm yr^{-1}, Pethick and Orford, 2013), suggesting that the natural land surface is maintaining equilibrium with changes in mean high water. Overall, the findings of this research highlight the resiliency and responsiveness of the natural G-B tidal delta plain to maintain positive surface elevation in the face of locally accelerated sea-level rise. However, the long-term fate of the delta

hinges upon the continued supply of sediments from upstream source areas. Future infrastructure projects that re-route water and sediment conveyance pathways away from the lower G-B delta increases the vulnerability of this low-lying coastal region to sea-level rise and submergence.

CHAPTER 3. BIOPHYSICAL PROCESS CONTROLS AND CARBON SEQUESTRATION POTENTIAL OF THE SUNDARBANS MANGROVE FOREST, SOUTHWEST BANGLADESH

3.1. Introduction

Mangroves forests, and the ecosystems that they foster, are among the most valuable ecological and economic resources on Earth. Mangroves confer a wide range of benefits that improve human livelihoods, including providing a source of food and timber (Bandaranayake, 1998), attenuating cyclone-induced storm surges (Danielsen, 2005; Das and Vincent, 2009), and promoting land building through sediment capture (Furukawa et al., 1997; Victor et al., 2004) and below-ground biological processes (Krauss et al., 2014; McKee, 2011; McKee et al., 2007). Additionally, mangroves and other coastal vegetation represent a significant sink for atmospheric CO_2 (Mcleod et al., 2011), and they will play a critical role in offsetting accelerated greenhouse gas emissions and resultant sea level rise in the 21st century (IPCC, 2013; Meinshausen et al., 2011). Despite the general recognition of these benefits, mangroves are in a state of rapid decline: the global areal extent of mangrove forests is decreasing at an average rate of 1% per year (FAO, 2007), and 40% of species are at risk of extinction (Polidoro et al., 2010). While deforestation contributes to the degradation of mangroves, existing research also identifies sea level rise as a primary threat to their survival (e.g., Ellison and Stoddart, 1991; Gilman et al., 2008), providing numerous examples of mangrove soil surfaces failing to keep pace with the combined effects of sea level rise and subsidence ("relative sea-level rise" e.g., Ellison, 1993; Krauss et al., 2010; Lovelock et al., 2011; Lovelock et al., 2015). Research efforts that quantify mangrove surface elevation dynamics in response to relative sea-level rise will be paramount for assessing the sustainability of these valuable ecosystems now and into the future.

Among studies that investigate the surface elevation dynamics and sustainability of mangrove settings, much focus has been placed on changes in the sediment profile extending from the ground surface to the depth of incompressible substrate (e.g., consolidated sand, limestone, volcanic rock), generally occurring between 5 and 15 meters belowground (e.g., Bomer et al., *in review*; Cahoon and Lynch, 1997; Krauss et al., 2010; Lovelock et al., 2011). In contrast, comparatively little attention has been given to the uppermost half-meter to meter of the sediment profile, termed the "live root zone" (LRZ), where biological processes have a relatively high influence on surface elevation change (Carter and Gregorich, 2008; McKee et al., 2007; Rogers et al., 2005). The LRZ, owing to its relatively shallow position in the subsurface, is particularly sensitive to environmental disturbances that alter surface elevation. For instance, Cahoon et al. (2003) found that mangrove mortality associated with the landfall of Hurricane Mitch caused widespread root decomposition and peat collapse, ultimately resulting in increased shallow subsidence and losses in surface elevation as much as 1.1 cm yr^{-1}. Even subtle changes in surface elevation can dramatically change the frequency, duration, and depth of inundation by tidal waters (Hale et al., *in press*; Marion et al., 2009), which can lead to intolerable levels of root submergence and tree death (Krauss et al., 2014).

Within the LRZ is a site-specific mixture of mineral matter, pore-water and gases, and organic matter that includes roots, rhizomes, leaf litter, living organisms, and fine particulate organic material (e.g., Mitchell and Soga, 2005). Compared to terrestrial plants, mangroves are commonly cited to sequester proportionally more carbon belowground (i.e., in the LRZ) than aboveground (e.g., Alongi, 2012; Donato et al., 2011; Fourqurean et al., 2012), and worldwide estimates of the mangrove carbon burial often treat the storage ability of different mangrove ecosystems to be equivalent (Duarte et al., 2004; Twilley et al., 1992). This, however, is an

oversimplified approach that discounts the heterogeneity of sediment texture and composition in mangrove ecosystems (Rovai et al., 2018). While peat and organic-rich substrates are common in mangrove settings and well represented in the literature (Cahoon et al., 2003; Cameron and Palmer, 1995; Krauss et al., 2010; McKee, 2011; McKee et al., 2007; Vegas-Vilarrúbia et al., 2010; Whelan et al., 2005), examples of mineral-rich soils in mangrove environments also exist (Rogers et al., 2013; Swales et al., 2015).

Previous research stresses the importance of considering both physical and biological processes to explain changes in surface elevation of the LRZ (e.g., Krauss et al., 2014). Yet, there is currently a paucity of studies that link above-ground physical data (e.g., surface elevation change, hydroperiod) to below-ground process controls (e.g., seasonal changes in pore-water abundance, oxidation-reduction conditions) in the LRZ. In this study, we investigate the relative contributions of sedimentary and biotic parameters on controlling surface equilibrium of the LRZ, using the Sundarbans mangrove forest (SMF) of southwest Bangladesh as a study area. Specifically, we compare surface elevation change to: (1) oxidation-reduction potential, (2) pore-water content, and (3) sediment grain size (Fig. 3.1). Another key objective of the study is to evaluate the below-ground carbon sequestration potential of the SMF and compare our findings with other mangrove forests across the globe. The proceedings of this research provide new information on the bio-physical dynamics of the LRZ and have implications for the sustainability and carbon storage potential of mangrove ecosystems worldwide.

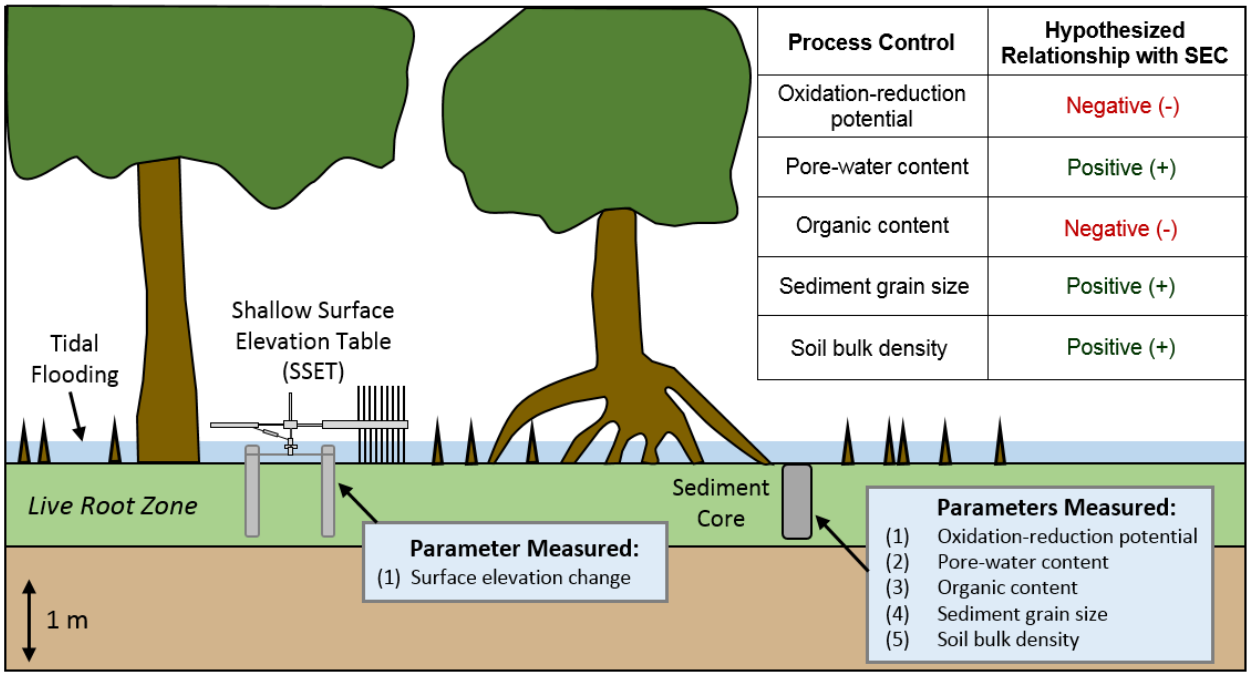

Fig. 3.1. Field techniques employed in this study and hypothesized relationships between process controls and surface elevation change (SEC) of the live root zone.

3.2. Study area

The Sundarbans mangrove forest (SMF), encompassing ~10,000 km^2 in coastal Bangladesh and India, represents the largest contiguous mangrove forest on Earth (e.g., Iftekhar and Saenger, 2008). The dominant mangrove species and namesake of the forest is the endangered Sundari (*Heritiera fomes*) (Ellison et al., 2000). Other species identified here include: Bain (*Avicennia marina*), Gewa (*Excoecaria agallocha*), and Kankra (*Bruguiera decandra*). Similar to other mangrove forests, the areal extent of the SMF has changed in response to the level of human activity. In the 18th century, the SMF was roughly twice its present-day size; the northern half of the forest was subsequently cleared to expand cultivated land (Ahmad, 1968; Allison, 1998). In more recent times, however, the forest has been largely robust, exhibiting 1.2% net land loss between 1973 and 2000 (Giri et al., 2007) and <2% infilled tidal channels since the 1960s (C. Wilson et al., 2017). The stability of the SMF can be attributed to preservation measures taken by the Bangladesh government establishing the forest as a

UNESCO World Heritage Site in 1997 (e.g., Rahman, 2000), as well as the efficient dispersal of fluvial- and marine-sourced sediments by tides throughout the mangrove islands (Hale et al., *in press*; Rogers et al., 2013).

The focus area for this study is located in the northernmost reaches of the SMF, covering ~20 km^2 of intertidal mangrove forest, mudflats, and tidal channels (Fig. 3.2). Water and sediments are distributed to the interior of the forest by tidal flooding of the Suterkhali River and its hierarchy of channels (~100-200 m wide, ~5-10 m deep; Fig. 3.2). The forest floor exhibits little topographic change apart from a network of primary creeks (~1-3 m wide, ~0.5 m deep) that accommodate the movement of tidal waters. Small-scale surface perturbations on the forest floor include pneumatophore roots, saplings, and mud crab (*Scylla serrata*) mounds. The frequency and duration of platform flooding is seasonally dependent, with higher water levels and ~70% of the annual flooding occurring during the summer monsoon season (June-September; Bomer et al., *in review*). During the monsoon, water in the local tidal channels is fresh (Shaha and Cho, 2016) and exhibits elevated levels of suspended sediment concentration (>1 g/L; Hale et al., *in press*). In the dry season (December-April), these tidal channel waters demonstrate higher salinity (5 - 25 ppt; Shaha and Cho, 2016) and lower suspended sediment concentration (0.1 – 0.6 g/L; Hale et al., *in press*). This seasonal pattern also applies to water that floods the forest floor here, though suspended sediment concentration is uniformly lower (Hale et al., *in press*), presumably due to particle settling and trapping by vegetation (e.g., Furukawa et al., 1997). In contrast to the human cultivated landscape to the north, tidal channels in the SMF are not artificially embanked. Hence, this region provides a unique opportunity to investigate surface elevation change and belowground processes of the LRZ under unimpeded and natural conditions.

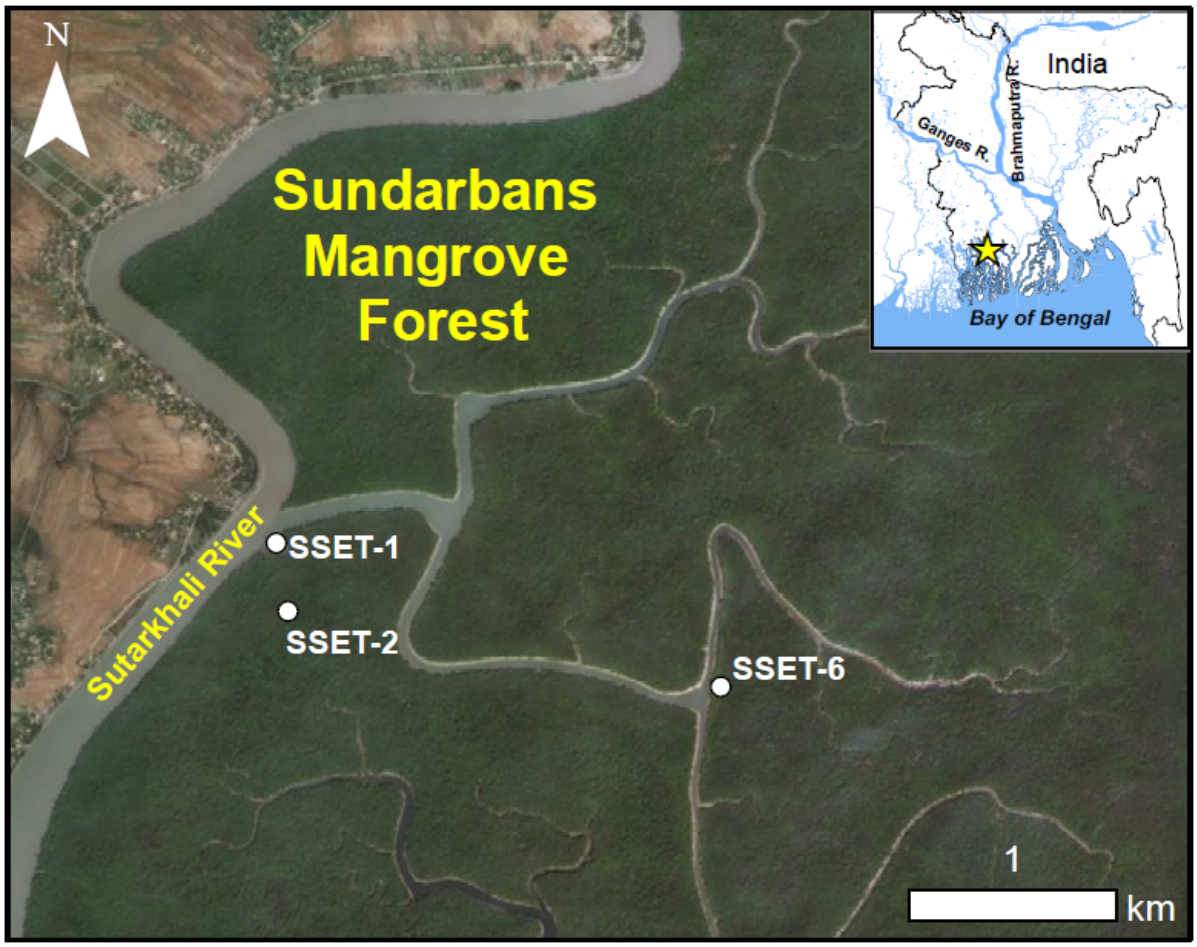

Fig. 3.2. Map of the study area with respect to greater Bangladesh and locations of Shallow Surface Elevation Table (SSET) stations. Shallow cores (depth up to 1 m) were taken seasonally within close proximity (<10 m away) of each station.

3.3. Methods

3.3.1. Near-surface elevation dynamics

Seasonal and inter-annual elevation change of the LRZ was recorded using shallow surface elevation table (SSET) instruments, a variant of the deeper rod surface elevation table (RSET; Cahoon et al., 2002) specifically designed to measure elevation dynamics to a benchmark depth of 0.75 m (Fig. 3.1). SSET's were installed in different hydrodynamic settings: SSET-1 is situated adjacent to the Suterkhali River, a first-order tidal channel; SSET-2 is located in the interior of the mangrove platform, distal (>100 m) from the major Suterkhali tidal channel; and SSET-6 is located adjacent to a smaller, second-order tidal channel (Fig. 3.2). SSET-1 and

SSET-2 were installed in October 2015 while SSET-6 was installed in May 2016. Data collection from all SSET's occurred approximately every six months.

3.3.2. Oxidation-reduction potential

To assess changes in oxidation-reduction potential (ORP) with depth, cores up to 1 m in length were collected in the vicinity of SSET locations using a 6-cm diameter half-cylinder auger (Fig. 3.1). Large mangrove pneumatophores and belowground roots were avoided during coring to obtain an undisturbed sediment profile and minimize compaction. Immediately after extraction, ORP measurements were taken on each core at 10-cm intervals using a handheld gel electrolyte ORP electrode with a platinum sensing pin (*Hanna Instruments HI3620D*). For calibration purposes, the electrode was soaked in pre-treatment solution for 15 minutes prior to analysis. ORP measurements were taken by inserting the electrode 2 cm into the sediment interface until the reading reached equilibrium. The electrode was rinsed with water following each measurement, and care was taken to shield core sediments from direct sunlight during data collection. Measurements were performed during two monsoon and dry season field campaigns to assess seasonal differences in ORP.

3.3.3. Soil pore-water content, organic content, and bulk density

Following ORP measurements, 2-cm thick subsamples were taken from cores every 10 cm and packed into air-tight bags. Upon return to the lab, wet sediment samples were weighed and placed in a drying oven at 60°C for at least 72 hours to attain a constant dry mass. The mass of the dehydrated sediment was recorded and compared to the wet weight using equation (1) to calculate the percent water content, where m_d and m_w refer to the dry and wet sediment mass, respectively.

$$((m_w - m_d) / (m_w)) * 100 \quad (1)$$

Soil total carbon (TC) and total organic carbon (TOC) were quantified by dry combustion in an induction furnace coupled to a Costech 1040 CHN Analyzer (Louisiana State University Wetland Biogeochemistry Laboratory). For TC analyses, 5 to 10 mg of dehydrated and homogenized sediment was sealed in tin capsules and combusted at ~1350 °C for 5 to 7 minutes (Schumacher, 2002). A similar approach was taken for TOC analyses, except sediments were fumigated overnight with HCl vapor before combustion to remove inorganic carbonate minerals (e.g., calcite, dolomite) (Harris et al., 2001). Soil organic matter was also assessed by the semi-quantitative loss-on-ignition (LOI) method for comparison (Heiri et al., 2001). Briefly, dehydrated sediments were homogenized using a mortar and pestle and combusted in a muffle furnace at 550°C for 5 hours to yield weight LOI. Percent organic matter was quantified following equation (2), where m_b and m_s refer to the biomass and pre-burn sample mass, respectively.

$$(m_b/m_s) * 100 \quad (2)$$

Dry soil bulk density was calculated by dividing the dry weight of each sediment sample by the volume of the sample (V = 61.33 cm^3). Values of soil bulk density were then multiplied by % TOC to obtain soil C density. C sequestration rates were calculated as the product of soil C density and average sediment accretion rates from Allison and Kepple (2001) and Bomer et al., (*in review*).

3.3.4. Granulometry

Grain size analysis was conducted at 10-cm intervals for all cores (Fig. 3.1). Wet sediment aliquots of ~2 g were placed in test tubes and stirred with 2 ml of 30% hydrogen peroxide (H_2O_2) to remove fine organic matter. Following digestion, 15 ml of 0.05% sodium metaphosphate (NaH_2PO_4) was added to each solution, stirred to de-flocculate clay particles, and

poured through an 850 μm sieve to remove large organic debris (e.g., shells, crab claws). Samples were then ultrasonically dispersed in a Beckman-Coulter laser diffraction particle size analyzer (Model LS 13 320) to calculate the relative abundance of grain sizes between 0.4 and 850 μm. The volumetric abundance of cohesive sediments for a particular sample was taken as the percentage sum of particle sizes <20 μm (Mehta, 1989).

3.3.5. Statistical analyses

Linear regression models were performed on the trends of dependent variables (e.g., pore-water content, surface elevation change, grain size) to ascertain whether the relationships between variables were statistically significant. Seasonal differences of process controls, including surface elevation change, water content, organic content, and oxidation-reduction potential, were tested for statistical significance using a two-sided t-test assuming equal variances (*sensu* Lovelock et al., 2011). Following the procedure of (Krauss et al., 2010), a significance level of $\alpha = 0.05$ was compared to the P-value to accept or reject the null hypothesis.

3.4. Results

3.4.1. Near-surface elevation dynamics

Inter-annual trends in surface elevation change of the LRZ demonstrated positive elevation change through time at all SSET locations (Table 3.1; Fig. 3.3). The annual rate of elevation change was similar at SSET-1 and SSET-2 (mean ± standard error = 2.06 ± 0.17 cm yr^{-1}) but higher at SSET-6 (3.14 ± 0.46 cm yr^{-1}, Table 3.1). Two distinct signatures in seasonal elevation change were identified: (1) seasonal step-wise increase or (2) non-seasonal near-linear increase (Fig. 3.3). SSET-1 and 2 exhibit the former trend and are characterized by greater elevation gain following the summer monsoon season (2.06 ± 0.09 cm) as compared to after the dry season (0.26 ± 0.08 cm) (Table 3.1; Fig. 3.3). Differences in seasonal elevation change were

statistically significant at SSET-1 (t-ratio = 9.01; P < 0.001) and SSET-2 (t-ratio = 3.29; P = 0.022). Conversely, SSET-6 does not display any evidence of seasonal variability in elevation change (t-ratio = 0.42; P > 0.05), exhibiting similar values after the monsoon (1.70 ± 0.22 cm) and dry seasons (1.44 ± 0.24 cm) (Table 3.1; Fig 3.3).

Table 3.1. Seasonal and inter-annual rates (± standard error) of surface elevation change (SEC) in the live root zone.

Station	Record (yr)	Mean Annual SEC (cm yr^{-1})	Mean Monsoon Season SEC (cm)	Mean Dry Season SEC (cm)
SSET-1	3.5	2.16 ± 0.19	2.22 ± 0.15	0.23 ± 0.08
SSET-2	3.5	1.95 ± 0.14	1.89 ± 0.05	0.29 ± 0.08
SSET-6	3.0	3.14 ± 0.46	1.70 ± 0.22	1.44 ± 0.24

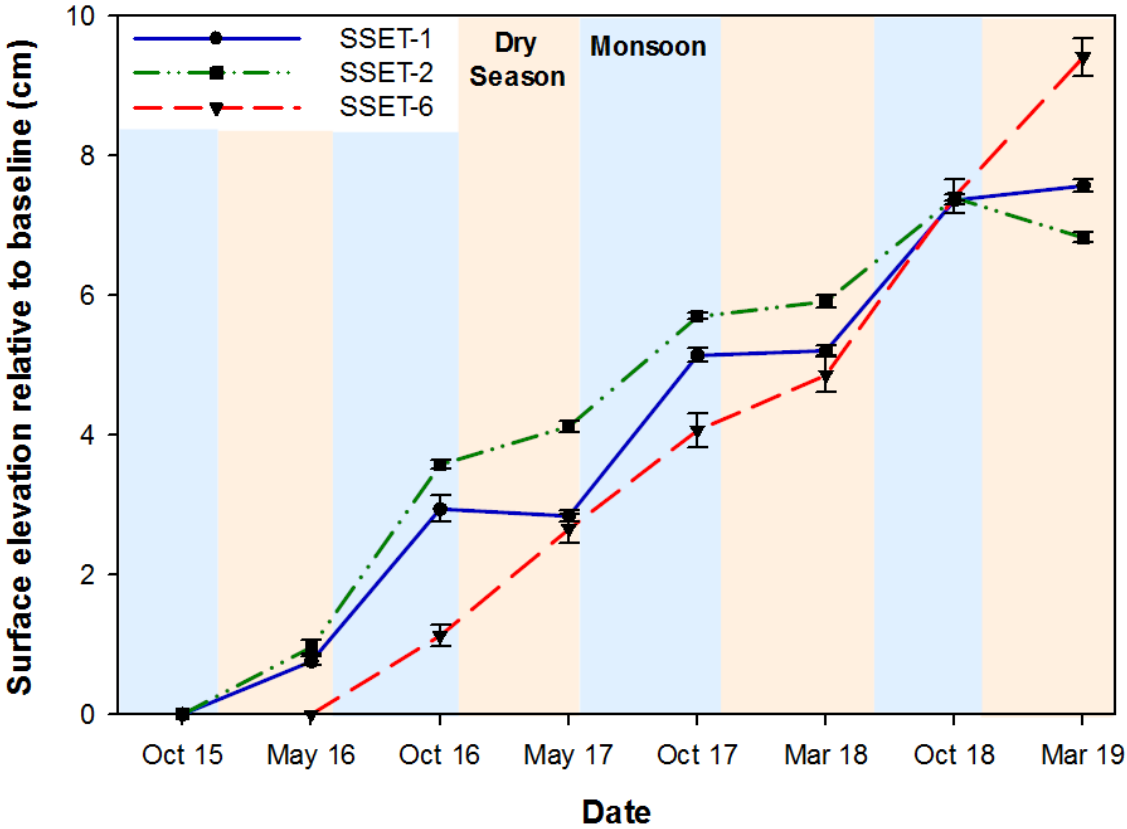

Fig. 3.3. Inter-annual change in surface elevation of the live root zone. Values represent longitudinal change relative to the baseline measurement. Error bars are the standard error for all measurements.

3.4.2. Oxidation-reduction potential

ORP measurements from sediment cores varied considerably depending on season, core location, and core depth, showing an overall range of -156 to +158 mV (Fig. 3.4). Cores taken during the monsoon season demonstrated uniformly reduced conditions (i.e., <0 mV) throughout the sediment profile, ranging between -156 and -17 mV among all cores (Fig. 3.4). ORP trends for cores at SSET-1 and 6 exhibited minimal variance with depth (mean = -140 mV) (Fig. 3.4). SSET-2, on the other hand, displayed a much more reduced condition at the surface (Eh = -156 mV, peaking at -17 mV) followed by more reducing conditions to 90 cm depth (Eh decreasing to -133 mV) (Fig. 3.4). On the whole, soil conditions were more oxidized in the dry season relative to the monsoon season, ranging between -140 and +158 mV among all cores (Fig. 3.4). The most notable down-core trend in dry season ORP is that the uppermost 30 cm of the soil profile was substantially more oxidized than depths below 30 cm (mean = -4mV compared to -105 mV, respectively) (Fig. 3.4). Apart from this trend, ORP measurements below 30 cm were generally invariant with depth in the dry season (Fig. 3.4). Significant seasonal differences in ORP were observed at SSET-1 (t-ratio = 2.52; P = 0.0227) and SSET-2 (t-ratio = 2.29; P = 0.0341) locations, but not at SSET-6 (t-ratio = 1.45; P > 0.05).

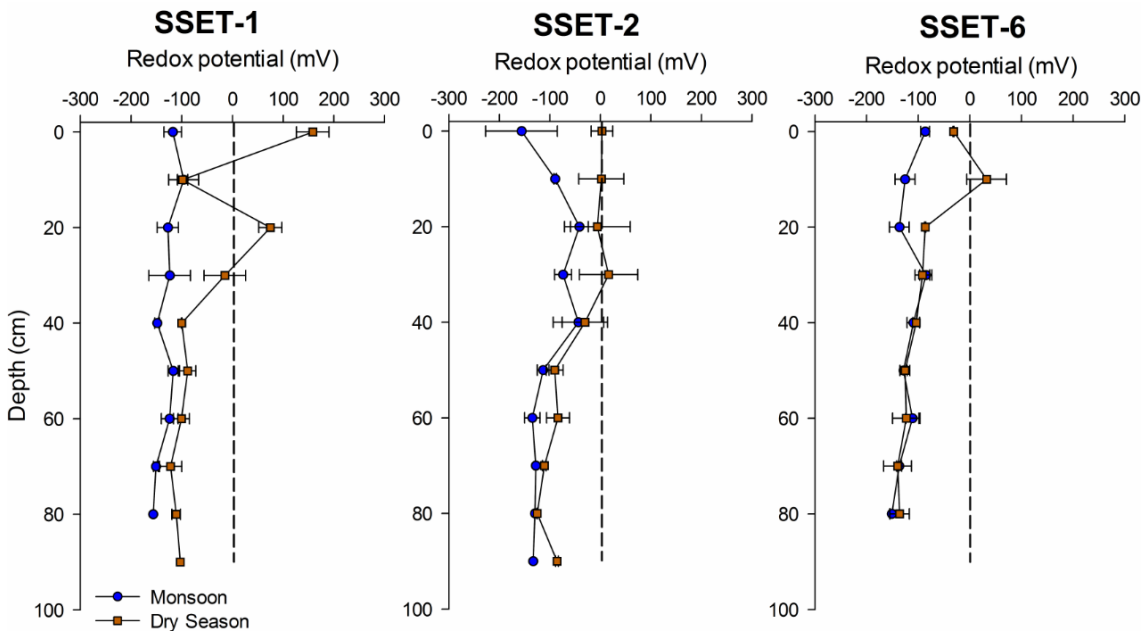

Fig. 3.4. Seasonal oxidation-reduction potential of shallow core sediments. Each data point represents the average measurement from two field seasons. Error bars correspond to the standard error of the measurement components. The dashed vertical line indicates the boundary between reduced (negative mV) and oxidized (positive mV) soil conditions. Note that soils are generally reduced with the exception of the upper ~20-30 cm in the dry season.

3.4.3. Soil pore-water content, organic content, and bulk density

Pore-water content in the LRZ varied primarily based on season, and to a lesser extent, core location and depth (Fig. 3.5). Seasonal differences in pore-water abundance were found to be significant in cores taken near SSET-1 (t-ratio = 9.39; $P < 0.0001$) and SSET-2 (t-ratio = 11.9; $P < 0.0001$). For these locations, the average pore-water content during the monsoon and dry seasons were 33.4% and 26.1%, respectively. However, seasonal variability in pore-water content is not evident for cores taken near SSET-6 (t-ratio = 1.73; $P > 0.05$). Here, average pore-water content during the monsoon and dry seasons were roughly equivalent at 28.4% and 26.7%, respectively. Trends in down-core water content were not seen in any of the cores apart from a slight increase in pore-water with depth for cores taken near SSET-6 during the monsoon season (Fig. 3.5).

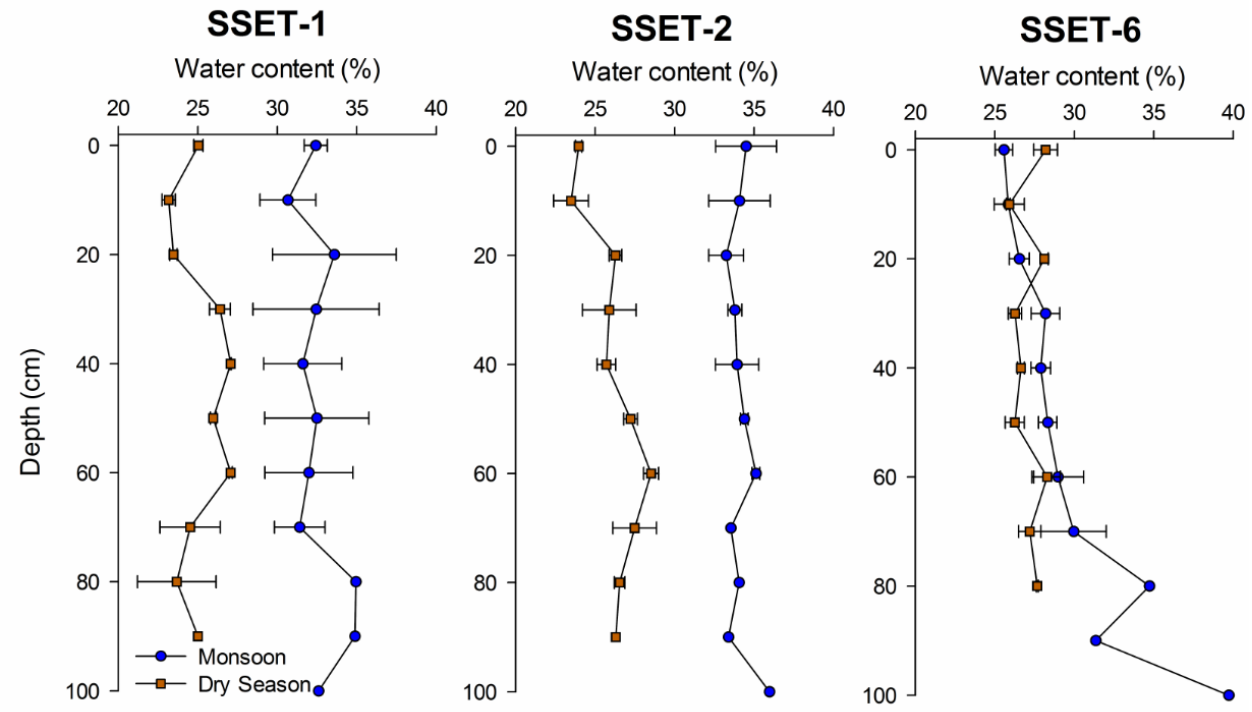

Fig. 3.5. Seasonal pore-water content of shallow core sediments. Each data point represents the average measurement from two field seasons. Error bars correspond to the standard error of the measurement components. Note that seasonal differences are present at SSET-1 and SSET-2, but not at SSET-6.

TC and TOC analyses demonstrate uniformly low organic matter content throughout the shallow subsurface, averaging 1.2 ± 0.1% and 0.9 ± 0.1%, respectively, among all samples (n = 56; Figs. 3.6A, 3.6B). No evident down-core trends were observed, and no significant differences in TC or TOC values existed among the coring locations. Average TOC values among all cores were 23.6% lower than average TC values, indicating the presence of inorganic carbon in SMF soils. Organic matter content as measured by LOI was higher than TC and TOC values but still generally low at all locations, ranging from 3.7% to 6.5% (Fig. 3.6C). Dry bulk density of the shallow subsurface ranges from 0.6 to 1.0 g cm^{-3}, with an average value of 0.81 ± 0.08 g cm^{-3}. Bulk density trends are invariant with depth at all of the core locations (Fig. 3.6D).

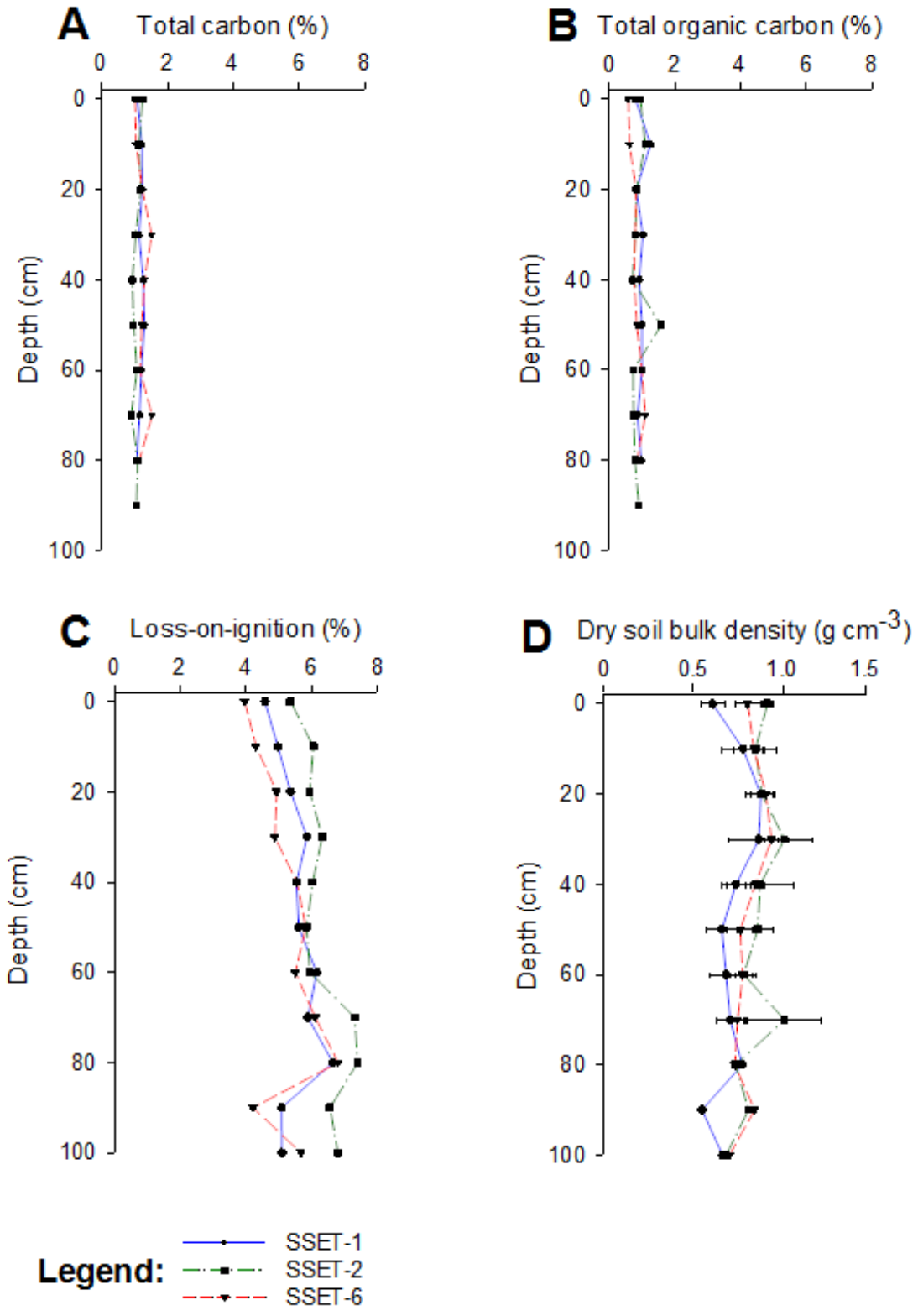

Fig. 3.6. Down-core changes in soil (A) total carbon, (B) total organic carbon, (C) loss-on-ignition, and (D) dry bulk density. Note the change in scale for dry bulk density relative to the other graphs.

3.4.4. Granulometry

Grain size analysis of sediments in the LRZ illustrate that the volumetric abundance of cohesive sediments (defined as <20 µm in particle diameter, Mehta, 1989) varies depending on core location and depth (Fig. 3.7). Cores at SSET-2, situated relatively deep in the forest and distal from tidal waterways (Fig. 3.1), exhibited the greatest abundance of cohesive sediments (54.0 ± 1.3%). Cores at SSET-1, located proximal to a tidal channel (Fig. 3.1), display lower abundances of cohesive sediments (45.0 ± 1.3%). Cores at SSET-6, also proximal to a tidal channel (Fig. 3.1), display relatively low abundances of cohesive sediments (37.9 ± 1.1%).

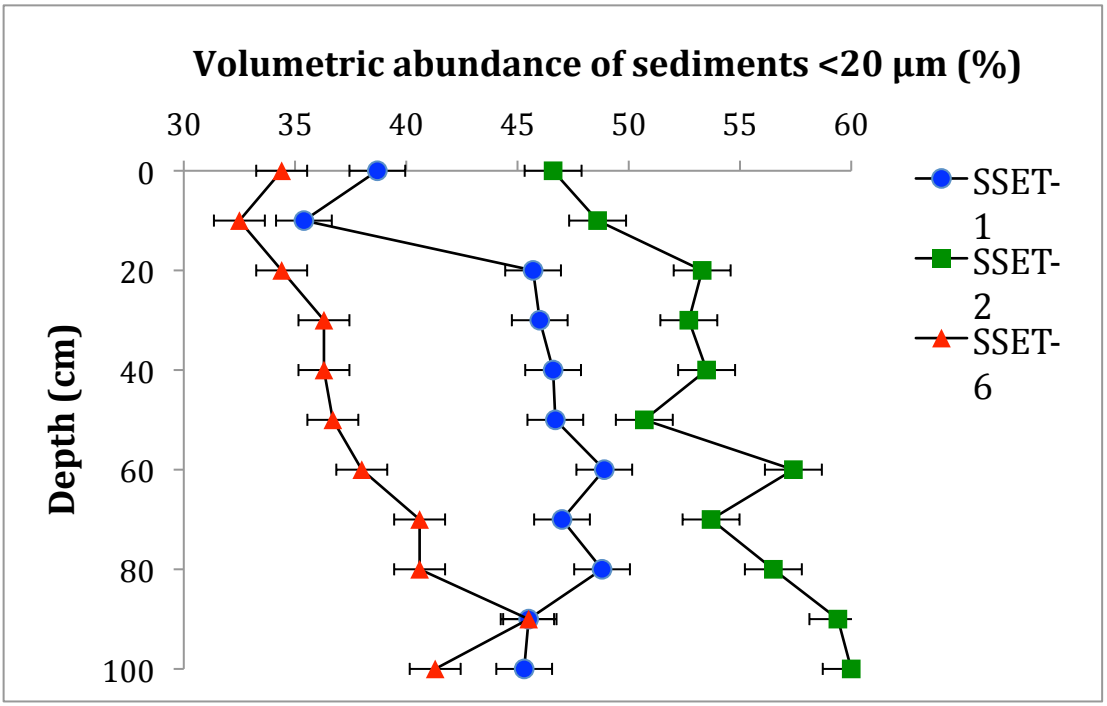

Fig. 3.7. Granulometry of sediment cores taken near respective SSET stations. Inset bar graph illustrates the volumetric abundance of cohesive sediments, taken to be particles finer than 20 µm (Mehta, 1989). Note that all cores exhibit a slight coarsening upward succession of median grain size.

3.5. Discussion

3.5.1. Effects of below-ground process controls on surface elevation change

Studies reporting the relative importance of subsurface processes on changes in surface equilibrium are uncommon but vital for understanding how mangrove forests and other coastal

ecosystems will adjust to environmental disturbances, like locally accelerated sea-level rise (Pethick and Orford, 2013). Our results indicate that seasonal changes in soil pore-water storage and oxidation-reduction potential, as well as spatial differences in sediment texture, all influence elevation dynamics in the Sundarbans mangrove forest (SMF; Fig. 3.8). For example, seasonal soil pore-water content exhibits a positive and significant relationship with changes in surface elevation of the LRZ ($r^2 = 0.77$, $P = 0.0218$, Fig. 3.8A). Greater soil pore-water storage during the wet season (Figs. 3.5, 3.8A) likely reflects increased platform hydroperiod (Bomer et al., *in review*) and infiltration from monsoonal rainfall (BMD, 2016). The combination of these factors raises the groundwater table and saturates the substrate, ultimately causing elevation gain via soil swelling (i.e., "dilation water storage," Cahoon et al., 2011; Nuttle et al., 1990). Conversely, decreased soil pore-water content during the dry season (Figs. 3.5, 3.8A) is caused by evapotranspiration (Brammer, 2004) and lowering of the water table (by up to 1 m; Bomer et al., *in review*), contributing to less elevation gain or even elevation loss (Fig. 3.3, Table 3.1). These trends did not apply to all locations, however, as SSET-6 exhibited minimal changes in seasonal pore-water content (Figs. 3.5, 3.8A). This may be due to differences in soil texture: SSET-6 contains a lower abundance of cohesive sediments (<40%) and therefore may have better soil drainage in comparison to SSET-1 and SSET-2 sites (Fig. 3.7). Seasonal expansion and contraction of the shallow subsurface due to fluctuations in pore-water content and groundwater level have been observed elsewhere, notably in the wetlands of the Florida Everglades (Whelan et al., 2005) and southeast Australia (Rogers et al., 2005; Rogers and Saintilan, 2008), however this is the first study to document this in the SMF.

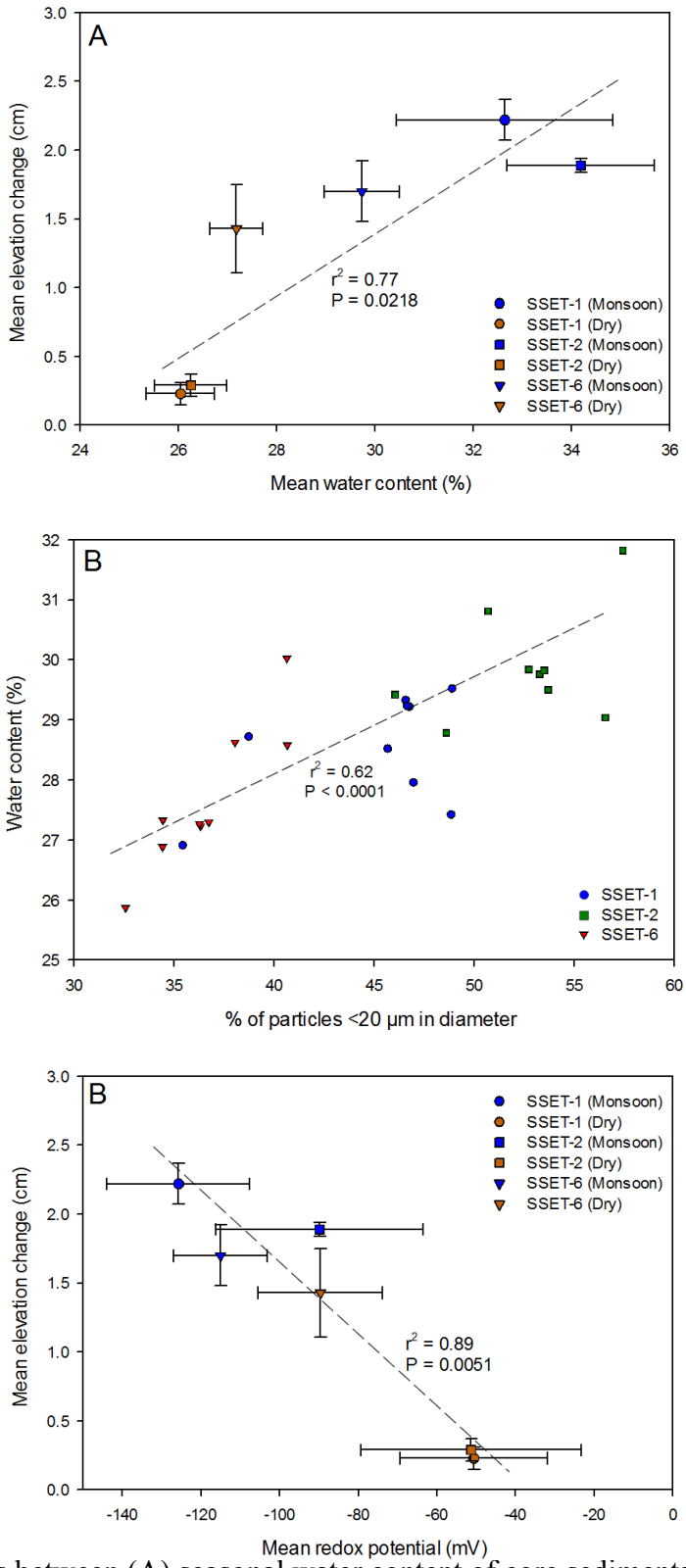

Fig. 3.8. Relationships between (A) seasonal water content of core sediments and elevation change, (B) volumetric abundance of cohesive sediment and water content, and (C) seasonal oxidation-reduction potential and elevation change. Error bars correspond to the standard error for all associated measurements.

Rogers and Saintilan (2008) found in the mangrove forests of Homebush Bay, Australia, that incremental changes in surface elevation over a four-month period were strongly correlated to groundwater depth, which in turn was influenced by the magnitude of monthly precipitation. It follows that locations with seasonal precipitation regimes are more likely to display marked seasonal differences in surface elevation change. In southwest Bangladesh, ~80% of the annual rainfall occurs between May and September (BMD, 2016), supporting the idea that seasonal variability in pore-water storage forms a strong control on local shallow surface elevation change. This appears to be evident at some locations (e.g. SSET-1 and -2) but not all (SSET-6).

Another parameter that appears to influence shallow elevation dynamics is sediment grain size and, more specifically, the abundance of clay minerals and other cohesive sediments capable of volumetric change (e.g., Boivin et al., 2004). Although the soil pore matrix hosts a large proportion of groundwater, a significant positive relationship ($r^2 = 0.62$, $P < 0.0001$) was observed between the abundance of cohesive sediment (<20 μm; Mehta, 1989) and average pore-water content (Fig. 3.8B), suggesting accommodation of water in the mineral structure of clays and other fine-grained particles (e.g., Fredlund et al., 2002; Gupta and Larson, 1979). The potential for soils to exhibit shrink-swell dynamics, and therefore impact shallow elevation change, depends on the local clay assemblage, as certain clay minerals (e.g., smectite and illite) are more prone to hydro-expansion and contraction than others (e.g., kaolinite and chlorite) (Mitchell and Soga, 2005). Allison et al. (2003) showed that the soils of the SMF are dominantly composed of illite (~60%) with smaller and roughly equivalent proportions of smectite, kaolinite, and chlorite (10-15% each). Given that illite and smectite together account for >70% of the total clay assemblage, the soils of the SMF are likely to exhibit moderate to high shrink-swell characteristics (Mitchell and Soga, 2005). Areas with a locally high abundance of fine-grained

sediments in the LRZ are therefore more likely to exhibit seasonal fluctuations in surface elevation and pore-water content, as is observed at SSET-1 and 2 (Figs. 3.3, 3.5). The relatively low abundance of cohesive sediments at SSET-6 (<40%) may explain why this location does not display seasonal differences in surface elevation change (Fig. 3.3; Table 3.1).

Hydroedaphic conditions, including soil redox potential, have long been recognized as an important control on the physicochemical composition of soils, especially with respect to the preservation or decomposition of organic matter (e.g., Brinson et al., 1981; McKee, 2011; Middleton and McKee, 2001). In general, vascular plant tissue is less likely to be preserved under aerobic soil conditions, as high oxygen levels enhance respiration and microbial activity responsible for the breakdown of lignin and other structural polymers (e.g., Kristensen et al., 2008). Measurements of soil ORP are thus pertinent for assessing changes in surface elevation as oxidized conditions facilitate the degradation of organic matter (e.g., roots, pneumatophores, buried litterfall) and can lead to compaction-induced shallow subsidence (e.g., Cahoon et al., 2006, 2003; Krauss et al., 2014; McIvor et al., 2013). In this study, oxidation of the uppermost ~30 cm of the soil profile was observed at all SSET locations during the dry season (Fig. 3.4) and likely occurs in response to reduced hydroperiods and lowering of the groundwater table (Bomer et al., *in review*). Mean seasonal ORP demonstrates a negative and significant relationship with seasonal shallow elevation change (r^2 = 0.89, P = 0.0051, Fig. 3.8C), suggesting that enhanced soil aeration contributes to surface elevation loss via degradation and remineralization of dead biomass. Seasonal changes in ORP vary depending on location: soils at SSET-1 and SSET-2 exhibit similar and highly seasonal differences in ORP while those at SSET-6 demonstrate comparatively little seasonal change (Figs. 3.4, 3.8C). Similar to pore-water storage, these site-specific responses may reflect differences in hydraulic conductivity, which is

directly proportional to the square of sediment grain size (Boadu, 2000). Alternatively, a different parameter, like mangrove root production and density, may explain these trends (e.g., McKee, 2011). More studies in the SMF are needed to constrain the spatial variability of seasonal ORP and provide insights on the processes that control these relationships.

Dry bulk density values of the shallow subsurface in this study (mean = 0.81 g cm^{-3}, Fig. 3.6D) are considerably higher than those reported for other Indo-Pacific mangrove soils (mean = 0.44 g/cm^{-3}, Donato et al., 2011), reflecting the preponderance of relatively dense mineral matter and the scarcity of organic matter in the SMF soil profile (Fig. 3.6A-C). High soil bulk density may facilitate the maintenance of surface elevation as clastic sediments are less compressible than organic matter and therefore incur less compaction-induced subsidence with burial (Bird et al., 2004; van Asselen et al., 2009). Direct observational compaction data is sparse, but it is widely thought that most compaction in wetland soils occurs in the upper 1-2 meters of the soil profile (e.g., Meckel et al., 2006; Törnqvist et al., 2008), as measured here with SSET's and core data. With regard to compositional differences, numerical forward models suggest that stratigraphic profiles containing mainly peat compact and subside much more readily than those composed exclusively of silts and sands (Meckel et al., 2007). Large differences in bulk density within stratigraphic components (e.g. sand overlying peat) were also found to accelerate rates of compaction and subsidence (Meckel et al., 2007; Higgins et al. 2014). This does not apply to the SMF system, given its generally homogeneous sediment character (median grain size = 20-30 μm; organic content = 1-2%), but may be relevant to oceanic mangrove settings, where organic-rich peat is periodically blanketed with offshore sediments delivered by large storm events (e.g., Victor et al., 2006).

Comparisons between rates of shallow surface elevation change observed here (Fig. 3.3, Table 3.1) and sediment accretion in this system (Bomer et al., *in review*) indicate that ~70% of the shallow elevation dynamics can be explained by sediment deposition alone. However, the subsurface parameters investigated in this study (e.g., pore-water content, redox potential, sediment texture) influence shallow surface elevation change up to 30%. While this is not wholly unexpected given that surficial processes generally govern elevation change in sediment-rich, alluvial mangrove environments while subsurface processes play a more prominent role in sediment-deficient, oceanic mangrove systems (e.g., Cahoon et al., 2006; Krauss et al., 2014; McIvor et al., 2013), we argue that research initiatives aimed at identifying belowground influences on surface elevation change in alluvial mangrove forests are nonetheless important due to site-specific differences that exist both at regional and global scales.

3.5.2. Carbon sequestration potential of the SMF

The effectiveness of mangrove forests, along with other ecosystems, to function as a carbon sink hinges upon the preservation of organic material during and after burial (e.g., Lützow et al., 2006). Total organic carbon (TOC) of SMF soils averaged 0.9 ± 0.1% among all samples, which is considerably lower than comparable soils in other Indo-Pacific alluvial mangrove forests (7.9 ± 4.6%; Donato et al., 2011) and up to an order of magnitude lower than soils of oceanic mangrove forests (14.6 ± 5.8%; Donato et al., 2011). The overall dearth of organic matter in the Sundarbans mangrove forest can be explained by a variety of physical and biological mechanisms that operate in the shallow subsurface and living root zone. Perhaps the most likely explanation is that the enormous flux of clastic sediments throughout the Ganges-Brahmaputra (G-B) delta system (e.g., Goodbred and Kuehl, 2000; Hale et al., 2018; Rogers et al., 2013) simply dilutes the overall abundance of preserved organic matter in the subsurface

(e.g., Chmura et al., 2003; Mcleod et al., 2011). For instance, of the ~1000 Mt of sediment discharged each year by the Ganges and Brahmaputra rivers (Kuehl et al., 2005), approximately 100 Mt is deposited in the SMF and G-B tidal delta plain (Rogers et al., 2013). Consequently, sediment accumulation rates in the SMF range between 3 and 5 cm yr^{-1} (Bomer et al., *in review*), ranking among the highest recorded in the literature for mangrove settings (Sasmito et al., 2016). Another possible reason for the mineral-rich soil character is that monsoonal flooding and regular tidal inundation of the forest floor support an energetic hydrodynamic setting capable of entraining and exporting large volumes of organic debris to coastal waters and the open ocean (Aucour et al., 2006; Galy et al., 2007; Fig. 3.9). The extent of tidal flushing evidently extends to the forest interior, as cores taken near SSET-2 do not contain significantly more organic material than cores taken in proximity to tidal waterways (i.e., SSET-1 and 6; Figs. 3.2, 3.6A-C).

Fig. 3.9. Mangrove leaves, twigs, and other organic debris concentrated on the bank of a tidal channel adjacent to site SSET-6 (see Fig. 3.2 for location). Originally deposited on the intertidal platform, this litterfall is captured by energetic flood tides and is ultimately stored within the tidal channels or is exported to the open ocean.

Furthermore, organic matter in the shallow subsurface of the SMF can also be degraded by either biological or physical processes (e.g., Kristensen et al., 2008). Existing research in mangrove forests identifies the presence or absence of leaf-consuming organisms as a key control for retention of organic matter in the shallow subsurface (e.g., Jennerjahn and Ittekkot, 2002; Middleton and McKee, 2001; Robertson, 1988). The intertidal SMF ecosystem fosters a wide array of gastropod species (e.g., *Cerithedia cingulata*, *Cymia lacera*) that predominantly graze on leaf litter and other mangrove detritus (Nayak et al., 2014). In addition, juvenile mud crabs (*Scylla serrata*) consume organic litter both at the surface and belowground in burrows (Alberts-Hubatsch et al., 2016). Organic material that escapes faunal consumption or tidal export is then subject to saprophytic decay upon burial (e.g., Webster and Benfield, 1986). Mangrove leaves, which constitute the majority of litter fall in the SMF (Ghosh et al., 1990), degrade at an average rate of 0.32% per day upon burial (Middleton and McKee, 2001 and references therein), indicating that leaves should fully decompose after approximately one year. While measurements of organic decay in the SMF are outside the scope of this study (see Hossain et al., 2014), the general lack of macroparticulate organic matter found in cores supports the concept of consumption, decomposition, and rapid conversion to particulate and/or dissolved organic states. The occurrence of oxidized conditions during the dry season (Fig. 3.4) further substantiates aerobic decomposition of Sundarbans soils.

Despite generally high soil bulk density (mean = 0.81 g cm^{-3}), soil C density in the SMF is uniformly low (mean = 0.010 g C cm^{-3}), chiefly due to the scarcity of preserved organic matter in the shallow subsurface (Fig. 3.6). Indeed, the soil C density of the SMF is approximately 82% lower than the worldwide average for mangrove forests (0.055 g C cm^{-3}; Chmura et al., 2003). Although spatial heterogeneities throughout the forest are certain to exist, a separate study

undertaken in the Indian Sundarbans confirms similarly low soil C densities (0.016 g C cm^{-3}; Donato et al., 2011). An assessment of whether the SMF is an effective sink for terrestrial C depends on the rate of sediment accretion and time period considered. For instance, integrating annual-scale sediment accretion rates (~3 cm yr^{-1}; Bomer et al., *in review*) yields C sequestration rates of 240 g C m^{-2} yr^{-1} that exceed the worldwide mean for mangrove forests of 188 g C m^{-2} yr^{-1} (Chmura et al., 2003; see Fig. 3.10C). This indicates that the locally high rates of sediment accretion in this mangrove forest compensate for the organic-poor soil quality. This characteristic is mirrored offshore in the Bengal submarine fan, where rapid sedimentation rates and efficient C burial support one of the largest discrete C deposits on Earth – accounting for ~15% of the total terrestrial C buried in oceanic sediments (Galy et al., 2007). Application of decadal to centennial rates of sediment accretion as determined by ^{137}Cs geochronology (1.1 cm/yr; Allison and Kepple, 2001), however, yields comparatively low C accumulation rates (82 g C m^{-2} yr^{-1}). As noted in other studies, the period of time over which C accumulates at the surface and in the subsurface should be carefully considered when evaluating whether ecosystems are productive at sequestering C (e.g., Alongi, 2012; Lovelock et al., 2014). Nonetheless, the calculations of the present study underscore that in the Sundarbans mangrove forest of the G-B delta, and possibly other alluvial mangrove forests (Rovai et al., 2018), continued sediment deposition is critical for the accumulation and sequestration of terrestrial C. Anthropogenic manipulation of sediment-bearing waterways, like the India River Linking Project which is projected to reduce sediment load to the delta by 39 to 75% (Higgins et al., 2018), threatens the current and future potential of this alluvial mangrove forest to function as a C sink.

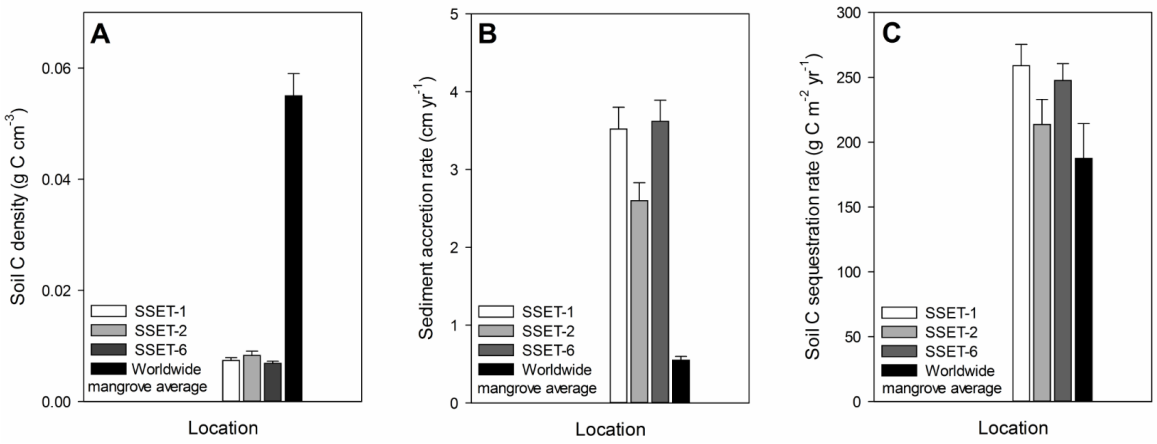

Fig. 3.10. Comparisons of mean soil C density (A), annual sediment accretion rates (B), and annual soil C sequestration rates (C) among the three SSET locations in this study and the worldwide average for mangrove forests. Error bars represent the standard error for all associated measurements. Soil C density is calculated as the product of soil bulk density and total organic carbon. Rates of C sequestration are calculated as the product of soil C density and the rate of sediment accretion. Data sources: SSET soil C density and soil C sequestration rates (*this study*); SSET sediment accretion rates (Bomer et al., *in review*); worldwide mangrove average soil C density and soil C sequestration rates (Chmura et al., 2003); worldwide mangrove average sediment accretion rate (Sasmito et al., 2016).

There are some limitations to the approach that we took when estimating belowground C densities and sequestration rates, primarily with respect to mangrove root production and biomass. In this study, aerial and belowground mangrove roots were avoided when coring to facilitate retrieval of the full sediment profile. Thus, our measurements of C density and sequestration (Fig. 3.10) only represent the amount of C sequestered by soil and underestimate the total belowground sequestration potential of the SMF. However, it has been shown in a variety of mangrove ecosystems that the majority (~75-90%) of the belowground carbon stock is sequestered within the soil component pool (Donato et al., 2011; Hutchison et al., 2014; Kauffman et al., 2011; Murdiyarso et al., 2009). Moreover, to ensure consistent analyses, we compared our rates of carbon sequestration exclusively with studies that reported values of organic content from soil (Chmura et al., 2003 and references therein). Measurements of belowground root and pneumatophore biomass are very difficult to compare owing to a wide variety of sampling procedures (Kauffman et al., 2011). These differences appear to be

manifested in data published in the literature. For instance, an extensive review of mangrove biomass studies found a wide range of reported belowground root biomass values (78.6 ± 94.6 Mg/ha), relative to soil organic content values (446.9 ± 175.4 Mg/ha) (Hutchison et al., 2014). Therefore, while root production biomass certainly constitutes a portion of belowground carbon storage, the lack of standardization in the associated sampling and analytical methodologies makes comparisons among different ecosystems nebulous. In the Sundarbans, Allison et al. (2003) document very low organic content (~1%) and no peat preservation in cores taken to ~5 m depth, indicating that mangrove roots quickly oxidize and decompose upon death. To refine estimations of total belowground biomass and carbon stocks, future studies would benefit from integrating root allometry and soil C measurements.

3.6. Conclusions

Although aboveground depositional processes like sedimentation and organic litter accumulation are critical components of surface elevation change, this study demonstrates that the role of belowground process controls should be taken into account when analyzing and interpreting elevation dynamics. Belowground process controls can be of physical or biological origin and vary in importance depending on the environmental conditions of the system involved (McKee, 2011; Rovai et al., 2018). In the SMF of southwest Bangladesh, both physical (e.g., seasonal pore-water content and particle size distribution) and biotic parameters (e.g., organic matter decomposition and remineralization) influence subsurface dynamics up to 30%, despite its status as a mineral-rich deltaic system where physical processes are expected to take precedence. Owing to high inputs of riverine sediments and seasonal aeration/oxidation of the shallow subsurface, the soils of the SMF volumetrically contain very little preserved organic matter (<2%). Nevertheless, locally high rates of sediment accretion compensate for the organic-poor

soil composition, causing C sequestration rates for the SMF to be higher than those of many mangrove systems worldwide. Continued research, especially in poorly-studied alluvial mangrove forests, is recommended for more accurate inventories of mangrove carbon sequestration and storage. Efforts to safeguard this valuable natural resource, along with other coastal ecosystems, are necessary for any hopes of re-shaping the trajectory of greenhouse gas emissions and minimizing the deleterious effects of climate change.

CHAPTER 4: AN INTEGRATED APPROACH FOR CONSTRAINING DEPOSITIONAL ZONES IN A TIDE-INFLUENCED RIVER: INSIGHTS FROM THE GORAI RIVER, SOUTHWEST BANGLADESH

4.1. Introduction

Rivers, estuaries, and other transitional bodies of water are subjected to varying degrees of terrestrial and marine influences on their journey from headwater source to open ocean, resulting in a complex spectrum of hydrodynamic and depositional conditions (e.g., Dalrymple and Choi, 2007). In landward regions, river currents, particularly those produced during flood events, represent the dominant hydrodynamic control on sediment transport and deposition (e.g., Milliman and Meade, 1983; Milliman and Syvitski, 1992). However, as rivers approach the coast, their currents are tempered by waning hydraulic gradients and the increasing influence of marine processes, namely waves and tides. The impact of waves is typically limited to the coastal zone as wave energy rapidly attenuates with distance inland through bottom friction (Madsen et al., 1989; Soulsby and Whitehouse, 1997) and interaction with vegetation (Jadhav et al., 2013; Kobayashi et al., 1993; Möller, 2006). Tides, on the other hand, can propagate upstream for tens to hundreds of kilometers, depending on river discharge, channel dimensions, and the gradient of the channel bed (e.g., Godin, 1999). Rivers connected to active tidal coasts are therefore characterized by reaches of tidal dominance, mixed influence, and fluvial dominance, together referred to in the literature as the tidal to fluvial transition zone (TFT, e.g., Dalrymple et al., 2015).

How this continuum of hydrodynamic processes controls the spatial distribution and preservation of sediments along tide-influenced rivers has only recently been investigated and is largely focused on interpretations from ancient tidal strata (e.g., Gugliotta et al., 2016; Jablonski and Dalrymple, 2016; Martin et al., 2018; Olariu et al., 2015; Prokocki et al., 2015; van den Berg

et al., 2007; Webb et al., 2015). Comparatively little work has been undertaken in the TFT of modern systems (Dashtgard et al., 2012; Ethridge et al., 1987; Gugliotta et al., 2017; Gugliotta and Saito, 2019), in spite of its dual applicability to economic and environmental issues. For instance, core data from modern tide-influenced channel bars readily allows the connection of hydraulic process to sedimentary product, which has proven useful for characterizing tidal-fluvial hydrocarbon reservoirs such as the Cretaceous McMurray Formation of Canada (Musial et al., 2012) and the Triassic Mungaroo Formation of Australia (Martin et al., 2018). Constraining the subsurface abundance of cohesive (i.e., mud) and non-cohesive (i.e., sand) sediments in the TFT is also critical for predicting geomorphic change along low-lying coastal rivers. Such findings, in turn, can guide management of environmental and societal matters like groundwater resources (Michael and Voss, 2009), aquaculture (Higgins et al., 2013), channel infilling and land reclamation (Wilson et al., 2017), and adaptation to lateral river migration and erosion (Das et al., 2014), all of which are pertinent to communities residing in fluvio-deltaic landscapes.

Previous research in both modern and ancient tidal-fluvial settings has demonstrated the importance of utilizing multiple proxies to accurately interpret and characterize depositional conditions (e.g., Gugliotta et al., 2017, 2016; La Croix and Dashtgard, 2015). The foundation of these studies has been sedimentological trends, namely changes in bulk grain size and stratal cyclicity as determined through sediment coring, outcrop observations, and channel bed grab sampling. Trace fossil assemblages (ichnofacies) have often been used to corroborate sedimentological findings, whereby faunal burrow size, intensity, and diversity relate to the level of physiochemical stress induced by the environment, therefore providing a proxy for salinity and marine influence (Díez-Canseco et al., 2015; Gingras et al., 2011; Johnson and Dashtgard,

2014). Separate efforts have been made to understand how the transition from backwater to normal flow hydrodynamics governs sediment transport (Nittrouer, 2013; Nittrouer et al., 2012) and river channel kinematics (Blum et al., 2013; Fernandes et al., 2018, 2016; Lamb et al., 2012). However, only preliminary relationships between backwater hydrodynamics and channel margin stratigraphy exist (Fernandes et al., 2016), and these have not been analyzed within the context of the TFT.

Among studies of tide-influenced rivers worldwide, much attention has been centered on systems in North America, notably the Fraser River (e.g., Czarnecki et al., 2014; Dashtgard et al., 2012; Johnson and Dashtgard, 2014; La Croix and Dashtgard, 2015; Sisulak and Dashtgard, 2012). Knowledge gaps exist elsewhere, especially in South Asia, a region that simultaneously hosts the largest tide-dominated deltas (e.g., Ganges-Brahmaputra, Indus, Ayeyawady) and population centers on Earth (Small et al., 2018b; Woodroffe et al., 2006b). The present study seeks to fill this gap by considering the mixed tidal-fluvial Gorai River, a distributary of the Ganges River in the Ganges-Brahmaputra Delta of Bangladesh (Fig. 4.1). The main objective of this study is to integrate a diverse assemblage of datasets, including core sedimentology, remote sensing, and channel bathymetry to provide a process-based depositional framework for the TFT of the Gorai River. The Gorai differs from many tidal-fluvial rivers in that its hydrology is highly regulated by seasonal conditions, exhibiting an order of magnitude difference in water discharge between wet and dry seasons (Shaha and Cho, 2016). Despite the growing body of literature in the TFT, very few studies have investigated systems with such pronounced hydrologic variation (Gugliotta et al., 2017), and it is presently unclear if and how these seasonal signals are preserved in the stratigraphy. Another key objective of the study is to explore the interactions among channel gradient, hydraulic conditions, and channel bank composition in modulating river

morphodynamics. Field and experimental work have demonstrated that the upstream limit of the backwater transition, that is the location where the channel bed elevation approximates mean sea level (Chow, 2009), exerts a strong control on the positioning of river avulsions (e.g., Chadwick et al., 2019; Chatanantavet et al., 2012; Edmonds et al., 2009; Fernandes et al., 2016; Ganti et al., 2016; Nittrouer et al., 2012), and it is hypothesized that similar phenomena occur in the Gorai River. Identification of areas likely to undergo morphologic change would be particularly relevant for southwest Bangladesh but would also contribute observational data to global modelling efforts that forecast river avulsion location and frequency (e.g., Ganti et al., 2014; Lamb et al., 2012).

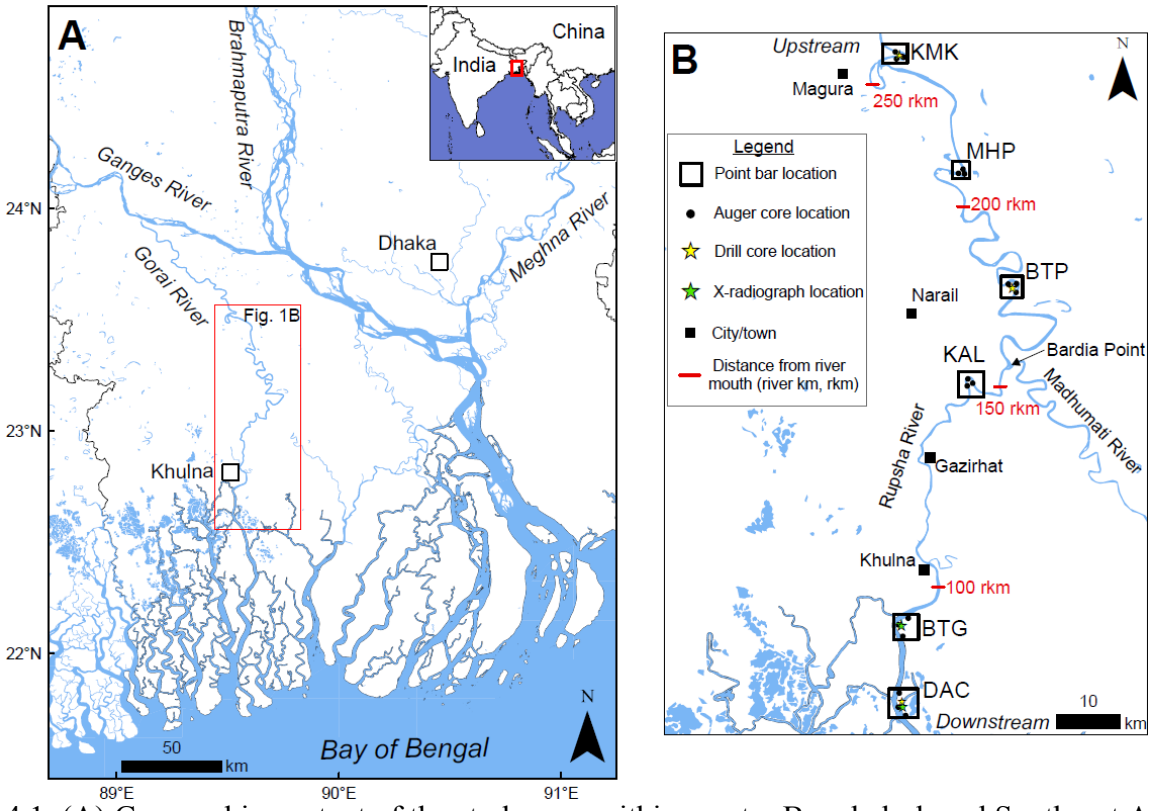

Fig. 4.1. (A) Geographic context of the study area within greater Bangladesh and Southeast Asia. The Gorai River is influenced by fluvial forces (e.g., monsoonal flood discharge) from the Ganges and marine forces (e.g., meso-scale tides) from the Bay of Bengal. (B) Map of the main stem of the Gorai River illustrating sampling locations codified by the names of nearby villages: Dacope (DAC), Batiaghata (BTG), Kalia (KAL), Bhatiapara (BTP), Mohammadpur (MHP), and Kamarkhali (KMK). Note that between Bardia Point and Khulna the Gorai is locally referred to as the Rupsha River. Downstream of Khulna the Gorai is locally known as the Pussur River.

4.2. Regional setting

The Gorai River is one of the largest distributaries of the Ganges and comprises the principal source of fresh river water for southwest Bangladesh, a region that hosts a burgeoning population of approximately 30 million (BBS, 2011). Originating from the Ganges in Kushtia District, the Gorai flows south-southeast for ~350 km through Quaternary alluvial and tidal delta plain sediments before emptying into the Bay of Bengal (Fig. 4.1A). In the upper reaches, the river exists as a single, meandering trunk channel with no natural bifurcations or distributaries (Fig. 4.1B). At Bardia Point, located ~150 river km upstream of the mouth, the Gorai bifurcates into the Rupsha and Madhumati Rivers (Fig. 4.1B). Historically, the Madhumati accommodated the majority of discharge from the Gorai until the beginning of the 20th century (Chamberlain et al., 2019), when the Rupsha off-take was extensively dredged to augment the delivery of river water to Khulna (EGIS, 2000). Since then, the Rupsha has taken precedence as the primary distributary, while the Madhumati has degraded as a result of waning fluvial input and channel siltation: between 1965 and 1998 the average depth of the Madhumati River decreased 55% from 4.86 to 2.76 m (EGIS, 2000). Downstream of Khulna, the Gorai-Rupsha enters the tidal delta plain and is locally referred to as the Pussur River. Here, the Pussur branches into a dense and interconnected network of tidal channels surrounding mangrove-vegetated forest (Sundarbans National Forest). For simplicity, the Gorai, Rupsha, and Pussur reaches of the river are hereafter referred to collectively as the Gorai River. In total, the drainage basin of the Gorai and its distributaries encompass ~16,000 km^2, roughly half of which is cultivated land (EGIS, 2000).

Similar to other tropical rivers in South and Southeast Asia, water discharge of the Gorai exhibits dramatic seasonality and is largely controlled by monsoonal precipitation and flooding. For instance, at the Kamarkhali gauging station located ~100 river-km downstream of the

Ganges off-take ("KMK" in Fig. 4.1B), ~95% of the annual discharge occurs between the months of July and November (Shaha and Cho, 2016). Due to the extreme variability of water discharge, the entire course of the river is fresh during the monsoon season but is saline in the dry season as far upstream as Gazirhat (see Fig. 4.1B for location; Winterwerp and Giardino, 2012). The upstream extent of tidal influence is similarly impacted by the magnitude of discharge: in the dry season, tides (range ~ 0.2 m) are observed up to Mohammadpur ("MHP" in Fig. 4.1B) whereas during the monsoon season tidal influence is dampened by the flood pulse and is limited to ~20 river km downstream of MHP (Fig. 4.1B; EGIS, 2000). The lower reach of the Gorai is characterized by a hypersynchronous tidal regime, wherein the tide range increases inland from ~2 m at the coast until reaching a maximum of ~3 m at Dacope ("DAC" in Fig. 4.1B; EGIS, 2000). This study is focused on a ~200-km reach of the Gorai River extending from a non-tidal, perennially fresh-water setting at KMK to a tide-dominated, seasonally saline setting at DAC (Fig. 4.1B).

4.3. Methods

4.3.1. Remote sensing

A digital elevation model (DEM) of the study area was constructed using data from the 2000 Shuttle Radar Topography Mission (SRTM; Farr et al., 2007). SRTM elevation data have a spatial resolution of 1 arc-second (~30 m) and were downloaded from the open source USGS EarthExplorer database (https://earthexplorer.usgs.gov/). Post-processing of the DEM and creation of elevation transects adjacent to the Gorai River were carried out in the software ArcMap 10.5. Regional trends in elevation change were identified using a running average (10 km window) of the raw data.

Present-day river channel sinuosity was calculated for each meander bend along the Gorai River by dividing the channel length by the linear downstream length (e.g., Bridge, 2003). The lateral mobility of point bars was determined by applying the "best-fitting circle" method (Finotello et al., 2018; Largasse, 2004) to georeferenced Landsat aerial photographs from 1972 and 2015 (resolution of 90 and 30 m, respectively), also obtained from the EarthExplorer database. This approach accounts for changes in meander bend extension (δE) by comparing bend radii (R_b) at two points in time (t and t + δt), represented by equation (1).

$$\delta E = R_b(t + \delta t) - R_b(t) \quad (1)$$

Bar migration via downstream translation (δT) is also calculated by comparing the change in location of the bend center point coordinates (δx and δy), represented by equation (2).

$$\delta T = \sqrt{(\delta x_c)^2 + (\delta y_c)^2} \quad (2)$$

The overall point bar migration rate (M_b), which combines the extension (δE) and translation (δT) components, is then calculated following equation (3).

$$M_b = \sqrt{\delta R^2 + \delta S^2} / (\delta t) \quad (3)$$

4.3.2. Hydrodynamic observations

Channel bathymetry of the Gorai River (Pethick, 2012) was incorporated with elevation measurements to constrain the vertical position of the channel bed with respect to mean sea level. The bathymetric survey consists of 183 bank-normal transects with ~1 km spacing between each transect. However, this study only utilizes 50 of the most inland transects, covering a segment of the river from Bardia Point to Dacope (DAC, Fig. 4.1B). Bathymetric data processing and presentation followed an approach similar to that of Nittrouer et al. (2012). Briefly, the average channel depth of each transect was calculated, and then a 10 km running average was applied to the trend to neutralize the effects of localized bathymetric irregularities, such as bed scouring

from channel confluences (e.g., Sambrook Smith et al., 2019). Bathymetric data were not corrected for water level changes induced by tides or river discharge.

Time-averaged hydrodynamic regions of the Gorai River were determined by analyzing annual-scale water level data from tide gauging stations across the TFT (BIWTA, 2019; EGIS, 2000) and salinity intrusion maps (Winterwerp and Giardino, 2012). Following a convention similar to that of La Croix and Dashtgard (2015), tide-dominated, or "tidal," reaches of the river were classified as having a mean tide range ≥ 2 m (i.e., meso-tidal or greater) and seasonal polyhaline conditions (18 to 30 psu); mixed tidal-fluvial, or "mixed," reaches were classified as having a mean tide range ≥ 0.2 m but ≤ 2 m (i.e., micro-tidal) and seasonal mesohaline conditions (5 to 18 psu); and fluvial-dominated, or "fluvial," reaches were classified as having a mean tide range of ≤ 0.2 m (i.e., non-tidal) and perennial fresh water conditions (< 0.5 psu).

4.3.3. Site selection and fieldwork

Core collection was undertaken during four field campaigns: following the summer monsoon in October 2017 and 2018, and during the dry season in March 2018 and 2019. Six point bars across the Gorai River TFT were cored in transects of ~1 km with ~300 m spacing between core sites (Fig. 4.1B). Sampling locations were pre-selected using satellite imagery and verified in the field with a Garmin eTrex 10 global positioning system (GPS) referenced to the WGS84 datum. Cores up to ~3 m length were extracted using a 3-cm diameter half-cylinder auger driven into the subsurface using an iron sledge. Sediment cores were taken along the accreting perimeter of the point bar with sites situated on the upstream (U), apex (A), and downstream (D) sides to capture along-strike depositional changes. In addition, acrylic box cores (30 cm length) were collected from DAC and BTG locations for x-radiograph imaging. To ensure consistent lateral positioning relative to the water line, all cores were collected following

the monsoon season (i.e., during high stage) in upstream locations and during or near high tide in tide-influenced areas. Following extraction, all auger cores were transported to the Department of Environmental Science at Khulna University where they were described and subsampled in regular intervals.

To constrain deeper stratigraphy and its effect on channel mobility, drill cores to ~45 m depth were taken at DAC, BTP, and KMK locations (Fig. 4.1B), representing tidal, mixed tidal-fluvial, and fluvial environments, respectively. Drilling was carried out using a local method for installing tube wells, previously described by Pickering et al. (2014). In brief, a drill string fitted with a steel cutting shoe was driven into the subsurface using a bamboo fulcrum-and-lever system facilitated by circulating drill fluid (water and organic matter). Sediment cuttings were collected from the expelled drill fluid in 1-m depth intervals for further analyses.

4.3.4. X-radiography

X-radiographs of sediments encased in acrylic box cores were collected to reveal sedimentological (e.g., bedding and laminations) and biological (e.g., burrows) features that were not visible otherwise. X-radiographs were carried out using a medical-grade X-ray detector (Khulna Health Diagnostic Center, Khulna, Bangladesh) illuminated by an X-ray unit operating at 40 keV and 10 mA. Individual x-radiograph films were developed and then photographed over a light table to maximize visibility. The intensity of bioturbation as revealed by x-radiographs was reported following the classification scheme of Taylor and Goldring (1993), wherein bioturbation intensity (BI) is quantified on a scale from 0 to 6. Lower values (0 to 3) represent high preservation of original sedimentary fabric and little to no bioturbation while higher values (4 to 6) indicate extensive biological overprinting and sediment reworking (Taylor and Goldring, 1993).

4.3.5. Granulometry

Grain size analysis was conducted at 10-cm intervals for all auger cores, and at finer resolution when distinct changes in sediment character were noted (n = 538). For deeper drill cores, analyses were undertaken at 1-m intervals (n = 135). In each case, sediment samples of ~2 g were exposed to 2 ml of 30% hydrogen peroxide (H_2O_2) to eliminate fine organic matter. Digested solutions were then stirred with 15 ml of 0.05% sodium metaphosphate (NaH_2PO_4) to de-flocculate clay particles. Prior to analyses, particulate organic debris and clastic material larger than 850 μm were removed by sieving. A total of 678 samples were analyzed for volumetric frequency distributions of grain size (range = 0.4-850 μm) and particle sorting using a Beckman Coulter laser diffraction particle size analyzer (Model LS 13 320).

4.4. Results

4.4.1. Surface and channel morphology

The surface elevation of the Gorai River floodplain gradually increases landward, ranging from 3 m immediately north of the Sundarbans Forest to 15 m near the Ganges-Gorai offtake (Figs. 4.2, 4.3). However, closer examination reveals two reaches with distinctly different gradients (*sensu* Wilson and Goodbred, 2015; Fig. 4.3). The first reach, which extends from the beginning of the transect ("A" in Figs. 4.2, 4.3) to ~10 km upstream of KAL, exhibits an average slope of 5×10^{-6} (Fig. 4.3). Inland of this point, the average slope of the floodplain increases by over an order of magnitude to 1×10^{-4} (Fig. 4.3). Integration of channel bathymetry (Pethick, 2012) with the elevation data indicates that the channel bed is situated below mean sea level (i.e., in the backwater zone) until approximately ~130 river km inland of the coast (Figs. 4.1B, 4.2, 4.3).

Although present-day channel sinuosity and channel migration rates (measured between 1972 and 2015) both generally increase landward, more detailed trends emerge when these geomorphic parameters are placed within the context of the hydrodynamic zones of the river (Fig. 4.4). In the downstream, tide-dominated tract of the river, channel sinuosity is relatively low and exhibits little variation along its course, with an average sinuosity coefficient (± standard deviation) of 1.2 ± 0.1 (Fig. 4.4A). Migration rates in the tide-dominated realm are similarly low, exhibiting an average migration rate of 6.6 ± 2.0 m/yr (Fig. 4.4B). Channel sinuosity and migration rates dramatically increase across the backwater (i.e., into the mixed tidal-fluvial zone), demonstrating a 50% increase in the sinuosity coefficient to 1.8 ± 0.6 and a nearly five-fold increase in migration rates to 32.4 ± 16.1 m/yr (Figs. 4.4A, 4.4B). In the purely fluvial zone, beyond the upstream limit of tidal influence, channel sinuosity is roughly the same as in the mixed tidal-fluvial zone (1.7 ± 0.9, Fig. 4.4A). However, channel migration rates decrease to 9.0 ± 11.4 m/yr, approximately the same level as the tide-dominated reach of the river (Fig. 4.4B).

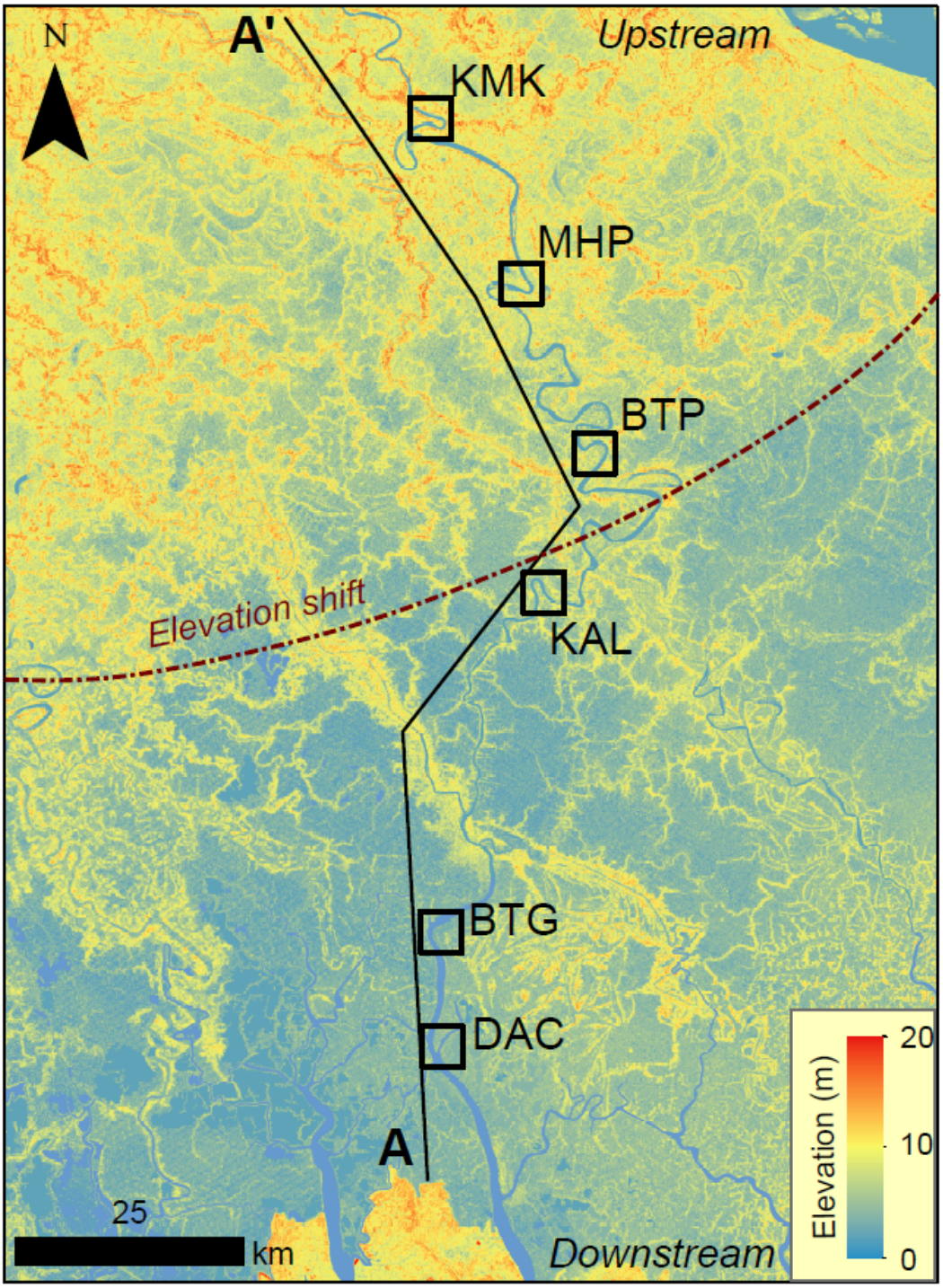

Fig. 4.2. Digital elevation model (DEM) of southwest Bangladesh constructed from the 2000 Shuttle Radar Topography Mission data illustrating a distinct shift in topography (adapted from Wilson and Goodbred, 2015). Transect A-A' runs alongside the Gorai River from the northern edge of the Sundarbans Forest to the Ganges-Gorai offtake.

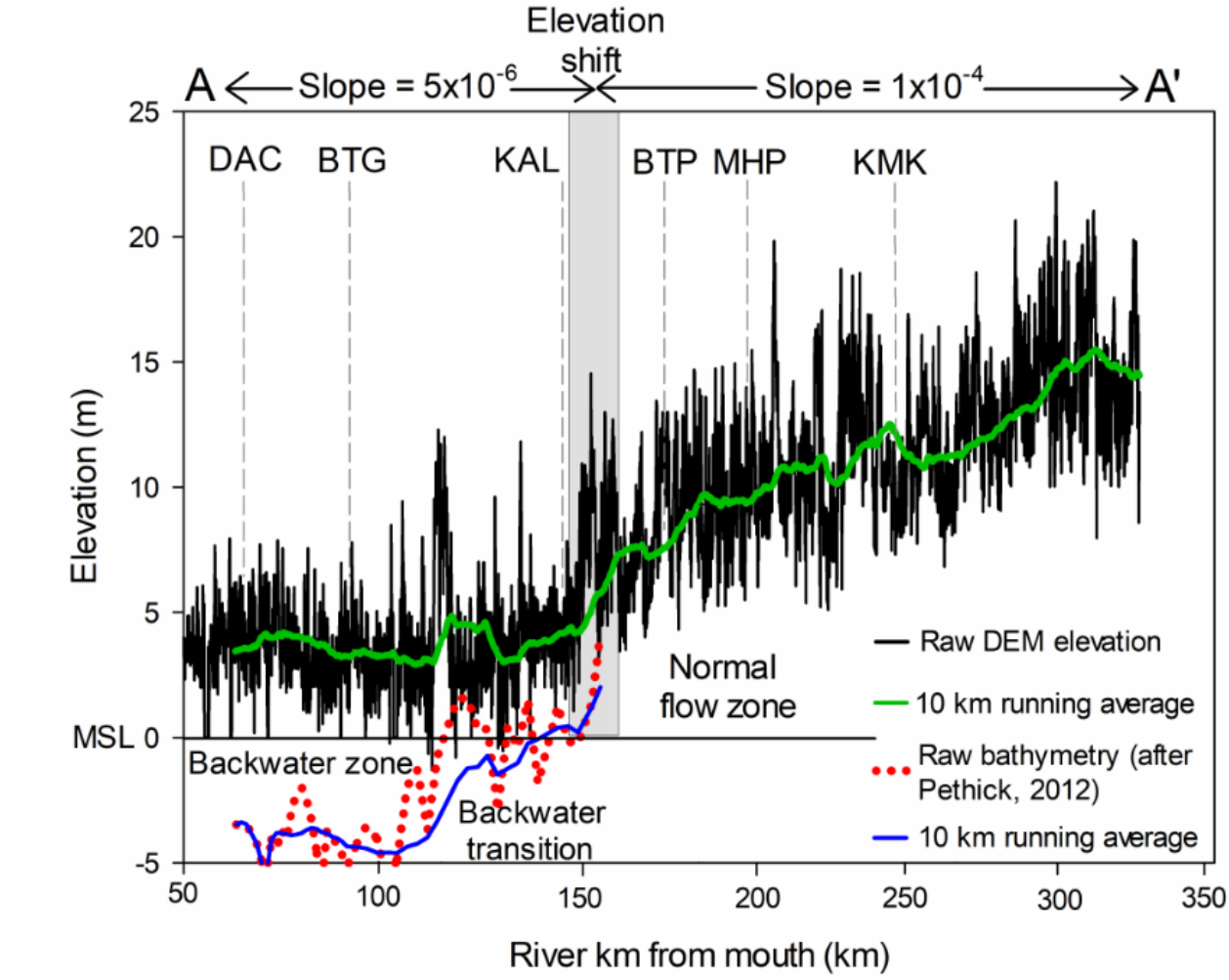

Fig. 4.3. Floodplain elevation measured adjacent to the Gorai River, following transect A-A' of Fig. 4.2. The vertical position of the channel bed, displayed in blue relative to mean sea level (MSL), is calculated as the 10 km running average of the floodplain elevation minus the 10 km running average of the channel depth (after Pethick, 2012). Note that the transition from backwater to normal flow hydrodynamics occurs immediately downstream of KAL and the elevation shift.

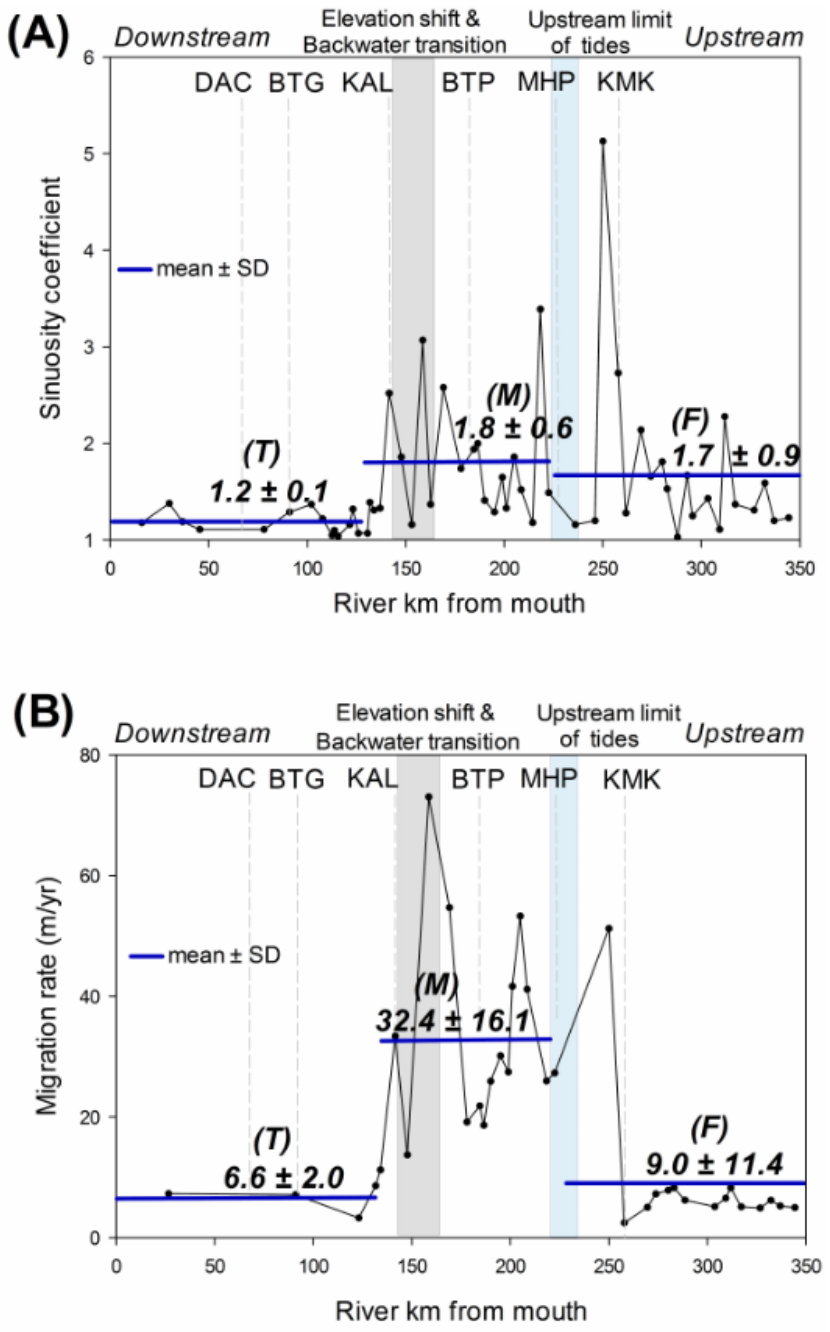

Fig. 4.4. Trends in channel morphodynamic properties as a function of distance from the river mouth, including: (A) present-day channel sinuosity and (B) meander bend migration rates between 1972 and 2015. Average ± standard deviation (SD) values for tidal (T), mixed tidal-fluvial (M), and fluvial (F) hydrodynamic zones are indicated by blue horizontal lines. The elevation shift and backwater transition are displayed as a shaded envelope because they occur over an area of the river rather than at a single point. Similarly, the upstream limit of tidal influence is represented as an envelope because the limit depends on the magnitude of river discharge.

4.4.2. Shallow subsurface sedimentology and stratigraphy

4.4.2.1. Tide-dominated depozone (DAC & BTG)

Dacope (DAC), the most downstream core site, is located 70 river km upstream of the mouth and 60 river km downstream of the backwater limit (Figs. 4.1B, 4.3). The mean tide range of this area is estimated to be ~3.2 m based on tide gauge data at Mongla (~3.1 m, BIWTA, 2019), located 15 river km downstream of DAC. The stratigraphy of DAC cores is dominantly composed of medium silt (72.3%) with occasional coarse silt (15.7%) and fine silt beds (12.0%, Table 4.1; Fig. 4.5). Down-core grain size trends display either weak reverse grading (i.e., coarsening upward, see DAC-D, Fig. 4.5) or are invariant with depth (e.g., DAC-U, Fig. 4.5). Although core profiles appear homogeneous, x-radiographs reveal that the sedimentary fabric is composed of rhythmic, mm-scale laminations of medium silts (Fig. 4.6A). Apart from human influences, bioturbation is minimal and much of the original sedimentary fabric is present (BI = 0-2, Fig. 4.6A).

Batiaghata (BTG) is situated 20 river km upstream of DAC and 40 river km downstream of the backwater limit (Figs. 4.1B, 4.3). The local tide range is estimated to be ~2.9 m based on tide gauge data at Khulna (~2.3 m, Pethick and Orford, 2013) and Mongla (~3.1 m, BIWTA, 2019). The stratigraphy of apex and upstream cores on this point bar consists of moderately well-sorted coarse silt with occasional medium silt and rare very fine sand beds (Fig. 4.5). Sediments of the downstream core are comparatively finer, dominantly composed of well-sorted fine silt (Fig. 4.5). All BTG cores exhibit gradual normal grading but rarely depart from the median grain size (Fig. 4.5). Due to the relative invariance in grain size, the thickness of depositional packages is usually unclear. However, in a few cases, fining-upward units of ~20 to 30 cm thickness are observed (e.g., BTG-U, 0.3-0.5 m depth; Fig. 4.5). X-radiographs indicate that the sedimentary

fabric is characterized by sections containing rhythmic mm-scale laminations of silts (e.g., 5-10 cm depth and 12-17 cm depth, Fig. 4.6B) as well as sections containing non-rhythmic, cm-scale laminations and beds (e.g., 3.5-4.5 cm depth and 10-12 cm depth, Fig. 4.6B). Faunal burrows are occasionally observed (e.g., 18-19 cm depth, Fig. 4.6B), but for the most part the original sedimentary fabric is intact (BI = 0-2, Fig. 4.6B). Overall, mud (grain size = 4-63 μm) composes 98.8% of sediments in the tide-dominated depozone (DAC and BTG, Table 4.1).

4.4.2.2. Mixed tidal-fluvial depozone (KAL & BTP)

Kalia (KAL) is situated 50 river km upstream of BTG and 10 river km upstream of the backwater limit (Figs. 4.1B, 4.3). The mean tide range of this area is inferred to be ~1.8 m based on tide gauge data at Khulna (~2.3 m, Pethick and Orford, 2013) and Lohagara (~1.5 m, Wilson and Valentine, *pers. comm.*), located 40 river km upstream of KAL. Sediment cores taken at KAL are chiefly composed of moderately well-sorted coarse silt (41.6%), with roughly equal proportions of medium silt (27%) and very fine sand (26.9%, Table 4.1; Fig. 4.7). KAL cores contain a notably higher sand content (26.9%) in comparison to those at BTG (2.3%, Table 4.1). Individual beds are also more readily observable in KAL cores: KAL-D, for instance, contains at least eight fining-upward units that range from 0.2 to 0.5 m in thickness (Fig. 4.7). Bed contacts are uniformly sharp at the base and fine upward either gradually (e.g., KAL-D, 1.0-1.3 m depth; Fig. 4.7) or abruptly (e.g., KAL-A, 1.3-1.5 m depth; Fig. 4.7). On the whole, fining-upward successions do not occur in consistently spaced intervals (Fig. 4.7). In contrast to DAC and BTG, no sedimentological trends or structures indicative of tidal influence were seen in the stratigraphy of KAL cores.

Table 4.1. Median grain size proportions for auger core locations and depositional zones. Note that changes in sand (and mud) content are particularly pronounced between BTG and KAL (across the backwater), as well as between MHP and KMK (near the limit of tidal influence). Mean tide ranges, originally reported by EGIS (2000) and BIWTA (2019), take into account neap/spring variation and seasonal conditions. Water salinity values for the dry season were reported by Winterwerp and Giardino (2012); water salinity is negligible for all sites during the monsoon season.

TFT hydrodynamic conditions	Tide-dominated		Mixed tidal-fluvial		Fluvial-dominated	
Auger core location/ Grain size (%)	DAC	BTG	KAL	BTP	MHP	KMK
Fine - medium silt (8-32 µm)	84.3	36.5	31.5	11.8	7.0	0
Coarse silt (32-63 µm)	15.7	51.2	41.6	54.1	37.2	13.3
Very fine sand (63-125 µm)	0	2.3	26.9	32.9	45.3	84.5
Fine sand (125-250 µm)	0	0	0	1.2	10.5	2.2
Grain size distribution	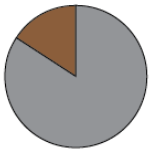				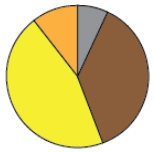	
Sand : mud ratio	0 : 100	2.3 : 97.7	26.9 : 73.1	34.1 : 65.9	55.8 : 44.2	86.7 : 13.3
Mean tide range (m)	3.2	2.9	1.8	1.4	0.2	0
Water salinity, dry season (psu)	23.0	22.0	10.0	4.0	0.5	0

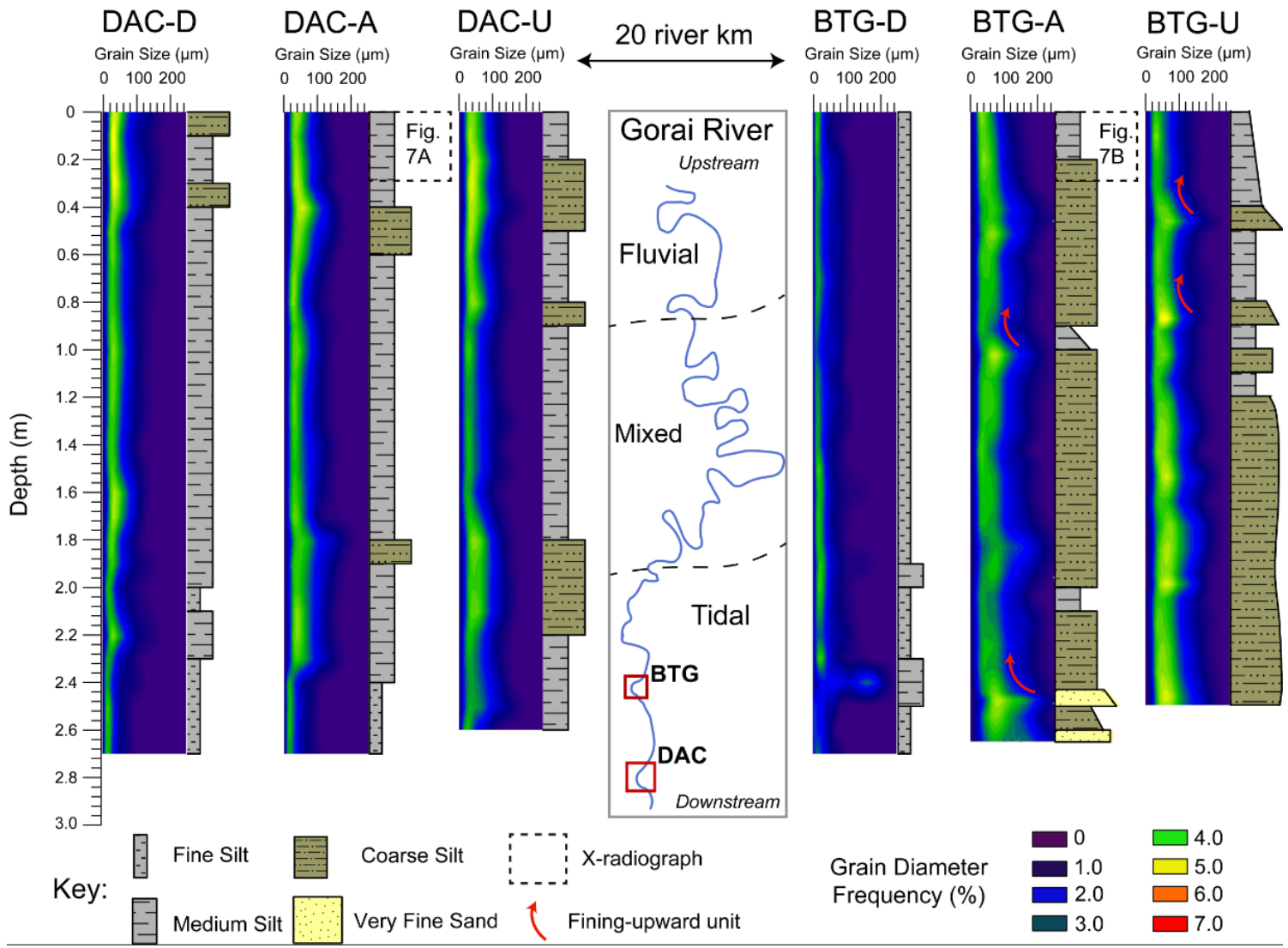

Fig. 4.5. Core stratigraphy at Dacope (DAC) and Batiaghata (BTG) sites, located within the tidal depositional zone (mean tide range at DAC and BTG are 2.8 m and 2.4 m, respectively). Down-core trends in grain size are represented by two panels for each core: volumetric frequency distributions between 0 and 250 µm (left), and median grain size (right).

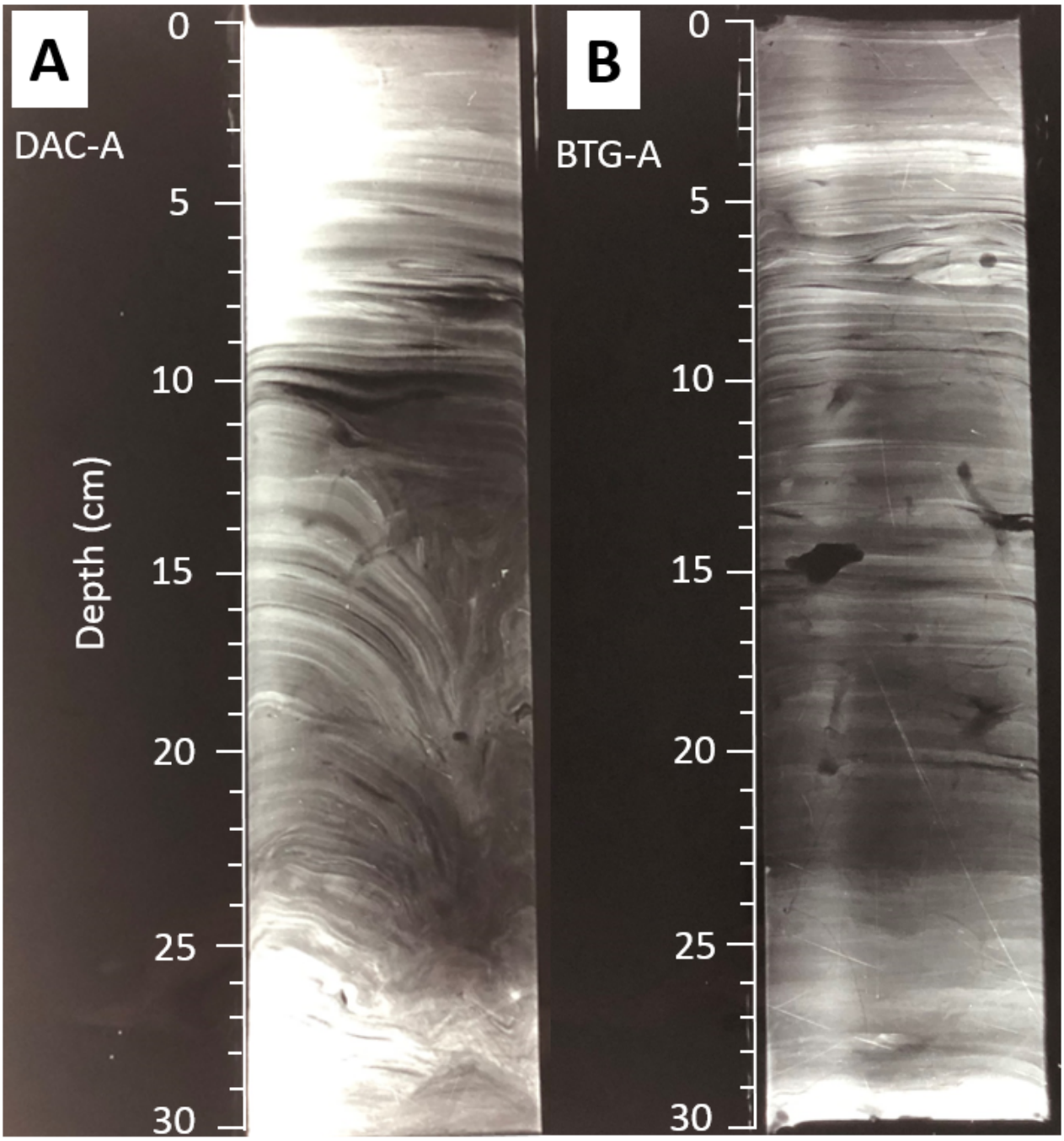

Fig. 4.6. X-radiograph negatives collected from box cores at (A) DAC-A and (B) BTG-A locations illustrating evidence of tidal and seasonal depositional influences (see Fig. 4.5 for core locations and position within the stratigraphy). Darker colors represent less dense sediments (e.g., fine silts) while light colors correspond to sediments with relatively high density (e.g., coarse silts and sands). Extensive deformation of bedding below 10 cm depth at DAC-A was likely produced by human activity (footprint).

Bhatiapara (BTP) is located 45 river km upstream of KAL and 35 river km upstream of the backwater (Figs. 4.1B, 4.3). The mean tide range of this area is estimated to be ~1.4 m based on tide gauge data at Lohagara (~1.5 m, Wilson and Valentine, *pers. comm*.), located 10 river km downstream of BTP. Cores at BTP are dominantly composed of coarse silt (54.1%) and very fine sand (32.9%) with lesser amounts of medium silt (11.8%, Table 4.1; Fig. 4.7). Normal grading is evident in downstream and apex cores from this point bar: from the surface to ~1.8 m depth the stratigraphy largely consists of medium and coarse silt beds, whereas the lowermost sections are predominantly composed of very fine sand beds (Fig. 4.7). Conversely, the upstream core along this point bar does not exhibit any clear grain size trends with depth (Fig. 4.7). Irregularly spaced fining-upward units of 0.2-0.5 cm thickness, similar to those in KAL cores, are seen in all BTP cores (e.g., BTP-D, 1.6-1.8 m depth; Fig. 4.7). Disseminated organic debris, including stems, twigs, and other fine particulate plant matter, are often found in silt beds associated with fining-upward units in KAL and BTP cores (Fig. 4.7). When partitioned by hydrodynamic zone, the mixed tidal-fluvial setting contains substantially more sand than the tidal setting (29.3% vs. 1.2%, Table 4.1).

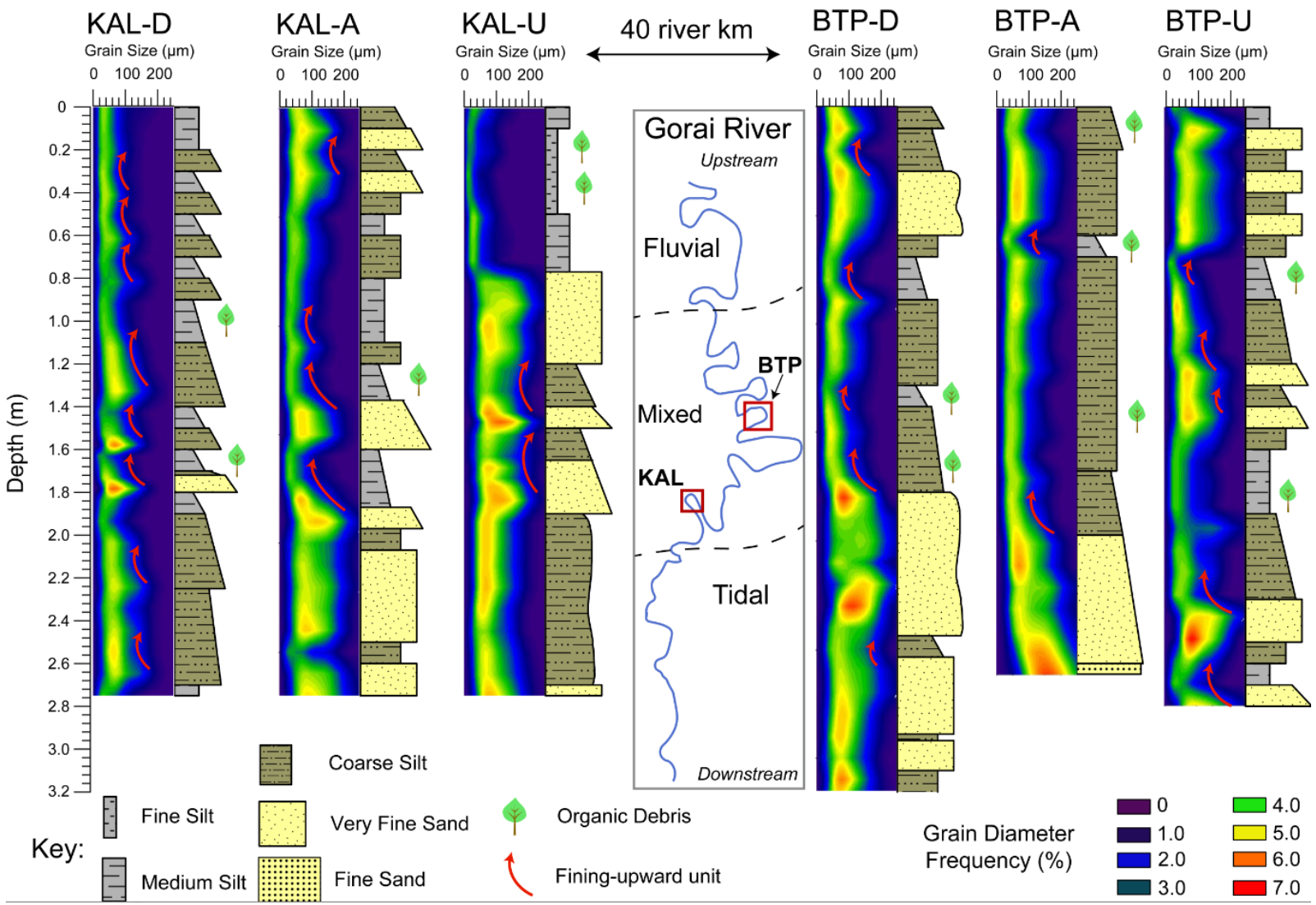

Fig. 4.7. Core stratigraphy at Kalia (KAL) and Bhatiapara (BTP) locations, both of which situated within the mixed tidal-fluvial depositional realm (mean tide range at KAL and BTP are ~1.8 m and ~1.4 m, respectively). Note the abundance of dm-scale fining-upward units, which are interpreted to represent monsoonal flood deposits.

4.4.2.3. Fluvial-dominated depozone (MHP & KMK)

MHP is located 40 river km upstream of BTP and 35 river km downstream of KMK (Fig. 4.1B). This area is inferred to be in the vicinity of the upstream limit of tidal influence based on hydrologic data from (BIWTA, 2019) and anecdotal evidence from local villagers who observe minor tide-induced water level changes (tide range ~ 0.2 m) during the dry season but no tides during the monsoon (Rahman, *pers. comm.*). MHP cores mainly contain very fine sand (45.3%) and coarse silt (37.2%), with roughly equal parts medium silt (7%) and fine sand (10.5%, Table 4.1; Fig. 4.8). All cores exhibit normal grading with a ~1.2 m thick section of very fine and fine sands overlain by ~1.5 m of silt and very fine sand (Fig. 4.8). Bed contacts, especially in the apex and upstream cores of this point bar, tend to be very abrupt at the base (e.g., MHP-A, 1.5-1.6 m depth; Fig. 4.8). KMK, the most upstream core site, is situated 35 river km upstream of MHP and 30 river km upstream of the limit of tidal influence (BIWTA, 2019). Cores from KMK are dominantly composed of very fine sand (84.5%), with lesser proportions of coarse silt (13.3%) and fine sand (2.2%, Table 4.1; Fig. 4.8). The general stratigraphy of KMK cores consists of dm- to m-scale very fine sand beds interspersed with cm- to dm-scale coarse silt beds (Fig. 4.8). Grain size fines upward, except for the core on the apex of the point bar (KMK-A, Fig. 4.8). Silt beds are irregularly spaced throughout the core profiles and often contain decomposed organic litter (Fig. 4.8). Sand beds appear to be massive and structureless, though volumetric frequency distributions of grain size reveal fining-upward and occasional coarsening-upward successions (Fig. 4.8). The difference in sand content between MHP (55.8%) and KMK (86.7%) represents the most pronounced change between two adjacent core sites in the study (Table 4.1).

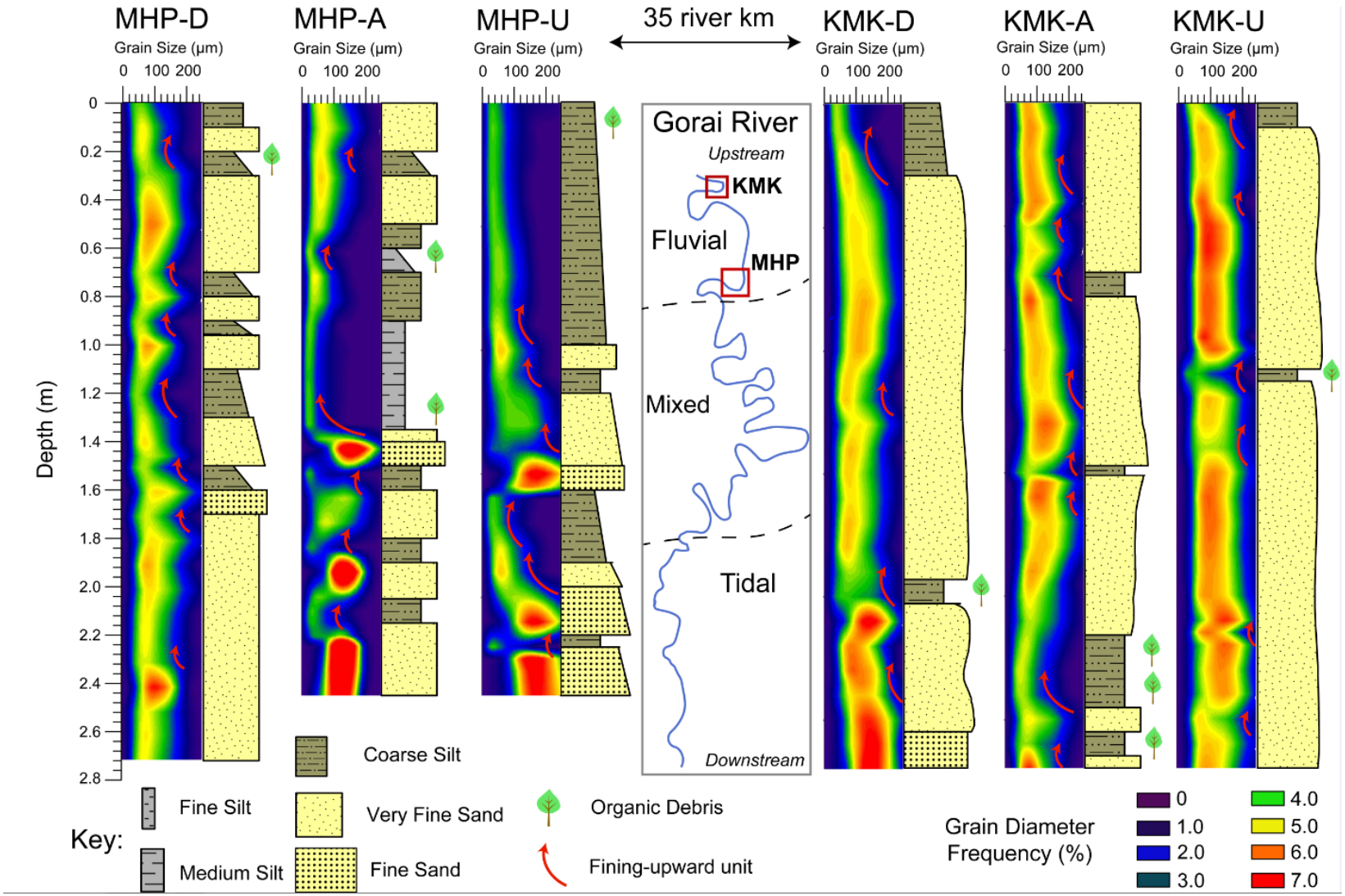

Fig. 4.8. Core stratigraphy at Mohammadpur (MHP) and Kamarkhali (KMK), both of which located within the fluvial depositional zone (mean tide range at MHP and KMK are ~0.2 m and 0 m, respectively). Note the thick (m-scale) and possibly amalgamated sand beds.

4.4.3. Deep subsurface sedimentology and stratigraphy

Drill cores from three point bar locations along the Gorai River (DAC, BTP, and KMK) extend stratigraphic profiles obtained by auger coring and demonstrate that along-channel stratigraphy varies substantially among the sites (Fig. 4.9). A drill core from DAC indicates that the overbank muds observed throughout the auger cores in this location (Fig. 4.5) continue to 13 m depth and overlie a 5 m thick bed of well-sorted fine sands (Fig. 4.9). Underlying this sand bed is a 17 m section characterized by alternating sands and muds (DAC-Drill, 17-34 m depth, Fig. 4.9). Individual sand beds in this section are relatively thin (mean thickness ± standard deviation = 1.8 ± 0.4 m), fine upward, and contain particulate organic debris at the top of bed contacts (Fig. 4.9). Mud beds are comparatively thicker (2.8 ± 2.0) and are composed of fine or medium silt (Fig. 4.9). The deepest section recorded in the core is a 12 m layer of amalgamated sand beds (DAC-Drill, 34-46 m depth, Fig. 4.9). Overall, the abundance of mud (47.8%) and sand (52.2%) is roughly equal throughout the core (Table 4.2), though muddy units are concentrated in the upper half of the core profile (Fig. 4.9).

The stratigraphy at BTP contains considerably more sand in comparison to that of DAC (89.2% vs. 52.2% respectively, Table 4.2), as suggested by auger core results (Figs. 4.5, 4.7). Sand beds at BTP are relatively thick (5.7 ± 4.0 m), well sorted, and often display fining upward trends (e.g., BTP-Drill, 22-29 m depth, Fig. 4.9). Fine sand is the most common grain size of these beds, but lesser amounts of very fine and medium sand are also present (Table 4.2; Fig. 4.9). Mud beds are thin (1.5 ± 0.5 m) and relatively scarce throughout the stratigraphy (Fig. 4.9). The stratigraphy of KMK, like BTP, is dominantly composed of well-sorted fine and medium sands (combined = 80.9%, Table 4.2; Fig. 4.9). The primary difference between these two sites is that the stratigraphy of KMK exhibits a greater abundance of interspersed mud beds (7 at KMK

vs. 4 at BTP, Fig. 4.9), a quality that is also reflected in the overall proportion of mud in the stratigraphic profiles (19.1% at KMK vs. 10.8% at BTP, Table 4.2).

4.5. Discussion

4.5.1. Sedimentological trends across the TFT

Core data from point bars across the Gorai River TFT reveal three sedimentological and stratigraphic trends that reflect the relative influence of fluvial and tidal hydrodynamics and associated depositional processes. The three recognized trends correspond to: (1) down-core changes in grain size (2) the extent and type of bedding exhibited; and (3) the relative abundance of sand and mud preserved in the stratigraphy.

4.5.1.1. Down-core trends in grain size

Sediment cores collected from tide-dominated point bars (DAC and BTG) do not exhibit any consistent vertical changes in grain size, demonstrating fining-upward (BTG-A and BTG-U), coarsening-upward (DAC-D and DAC-A), and invariant trends (DAC-U and BTG-D) (Fig. 4.5). These observations are in line with conflicting reports in the literature of fining-upward (Brivio et al., 2016; Choi et al., 2004; Ethridge et al., 1987) and coarsening-upward (Johnson and Dashtgard, 2014; Sidi et al., 2003) successions occurring in tidal point bars. Detailed research on a tidal point bar in Venice Lagoon, Italy indicates that asymmetries in ebb- and flood-tide flow velocities can construct complex stratigraphic architecture, including the presence of fining- and coarsening-upward sequences in the same point bar (Ghinassi et al., 2018). We postulate that similar hydrodynamic conditions lead to the inconsistent down-core grain size trends observed in the present study (Fig. 4.5), especially in light of recent work demonstrating that the Ganges-Brahmaputra tidal delta plain is characterized by a tidal prism that is both seasonally and directionally asymmetric (Hale et al., 2019). Localized geomorphological elements, such as channel confluences, can also impact hydraulic conditions and resultant channel margin sedimentology (e.g., Best and Rhoads, 2008; Sambrook Smith et al., 2019). Both of the tidal point bars investigated in this study (DAC and BTG) are situated adjacent to major tidal channel

confluences (Fig. 4.1B), which may generate irregular hydrodynamic conditions (e.g., eddying and rapid flow reversals, Hale et al., *in press*) and stratal architecture. In the mixed tidal-fluvial realm, normal gradation is the primary vertical grain-size trend, occurring in 4 out of the 6 cores taken in this setting (KAL-A, KAL-U, BTP-D, and BTP-A, Fig. 4.7). Cores that did not display normal gradation (KAL-D and BTP-U, Fig. 4.7) were generally invariant with depth and may have exhibited normal grading if the cores were deep enough to reach the channel thalweg sands (see BTP-Drill, Fig. 4.9). Normal gradation is a common element of fluvial point bar depositional models and is attributed the progressive accumulation of finer overbank sediments over coarser thalweg sands as the channel migrates across the floodplain (e.g., Bridge, 2003; Clift et al., 2019; Ethridge et al., 1987; Jackson, 1976). Inherent to this model of formation is the notion that fluvial point bars are laterally mobile features, migrating over time through extension and down-valley translation (e.g., Ikeda, 1989; Largasse, 2004). Thus, the prevalence of normal grading in the KAL and BTP cores (Fig. 4.7), along with elevated rates of channel sinuosity and mobility (Fig. 4.4), suggests that fluvial processes are, at least in part, operating in this hydrologic domain. Likewise, cores from the fluvial realm almost exclusively demonstrate normal gradation, with the only exception being KMK-A, which shows reverse gradation (Fig. 4.8). The drill core from KMK contains multiple instances of m-scale fining-upward successions that may represent buried point bars (e.g., KMK-Drill, 8-13 m depth and 27-35 m depth, Fig. 4.9), suggesting that similar hydrodynamic conditions have persisted in this region for extended periods of time (*sensu* Goodbred et al., 2014).

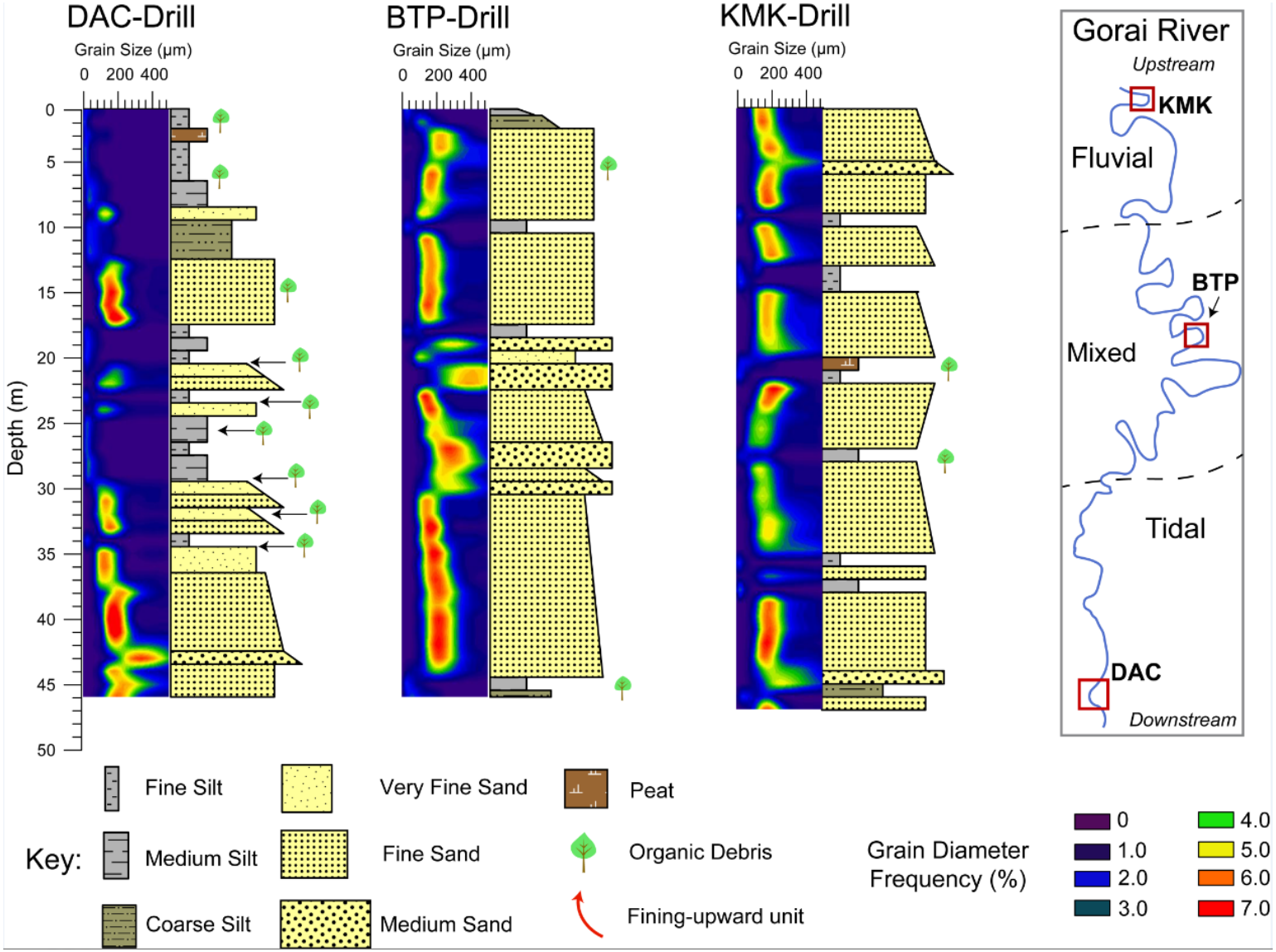

Fig. 4.9. Drill core stratigraphy at DAC, BTP, and KMK point bars, representing tidal, mixed tidal-fluvial, and fluvial depositional settings. Note the change in scale for core depth relative to cores shown in Figs. 4.5, 4.7, and 4.8.

Table 4.2. Grain size proportions for drill core locations.

TFT hydrodynamic conditions	Tide-dominated	Mixed tidal-fluvial	Fluvial-dominated
Drill core location/ Grain size (%)	DAC	BTP	KMK
Peat	2.2	0	2.1
Fine - medium silt (8-32 μm)	35.6	6.7	14.9
Coarse silt (32-63 μm)	6.7	4.4	2.1
Very fine sand (63-125 μm)	15.6	2.2	0
Fine sand (125-250 μm)	37.7	71.1	76.6
Medium sand (125-250 μm)	2.2	15.6	4.3
Grain size distribution		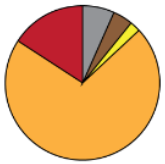	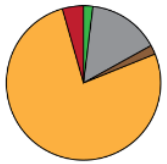
Sand : mud ratio	55.5 : 44.5	88.9 : 11.1	80.9 : 19.1

4.5.1.2. Progressive changes in bedding type

The stratigraphy of point bars in the tidal realm (DAC and BTG) appears to be composed of texturally homogeneous muds with no readily distinguishable bedding or sedimentary structures (Fig. 4.5). However, x-radiographs reveal the presence of rhythmic, mm-scale laminations of mud ("tidal rhythmites," Fig. 4.6), which reflect regular variations in hydraulic energy during the tidal cycle (e.g., Kvale, 2012). Tidal rhythmites are commonly observed in tide-influenced sedimentary features, including point bars (Choi et al., 2004; Dashtgard et al., 2012; Ethridge et al., 1987; Pearson and Gingras, 2006), in-channel bars (Johnson and Dashtgard, 2014), and channel fill deposits (Gugliotta et al., 2017; Wilson et al., 2017). The non-rhythmic, cm-scale beds observed in the x-radiograph of BTG (Fig. 4.6B) may have been deposited during time periods when tides are subordinate to river discharge, such as during the summer monsoon season. The preservation of original sedimentary fabric and low bioturbation index (BI = 0-2) at DAC and BTG (Fig. 4.6) suggest rapid sedimentation (e.g., Taylor et al., 2003) and a high degree of physiochemical stress (e.g., alternating fresh and saline water conditions, Gingras et al., 2011; Johnson and Dashtgard, 2014; Pearson and Gingras, 2006). These interpretations are in accordance with observational studies in the region documenting sediment accretion rates in excess of 1 cm/yr (Bomer et al., *in review*; Brown et al., 2018; Rogers et al., 2013) and seasonal differences in salinity of ~20 psu (Shaha and Cho, 2016).

Further upstream in the mixed tidal-fluvial realm, bedding becomes visually apparent and is characterized by cm- to dm-scale fining-upward packages that are irregularly spaced throughout the stratigraphy (Fig. 4.7). On the basis of their thickness, normal gradation, abrupt basal contacts, and non-rhythmic nature, we interpret that the deposition of these units is controlled by seasonal changes in fluvial discharge. Specifically, we propose that sandy beds are deposited during monsoon conditions while mud-rich beds are deposited during low flow conditions (i.e., dry season). Centimeter-scale sand beds (e.g., KAL-D, 1.75-1.80 m depth; Fig. 4.7) likely represent sedimentation from a single monsoon flood pulse, as supported by sediment tile accumulation measurements (Bomer et al., *in review*; Rogers et al., 2013). Sand beds on the

order of decimeters (e.g., BTP-D, 1.80-2.40 m depth; Fig. 4.7) may indicate the amalgamation of several monsoon flood deposits, a possible product of time periods when repeatedly strong flood pulses eroded fine-grained low-flow deposits (*sensu* Jablonski and Dalrymple, 2016). Mud-rich beds are homogeneous in texture (Figs. 4.7, 4.8) with the exception of intercalated organic detritus, a common constituent of slackwater flood deposits (Baker, 1987). Despite the presence of tides in the mixed tidal-fluvial realm (range ~ 0.5-2.0 m), any evidence of tidal influence in the stratigraphy has been completely overprinted by seasonal signals. This contrasts with findings in the Fraser River, where the co-presence of rhythmic and non-rhythmic heterolithic bedding was documented in point bars and in-channel bars in a mixed tidal-fluvial setting (Johnson and Dashtgard, 2014; Sisulak and Dashtgard, 2012). Stratigraphic differences between these locations may reflect the overall importance of seasonal (e.g., Gorai River) vs. tidal (e.g., Fraser River) hydrodynamic conditions throughout the respective systems, applying to each mixed tidal-fluvial zone.

The abundance and greater thickness (i.e., m-scale) of sand beds in the stratigraphy of the fluvial realm (Figs. 4.8, 4.9, Table 4.1) suggest that most suspended load sediments (e.g. silts and clays) bypass this reach of the river and are conveyed downstream to regions of lower hydraulic gradient (Figs. 4.2, 4.3). Although fining-upward packages are detected in volumetric frequency distributions of the fluvial cores (e.g., KMK-A, 1.0-1.35 m depth; Fig. 4.8), they are less commonly observed than in the mixed tidal-fluvial realm (Fig. 4.7), which may be due to the greater erosive potential of monsoonal flood flows in the upstream tract of the river. In other words, monsoon flood flows may winnow relatively fine sediments from the point bar surface, ultimately yielding clean, well-sorted sands and a homogeneous stratigraphic profile over time (Fig. 4.8, see also Bridge, 2003).

4.5.1.3. Relative abundance of sand and mud

Examination of grain size partitioning across the Gorai River TFT reveals that downstream changes in the relative proportions of sand and mud do not occur in a uniform manner, but rather exhibit two reaches with pronounced differences – the first occurring between

BTG and KAL, where sand content decreases from 26.9% to 2.3%, and the second occurring between MHP and KMK, where sand content decreases from 86.7% to 55.8% (Fig. 4.10; Table 4.1). We attribute the former shift in grain size to mass extraction of bedload sediments (i.e., sand) at the upstream limit of the backwater zone, which is situated immediately downstream of KAL (Figs. 4.3, 4.10). Backwater hydrodynamics have been shown to fundamentally influence sediment transport capacity in coastal rivers through the introduction of non-uniform water-flow conditions (e.g., Fernandes et al., 2016; Martin et al., 2018; Nittrouer, 2013; Nittrouer et al., 2012, 2011; Smith, 2012). For instance, Nittrouer (2013) demonstrated in the Mississippi River, USA that the rate of downstream fining of channel-bed sediments dramatically increases downstream of the backwater transition zone. We document a similar phenomenon in the present study wherein point bar sediments become notably coarser and sand-rich upstream of the backwater zone (Figs. 4.5, 4.7, 4.8, 4.9; Tables 4.1, 4.2). The spatial coincidence of the backwater transition and coarsening of channel-bank particle size holds important implications for modern and ancient fluvial-tidal rivers. First, the preferential sequestration of bedload sediments induced by the backwater suggests that this reach of the river is a site of facilitated deposition and thus may be susceptible to channel-bed aggradation over time. This notion is supported by bathymetric data indicating marked shallowing of the channel bed between BTG and KAL (Fig. 4.3). Second, many workers have hypothesized that channel-bed aggradation at the backwater dictates the location of avulsion nodes in fluvio-deltaic systems (Chadwick et al., 2019; Chatanantavet et al., 2012; Edmonds et al., 2009; Ganti et al., 2016; Jerolmack and Swenson, 2007).

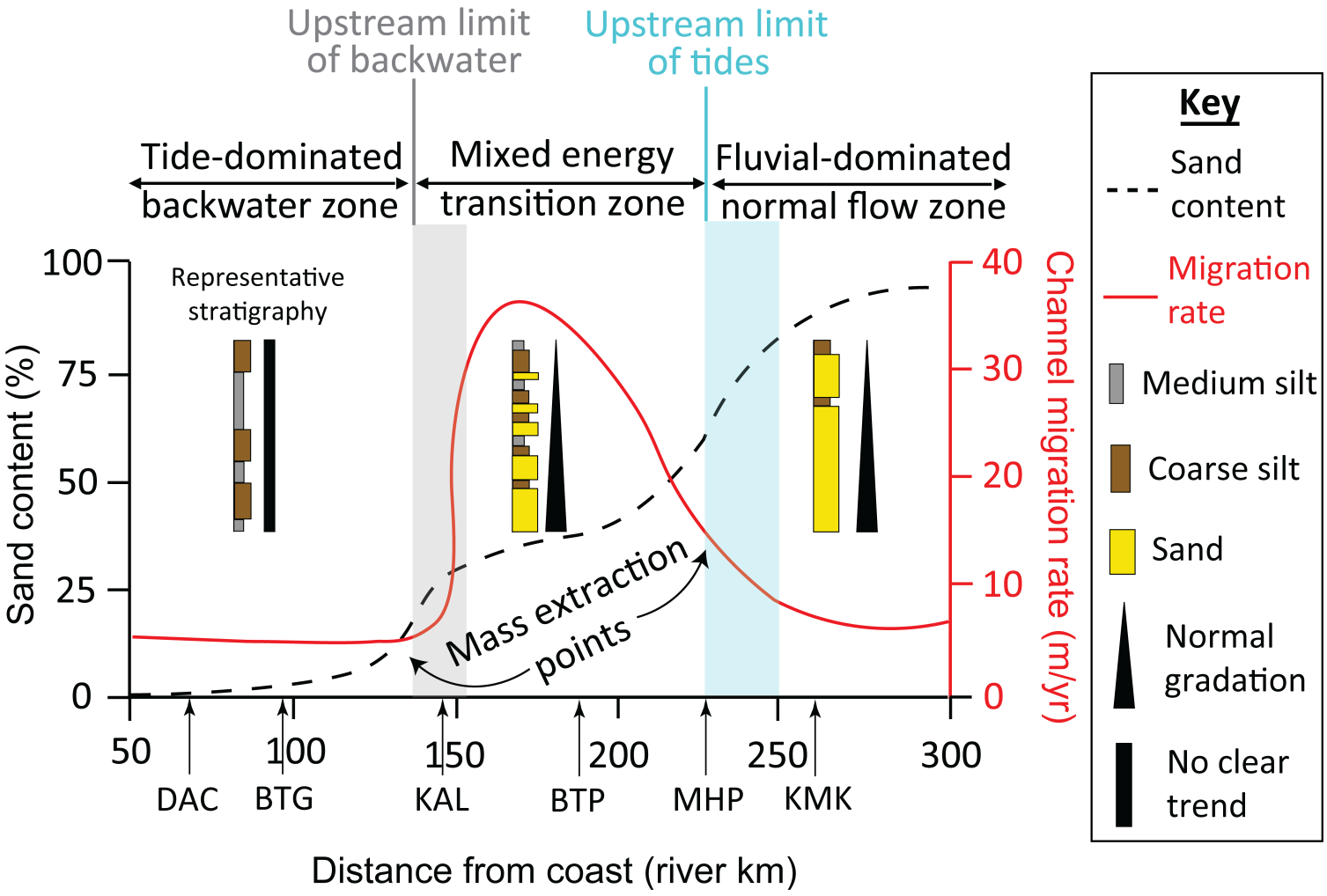

Fig. 4.10. Integrated depositional framework for the tidal to fluvial transition of the Gorai River with representative core profiles for each depositional zone. The upstream extents of the backwater and tidal influence are not singular points in space or time (e.g., Dalrymple and Choi, 2007), and as such, are represented as shaded envelopes. The gray shaded zone represents the backwater transition, where parts, but not all, of the channel bed is situated above mean sea level (see Fig. 4.3). The blue shaded zone represents the limit of tidal influence, which varies depending on seasonal conditions – in particular, the magnitude of fluvial discharge.

Although the Gorai River is not likely to avulse in the near future, we suggest that this may have occurred when the active lobe of the Ganges-Brahmaputra Delta occupied this region ~2000-4000 years before present (Allison et al., 2003). Third, spatially constraining the paleo-backwater zone in ancient fluvial and tidal depositional environments is useful for predicting the quality of channel fill and point bar hydrocarbon reservoirs (e.g., sand-mud ratio, lateral continuity of beds, porosity and permeability). In a recent example, Martin et al. (2018) generated amplitude extraction maps of interpreted channel belt horizons from a 3-D seismic dataset to identify the ancient planform geomorphology of the Triassic Mungaroo paleo-delta system. If a similar approach is taken, and the sediment source direction (i.e., provenance) can be determined (e.g., Cao et al., 2015), then the results of this study suggest that point bar deposits upstream of the paleo-backwater should be sought out to maximize the potential of encountering high-quality reservoir sands.

The second shift in grain size, occurring between MHP and KMK (Fig. 4.10, Table 4.1), is hypothesized to result from the landward extent of tidal influence. Similar to the backwater effect, non-uniform water flow conditions induced by tides (i.e., current reversals) are space- and time-dependent (e.g., Guo et al., 2015). Specifically, these hydraulic conditions only occur during landward-directed flood tides and are amplified during periods of low river discharge (e.g., Zhang et al., 2016). Although the most landward extent of tide-induced current reversals does not necessarily overlap with the limit of tidal influence (Gugliotta and Saito, 2019; La Croix and Dashtgard, 2015), the exceedingly low discharge of the Gorai River during the dry season (~10 m^3/s, compared to ~2000 m^3/s during the monsoon, Shaha and Cho, 2016) indicates that flood tides experience little resistance from fluvial forces and therefore likely induce changes in current direction near the tidal limit. Previous studies on sediment grain size partitioning in rivers

have examined microtidal systems (e.g., Mississippi River, Fernandes et al., 2016; Trinity River, Smith, 2012) to focus on the effects of the backwater and avert instances of non-uniform flow induced by tides. In these cases, one distinct shift in grain size was noted, which was coincident with the upstream limit of the backwater (e.g., Nittrouer, 2013). Based on the results of this study, we suggest that tide-influenced rivers may display two separate shifts in sediment grain size – the first occurring near the backwater and the second occurring near the landward extent of current reversals induced by tides (Fig. 4.10), with the expectation that the distance between these two sedimentological shifts is highly site-specific.

4.5.2. Channel morphodynamics across the TFT

The planform expression and recent (i.e., decadal) evolution of the Gorai River indicate a downstream-to-upstream pattern of channel morphodynamics characterized by: (i) non-sinuous and relatively immobile in the tidal realm, (ii) sinuous and mobile in the mixed tidal-fluvial realm, and (iii) sinuous and relatively immobile in the fluvial realm (Figs. 4.1, 4.4, 4.10). A similar "straight-meandering-straight" channel pattern was initially described by (Dalrymple et al., 1992) and is often associated with tide-dominated estuaries (Dalrymple and Choi, 2007). Although the Gorai River is not an estuary in a strict sense, it functions much like one during the dry season when water discharge is reduced to ~10 m^3/s (Shaha and Cho, 2016) and flood tides take precedence over ebb tides (Hale et al., 2019).

In the downstream tide-dominated depozone, uniformly low sinuosity and channel migration rates (Figs. 4.4, 4.10) likely result from a combination of factors inherent to this realm of the TFT, including relatively low hydraulic gradient and flow strength (Fig. 4.2; see also Bridge, 2003) and an abundance of fine-grained, cohesive sediments (Figs. 4.5, 4.9, 4.10; Tables 4.1, 4.2). Indeed, mud, which composes 98.8% of point bar sediments in the tidal realm (Table

4.1), has been shown to restrict lateral channel mobility both in physical experiments (e.g., Hoyal and Sheets, 2009; Li et al., 2017) and observational studies (e.g., Ikeda, 1989; Kolb, 1963; Orton and Reading, 1993; Tornqvist, 1993) owing to its relatively high critical shear stress (e.g., Mehta, 1991). Low channel sinuosity and mobility may also be ascribed to the predominance of tidal hydrodynamics (Hoitink et al., 2017; Lentsch et al., 2018). For instance, Lentsch et al. (2018) demonstrated through a series of physical delta models that distributary channel mobility systematically decreases as the ratio of tidal to fluvial energy increases. Enhanced channel stability in tide-dominated settings was attributed to channel deepening and sediment flushing via ebb tide-enhanced river flow (Lentsch et al., 2018). These findings are consistent with observations of the present study in that channel depth markedly increases (Fig. 4.3) while sinuosity and migration rates decrease downstream of KAL (Fig. 4.4), the reach of the Gorai River where tides are the predominant hydraulic force (EGIS, 2000).

An abrupt increase in channel mobility and sinuosity occurs immediately upstream of the tide-dominated realm and persists throughout the mixed tidal-fluvial realm (Figs. 4.4, 4.10). This shift in river kinematics coincides with the upstream limit of the backwater zone (Figs. 4.3, 4.4), suggesting an interconnected relationship among changes in hydrodynamics, bank sedimentology, and channel morphodynamics (e.g., Blum et al., 2013). In particular, we suggest that this marked change in channel mobility arises from backwater-induced modification of sediment composition and sediment storage (*sensu* Fernandes et al., 2016). At the upstream limit of the backwater (Fig. 4.3), the capture and preservation of non-cohesive sediments in channel margin bodies (Fig. 4.6, Table 4.1) facilitates bank erodibility and therefore channel mobility across the floodplain (Fig. 4.4; see also Orton and Reading, 1993). Augmented sediment storage and lateral building of point bars upstream of the backwater also drives fluvial erosion by

constricting channel flow and redirecting high-energy flows of the channel thalweg toward the cutbank (Hasegawa, 1989; Ikeda et al., 1981).

Stratigraphic profiles at KMK indicate an abundance of non-cohesive, sandy sediment (Figs. 4.8, 4.9, 4.10), a feature that presumably applies to channel banks upstream of KMK. Yet, lateral channel migration rates conspicuously decrease upstream of KMK to values similar to those of the tidal realm (Figs. 4.4B, 4.10). (EGIS, 2000) speculated that this relatively straight and immobile reach of the Gorai is caused by the older and more consolidated substrate of the upper Ganges floodplain. An alternative explanation for restricted channel mobility in this area could be an abundance of subsurface clay plugs that formed following meander cutoff and oxbow lake infilling. Indeed, similar upstream decreases in channel migration rates have also been observed in the Mississippi River and attributed to the abundance of clay plugs (Fisk, 1947; Hudson and Kesel, 2000). Deep drill cores from this study indicate nearly twice as many intercalated mud units in the stratigraphy of KMK when compared to BTP (Fig. 4.9). Similar findings have been noted in cores collected from the floodplain of the Gorai River (Goodbred et al., 2014). For example, a drill core taken at Magura, which is situated ~8 km southwest of KMK (see Fig. 4.1B for location), documented stratigraphy consisting of roughly equal proportions of channel sands and floodplain muds (Goodbred et al., 2014). In contrast, a drill core taken at Narail, located ~20 km southwest of BTP (see Fig. 4.1B for location), was almost exclusively composed of fine and medium sands (Goodbred et al., 2014; Wilson et al., 2017). Taken together, the similarities of the deep stratigraphic profiles immediately adjacent to the Gorai River (*this study*) and in the floodplain (Goodbred et al., 2014) suggest that if substrate composition is a primary control on channel morphology, then the morphodynamics should operate in a similar fashion as the river continues to shift over time.

6. Conclusions

Careful integration of remote sensing, river bathymetry, and core sedimentology and stratigraphy reveal insights on the processes that govern the tidal-fluvial transition of the Gorai River, southwest Bangladesh. The conclusions of this study are summarized as follows:

(1) The Gorai River can be divided into three tracts with distinct hydrodynamic and morphological properties: (i) a downstream tract dominated by meso-scale tides (range ~ 2-4 m) that exhibits uniformly low channel sinuosity and migration rates; (ii) a mixed tidal-fluvial tract affected by micro-scale tides (range < 2 m) and seasonal flood pulses that displays high channel sinuosity and migration rates; and (iii) an upstream tract dominated by fluvial processes with little to no tidal influence (range < 0.2 m) that demonstrates moderate channel sinuosity and low migration rates.

(2) Point bar sedimentary architecture differs substantially among the three depositional zones. Point bars from the tide-dominated depo-zone are characterized by cohesive muds with no readily discernable bedding and no consistent vertical (i.e., down-core) grain-size trends. However, x-radiographs reveal rhythmic, mm-scale laminations (tidal rhythmites) and occasional cm-scale beds. The stratigraphy of the mixed tidal-fluvial realm is primarily composed of non-rhythmic, cm- to dm-scale sand beds that are interbedded with dm-scale mud beds containing particulate organic matter. These sand beds, which display erosive basal contacts and fine upward, are interpreted to represent monsoonal flood deposits. In the fluvial depositional realm, point bars consist of dm- to m-scale sand beds interbedded with organic-rich mud and almost exclusively display normal gradation.

(3) Comparisons of river channel bathymetry with elevation control of the adjacent floodplain indicate that the channel bed approximates mean sea-level ~135 river-km inland of the coast. This location, also known as the upstream limit of the backwater zone, may be a site of accelerated in-channel deposition due to the introduction of non-uniform water-flow conditions and resultant sequestration of bedload sediments. The spatial coincidence of the backwater limit and shift in river channel morphology suggests

that this change in hydrodynamics may also locally influence the kinematics of the channel over time.

(4) Two pronounced shifts in point bar bulk sedimentology are observed along the course of the tide-influenced Gorai River: the first occurs between KAL and BTP and is spatially coincident with the upstream limit of the backwater zone (i.e., persistent non-uniform water-flow conditions); the second occurs between MHP and KMK and broadly coincides with the upstream limit of tidal influence (i.e., transient non-uniform water-flow conditions).

CHAPTER 5. SUMMARY AND CONCLUSIONS

Deltaic landscapes are inherently dynamic systems that have changed over time in response to processes such as eustasy, subsidence, river avulsions, and more recently, to anthropogenic alteration. In order to properly assess the present and future sustainability of these low-lying landforms it is critical to understand the sedimentary and hydrodynamic processes associated with the system and the products that they yield. Accordingly, the primary objective of this dissertation was to investigate the processes that influence the geomorphic evolution of the Ganges-Brahmaputra (G-B) Delta – from its downstream, tide-dominated zone to its upstream, fluvial dominated zone – and to place these findings within the context of coastal hazards, namely sea-level rise and lateral channel migration. The following paragraphs summarize the key findings and significance of the three studies that comprise this dissertation.

In Chapter 2, an array of rod surface elevation tables, sediment traps, and groundwater piezometers were utilized to provide longitudinal trends of sedimentation and elevation dynamics with respect to local hydroperiod in the Sundarbans mangrove forest, a relatively natural setting within the G-B tidal delta plain. The results of this work indicate that local rates of elevation gain greatly exceed the rate of relative sea-level rise and more closely approximate the rate of relative sea-level rise augmented by human-induced tidal amplification. This finding implies adaptation of the Sundarbans forest to extensive human modification of the G-B tidal channel network and hydrodynamics. Nonetheless, continued research in the G-B tidal delta plain, especially with respect to elevation dynamics in the embanked polder landscape and longitudinal changes in upstream sediment supply (e.g., decreases in sediment discharge from river damming), are needed to clarify whether the results of the present study apply throughout the delta and will feasibly continue into the future.

Chapter 3 examined the relative impacts of physical and biological subsurface processes on surface elevation change in the Sundarbans mangrove forest, specifically within the uppermost meter of the soil profile (i.e., the "live root zone"). Although physical subsurface processes (e.g., seasonal changes in pore water content and porosity) are expected to control elevation dynamics in mineral-rich deltaic systems like the Sundarbans, this study demonstrated that biological processes, notably soil oxidation during the dry season, also govern seasonal and interannual surface evolution. This study also quantified rates of soil carbon accumulation in the Sundarbans, demonstrating that locally high rates of sediment accumulation can compensate for organic-poor soil quality, ultimately yielding carbon accumulation rates on par with mangrove forests with comparably organic-rich soils (e.g., peaty mangrove forests of Oceania and the Caribbean).

Chapter 4 investigated the interaction of stratigraphy and channel dynamics across the tidal-fluvial transition of the Gorai River, a major distributary of the Ganges that flows through southwest Bangladesh. Through the integration of multiple datasets – including core sedimentology, channel bathymetry, and remote sensing – results from this work reveal coincident, abrupt shifts in river channel morphology and sediment character that may be controlled by hydrodynamic shifts, such as the backwater zone and the limit of tidal influence. Specifically, lateral channel mobility (i.e., channel sinuosity and migration rates) is considerably higher in a section of the river that lies roughly between the upstream limit of the backwater zone and the upstream limit of tidal influence. Similar findings have been documented in the Mississippi River, USA, but additional studies, especially those in tide-influenced rivers, are necessary to determine whether these trends are site-specific or widespread.

Taken together, the proceedings of this dissertation underscore the robust nature of the Sundarbans, and possibly other pristine deltaic settings, in the face of human-induced modification of the natural environment (e.g., accelerated sea-level rise from embankment construction). Results from this dissertation demonstrate that deltas do not passively drown in response to rising water levels; rather, they adapt through processes such as increased sediment deposition with greater hydroperiods. However, the lifeblood of a river delta is sediment, and without continued sediment delivery, the existence of deltas and the valuable ecosystems that they foster is placed in jeopardy. Preservation measures in the greater G-B system, as well as in other deltas worldwide, would benefit by maintaining natural sediment delivery from upstream catchments.

REFERENCES

Ahmad, N., 1968. Economic geography of East Pakistan. Oxford University Press, London, UK.

Alam, M., 1996. Subsidence of the Ganges—Brahmaputra Delta of Bangladesh and Associated Drainage, Sedimentation and Salinity Problems, in: Milliman, J.D., Haq, B.U. (Eds.), Sea-Level Rise and Coastal Subsidence: Causes, Consequences, and Strategies, Coastal Systems and Continental Margins. Springer Netherlands, Dordrecht, pp. 169–192. https://doi.org/10.1007/978-94-015-8719-8_9

Alberts-Hubatsch, H., Lee, S.Y., Meynecke, J.-O., Diele, K., Nordhaus, I., Wolff, M., 2016. Life-history, movement, and habitat use of Scylla serrata (Decapoda, Portunidae): current knowledge and future challenges. Hydrobiologia 763, 5–21. https://doi.org/10.1007/s10750-015-2393-z

Allison, M., Kepple, E., 2001. Modern sediment supply to the lower delta plain of the Ganges-Brahmaputra River in Bangladesh. Geo-Mar. Lett. 21, 66–74. https://doi.org/10.1007/s003670100069

Allison, M.A., 1998. Geologic Framework and Environmental Status of the Ganges-Brahmaputra Delta. J. Coast. Res. 14.

Allison, M.A., Khan, S.R., Goodbred, S.L., Kuehl, S.A., 2003. Stratigraphic evolution of the late Holocene Ganges–Brahmaputra lower delta plain. Sediment. Geol. 155, 317–342. https://doi.org/10.1016/S0037-0738(02)00185-9

Alongi, D.M., 2012. Carbon sequestration in mangrove forests. Carbon Manag. 3, 313–322. https://doi.org/10.4155/cmt.12.20

Alongi, D.M., 2008. Mangrove forests: Resilience, protection from tsunamis, and responses to global climate change. Estuar. Coast. Shelf Sci. 76, 1–13. https://doi.org/10.1016/j.ecss.2007.08.024

Aucour, A.-M., France-Lanord, C., Pedoja, K., Pierson-Wickmann, A.-C., Sheppard, S.M.F., 2006. Fluxes and sources of particulate organic carbon in the Ganga-Brahmaputra river system: ORGANIC CARBON FLUXES IN GANGA-BRAHMAPUTRA. Glob. Biogeochem. Cycles 20, 1–12. https://doi.org/10.1029/2004GB002324

Auerbach, L.W., Goodbred Jr, S.L., Mondal, D.R., Wilson, C.A., Ahmed, K.R., Roy, K., Steckler, M.S., Small, C., Gilligan, J.M., Ackerly, B.A., 2015a. Flood risk of natural and embanked landscapes on the Ganges–Brahmaputra tidal delta plain. Nat. Clim. Change 5, 153–157. https://doi.org/10.1038/nclimate2472

Auerbach, L.W., Goodbred Jr, S.L., Mondal, D.R., Wilson, C.A., Ahmed, K.R., Roy, K., Steckler, M.S., Small, C., Gilligan, J.M., Ackerly, B.A., 2015b. Reply to “Tidal river

management in Bangladesh." Nat. Clim. Change 5, 492. https://doi.org/10.1038/nclimate2472

Baker, V.R., 1987. Paleoflood hydrology and extraordinary flood events. J. Hydrol. 96, 79–99. https://doi.org/10.1016/0022-1694(87)90145-4

Bandaranayake, W.M., 1998. Traditional and medicinal uses of mangroves. Mangroves Salt Marshes 2, 133–148. https://doi.org/10.1023/A:1009988607044

Barua, D.K., 1990. Suspended sediment movement in the estuary of the Ganges-Brahmaputra-Meghna river system. Mar. Geol. 91, 243–253. https://doi.org/10.1016/0025-3227(90)90039-M

Barua, D.K., Kuehl, S.A., Miller, R.L., Moore, W.S., 1994. Suspended sediment distribution and residual transport in the coastal ocean off the Ganges-Brahmaputra river mouth. Mar. Geol. 120, 41–61. https://doi.org/10.1016/0025-3227(94)90076-0

BBS, 2011. Population and Housing Census 2011. Bangladesh Bureau of Statistics.

Best, J.L., Rhoads, B.L., 2008. Sediment Transport, Bed Morphology and the Sedimentology of River Channel Confluences, in: Rice, S.P., Roy, A.G., Rhoads, B.L. (Eds.), River Confluences, Tributaries and the Fluvial Network. John Wiley & Sons, Ltd, Chichester, UK, pp. 45–72. https://doi.org/10.1002/9780470760383.ch4

Bird, M.I., Fifield, L.K., Chua, S., Goh, B., 2004. Calculating Sediment Compaction for Radiocarbon Dating of Intertidal Sediments. Radiocarbon 46, 421–435. https://doi.org/10.1017/S0033822200039734

BIWTA, (Bangladesh Inland Water Transportation Authority), 2019. Bangladesh tide tables, 2019.

Blum, M., Martin, J., Milliken, K., Garvin, M., 2013. Paleovalley systems: Insights from Quaternary analogs and experiments. Earth-Sci. Rev. 116, 128–169. https://doi.org/10.1016/j.earscirev.2012.09.003

Blum, M.D., Roberts, H.H., 2009. Drowning of the Mississippi Delta due to insufficient sediment supply and global sea-level rise. Nat. Geosci. 2, 488–491. https://doi.org/10.1038/ngeo553

BMD, 2016. Normal monthly rainfall. Bangladesh Meteorological Department.

Boadu, F.K., 2000. Hydraulic conductivity of soils from grain-size distribution: new models. Journal of Geotechnical and Geoenvironmental Engineering, 126(8), pp.739-746.

Boivin, P., Garnier, P., Tessier, D., 2004. Relationship between Clay Content, Clay Type, and Shrinkage Properties of Soil Samples. Soil Sci. Soc. Am. J. 68, 1145. https://doi.org/10.2136/sssaj2004.1145

Bomer, E.J., Wilson, C.A., Hale, R.P., Hossain, A.N.M., Rahman, F.M.A., in review. Surface elevation and sedimentation dynamics in the Ganges-Brahmaputra tidal delta plain, Bangladesh: evidence for mangrove adaptation to human-induced hydrological distubances. Catena.

Bomer, E.J., Wilson, C.A., Quirk, T., 2019. Belowground controls on surface elevation change and carbon sequestration potential of the Sundarbans Mangrove Forest, Bangladesh. Society of Wetland Scientists Annual Meeting, Baltimore, MD.

Brammer, H., 2004. Can Bangladesh be protected from floods? University Press, Dhaka.

Bridge, J.S., 2003. Rivers and floodplains: forms, processes, and sedimentary record. Blackwell Pub, Oxford, UK.

Brinson, M.M., Lugo, A.E., Brown, S., 1981. Primary Productivity, Decomposition and Consumer Activity in Freshwater Wetlands. Annu. Rev. Ecol. Syst. 12, 123–161. https://doi.org/10.1146/annurev.es.12.110181.001011

Brivio, L., Ghinassi, M., D'Alpaos, A., Finotello, A., Fontana, A., Roner, M., Howes, N., 2016. Aggradation and lateral migration shaping geometry of a tidal point bar: An example from salt marshes of the Northern Venice Lagoon (Italy). Sediment. Geol. 343, 141–155. https://doi.org/10.1016/j.sedgeo.2016.08.005

Brown, K.F., Hale, R.P., Datta, D.K., Datta, S.B., 2018. Persistence of depositional features in a strongly seasonal, tide-dominated delta. American Geophysical Union Fall Meeting, Washington D.C.

Brown, S., Nicholls, R.J., 2015. Subsidence and human influences in mega deltas: The case of the Ganges–Brahmaputra–Meghna. Sci. Total Environ. 527–528, 362–374. https://doi.org/10.1016/j.scitotenv.2015.04.124

Cahoon, D.R., 2015. Estimating Relative Sea-Level Rise and Submergence Potential at a Coastal Wetland. Estuaries Coasts 38, 1077–1084. https://doi.org/10.1007/s12237-014-9872-8

Cahoon, D.R., Hensel, P., Rybczyk, J., McKee, K.L., Proffitt, C.E., Perez, B.C., 2003. Mass tree mortality leads to mangrove peat collapse at Bay Islands, Honduras after Hurricane Mitch. J. Ecol. 91, 1093–1105. https://doi.org/10.1046/j.1365-2745.2003.00841.x

Cahoon, D.R., Hensel, P.F., Spencer, T., Reed, D.J., McKee, K.L., Saintilan, N., 2006. Coastal Wetland Vulnerability to Relative Sea-Level Rise: Wetland Elevation Trends and Process Controls, in: Verhoeven, J.T.A., Beltman, B., Bobbink, R., Whigham, D.F. (Eds.),

Wetlands and Natural Resource Management. Springer Berlin Heidelberg, pp. 271–292. https://doi.org/10.1007/978-3-540-33187-2_12

Cahoon, D.R., Lynch, J.C., 1997. Vertical accretion and shallow subsidence in a mangrove forest of southwestern Florida, U.S.A. Mangroves Salt Marshes 1, 173–186. https://doi.org/10.1023/A:1009904816246

Cahoon, D.R., Lynch, J.C., Perez, B.C., Segura, B., Holland, R.D., Stelly, C., Stephenson, G., Hensel, P., 2002. High-Precision Measurements of Wetland Sediment Elevation: II. The Rod Surface Elevation Table. J. Sediment. Res. 72, 734–739. https://doi.org/10.1306/020702720734

Cahoon, D.R., Perez, B.C., Segura, B.D., Lynch, J.C., 2011. Elevation trends and shrink–swell response of wetland soils to flooding and drying. Estuar. Coast. Shelf Sci. 91, 463–474. https://doi.org/10.1016/j.ecss.2010.03.022

Cahoon, D.R., Reed, D.J., Day, J.W., 1995. Estimating shallow subsidence in microtidal salt marshes of the southeastern United States: Kaye and Barghoorn revisited. Mar. Geol. 128, 1–9. https://doi.org/10.1016/0025-3227(95)00087-F

Cahoon, D.R., Turner, R.E., 1989. Accretion and Canal Impacts in a Rapidly Subsiding Wetland II. Feldspar Marker Horizon Technique. Estuaries 12, 260. https://doi.org/10.2307/1351905

Cameron, C.C., Palmer, C.A., 1995. The mangrove peat of the Tobacco Range Islands, Belize Barrier Reef, Central America 35.

Cao, L., Jiang, T., Wang, Z., Zhang, Y., Sun, H., 2015. Provenance of Upper Miocene sediments in the Yinggehai and Qiongdongnan basins, northwestern South China Sea: Evidence from REE, heavy minerals and zircon U–Pb ages. Mar. Geol. 361, 136–146. https://doi.org/10.1016/j.margeo.2015.01.007

Carter, M.R., Gregorich, E.G. (Eds.), 2008. Soil sampling and methods of analysis, 2nd ed. ed. Canadian Society of Soil Science ; CRC Press, [Pinawa, Manitoba] : Boca Raton, FL.

Cazenave, A., Lombard, A., Llovel, W., 2008. Present-day sea level rise: A synthesis. Comptes Rendus Geosci. 340, 761–770. https://doi.org/10.1016/j.crte.2008.07.008

Chadwick, A.J., Lamb, M.P., Moodie, A.J., Parker, G., Nittrouer, J.A., 2019. Origin of a Preferential Avulsion Node on Lowland River Deltas. Geophys. Res. Lett. 46, 4267–4277. https://doi.org/10.1029/2019GL082491

Chamberlain, E.L., Goodbred, S.L., Hale, R., Steckler, M.S., Wallinga, J., Wilson, C., 2019. Integrating geochronologic and instrumental approaches across the Bengal Basin: Integrating geochronologic and instrumental approaches. Earth Surf. Process. Landf. https://doi.org/10.1002/esp.4687

Chatanantavet, P., Lamb, M.P., Nittrouer, J.A., 2012. Backwater controls of avulsion location on deltas: Backwater controls on delta avulsion. Geophys. Res. Lett. 39, n/a-n/a. https://doi.org/10.1029/2011GL050197

Chmura, G.L., Anisfeld, S.C., Cahoon, D.R., Lynch, J.C., 2003. Global carbon sequestration in tidal, saline wetland soils. Glob. Biogeochem. Cycles 17. https://doi.org/10.1029/2002GB001917

Choi, K.S., Dalrymple, R.W., Chun, S.S., Kim, S.-P., 2004. Sedimentology of Modern, Inclined Heterolithic Stratification (IHS) in the Macrotidal Han River Delta, Korea. J. Sediment. Res. 74, 677–689. https://doi.org/10.1306/030804740677

Chow, V.T., 2009. Open-channel hydraulics. Blackburn Press, Caldwell, NJ.

Church, J.A., Clark, P.U., Cazenave, A., Gregory, J.M., Jevrejeva, S., Levermann, A., Merrifield, M.A., Milne, G.A., Nerem, R.S., Nunn, P.D., Payne, A.J., Pfeffer, W.T., Stammer, D., Unnikrishnan, A.S., 2013. Sea-Level Rise by 2100. Science 342, 1445–1445. https://doi.org/10.1126/science.342.6165.1445-a

Church, J.A., White, N.J., 2006. A 20th century acceleration in global sea-level rise: An acceleration in global sea-level rise. Geophys. Res. Lett. 33, n/a-n/a. https://doi.org/10.1029/2005GL024826

Clift, P.D., Olson, E.D., Lechnowskyj, A., Moran, M.G., Barbato, A., Lorenzo, J.M., 2019. Grain-size variability within a mega-scale point-bar system, False River, Louisiana. Sedimentology 66, 408–434. https://doi.org/10.1111/sed.12528

Coleman, J.M., 1969. Brahmaputra river: Channel processes and sedimentation. Sediment. Geol. 3, 129–239. https://doi.org/10.1016/0037-0738(69)90010-4

Czarnecki, J.M., Dashtgard, S.E., Pospelova, V., Mathewes, R.W., MacEachern, J.A., 2014. Palynology and geochemistry of channel-margin sediments across the tidal–fluvial transition, lower Fraser River, Canada: Implications for the rock record. Mar. Pet. Geol. 51, 152–166. https://doi.org/10.1016/j.marpetgeo.2013.12.008

Dalrymple, R.W., Choi, K., 2007. Morphologic and facies trends through the fluvial–marine transition in tide-dominated depositional systems: A schematic framework for environmental and sequence-stratigraphic interpretation. Earth-Sci. Rev. 81, 135–174. https://doi.org/10.1016/j.earscirev.2006.10.002

Dalrymple, R.W., Kurcinka, C.E., Jablonski, B.V.J., Ichaso, A.A., Mackay, D.A., 2015. Deciphering the relative importance of fluvial and tidal processes in the fluvial–marine transition, in: Developments in Sedimentology. Elsevier, pp. 3–45. https://doi.org/10.1016/B978-0-444-63529-7.00002-X

Dalrymple, R.W., Zaitlin, B.A., Boyd, R., 1992. Estuarine facies models: Conceptual basis and stratigraphic implications. J. Sediment. Res. 62, 1330–1146.

Danielsen, F., 2005. The Asian Tsunami: A Protective Role for Coastal Vegetation. Science 310, 643–643. https://doi.org/10.1126/science.1118387

Das, S., Vincent, J.R., 2009. Mangroves protected villages and reduced death toll during Indian super cyclone. Proc. Natl. Acad. Sci. 106, 7357–7360. https://doi.org/10.1073/pnas.0810440106

Das, T.K., Haldar, S.K., Das Gupta, I., Sen, S., 2014. River Bank Erosion Induced Human Displacement and Its Consequences. Living Rev. Landsc. Res. 8. https://doi.org/10.12942/lrlr-2014-3

Dashtgard, S.E., Venditti, J.G., Hill, P.R., Sisulak, C.F., Johnson, S.M., LaCroix, A.D., 2012. Sedimentation across the Tidal-Fluvial Transition in the Lower Fraser River, Canada. Sediment. Rec. 10, 4–9. https://doi.org/10.2110/sedred.2012.4.4

Day, J.W., Boesch, D.F., Clairain, E.J., Kemp, G.P., Laska, S.B., Mitsch, W.J., Orth, K., Mashriqui, H., Reed, D.J., Shabman, L., Simenstad, C.A., Streever, B.J., Twilley, R.R., Watson, C.C., Wells, J.T., Whigham, D.F., 2007. Restoration of the Mississippi Delta: Lessons from Hurricanes Katrina and Rita. Science 315, 1679–1684. https://doi.org/10.1126/science.1137030

Day, J.W., Britsch, L.D., Hawes, S.R., Shaffer, G.P., Reed, D.J., Cahoon, D., 2000. Pattern and process of land loss in the Mississippi Delta: A Spatial and temporal analysis of wetland habitat change. Estuaries 23, 425–438. https://doi.org/10.2307/1353136

Day, J.W., Rybczyk, J., Scarton, F., Rismondo, A., Are, D., Cecconi, G., 1999. Soil Accretionary Dynamics, Sea-Level Rise and the Survival of Wetlands in Venice Lagoon: A Field and Modelling Approach. Estuar. Coast. Shelf Sci. 49, 607–628. https://doi.org/10.1006/ecss.1999.0522

Díez-Canseco, D., Buatois, L.A., Mángano, M.G., Rodriguez, W., Solorzano, E., 2015. The ichnology of the fluvial–tidal transition, in: Developments in Sedimentology. Elsevier, pp. 283–321. https://doi.org/10.1016/B978-0-444-63529-7.00009-2

Donato, D.C., Kauffman, J.B., Murdiyarso, D., Kurnianto, S., Stidham, M., Kanninen, M., 2011. Mangroves among the most carbon-rich forests in the tropics. Nat. Geosci. 4, 293–297. https://doi.org/10.1038/ngeo1123

Duarte, C.M., Middelburg, J.J., Caraco, N., 2004. Major role of marine vegetation on the oceanic carbon cycle. Biogeosciences Discuss. 1, 659–679.

Edmonds, D.A., Hoyal, D.C.J.D., Sheets, B.A., Slingerland, R.L., 2009. Predicting delta avulsions: Implications for coastal wetland restoration. Geology 37, 759–762. https://doi.org/10.1130/G25743A.1

EGIS, (Environmental Geographical Information Systems), 2000. Environmental baseline of Gorai River restoration project, EGIS-II. Bangladesh Water Development Board, Ministry of Water Resources, Government of Bangladesh, Delft, The Netherlands.

Ellison, A.M., Mukherjee, B.B., Karim, A., 2000. Testing patterns of zonation in mangroves: scale dependence and environmental correlates in the Sundarbans of Bangladesh: Patterns of zonation in mangroves. J. Ecol. 88, 813–824. https://doi.org/10.1046/j.1365-2745.2000.00500.x

Ellison, J.C., 1993. Mangrove Retreat with Rising Sea-level, Bermuda. Estuar. Coast. Shelf Sci. 37, 75–87. https://doi.org/10.1006/ecss.1993.1042

Ellison, J.C., Stoddart, D.R., 1991. Mangrove Ecosystem. Collapse During Predicted Sea-Level Rise: Holocene Analogues and Implications. J. Coast. Res. 7, 15.

Ethridge, F.G., Flores, R.M., Harvey, M.D. (Eds.), 1987. Recent Developments in Fluvial Sedimentology. SEPM (Society for Sedimentary Geology). https://doi.org/10.2110/pec.87.39

FAO, 2007. The world's mangroves 1980-2005 (FAO Forestry Paper). Food and Agricultural Organization of the United Nations.

Farr, T.G., Rosen, P.A., Caro, E., Crippen, R., Duren, R., Hensley, S., Kobrick, M., Paller, M., Rodriguez, E., Roth, L., Seal, D., 2007. The shuttle radar topography mission. Rev. Geophys. 45.

Feldman, H., Demko, T., 2015. Chapter 13 - Recognition and prediction of petroleum reservoirs in the fluvial/tidal transition, in: Ashworth, P.J., Best, J.L., Parsons, D.R. (Eds.), Developments in Sedimentology, Fluvial-Tidal Sedimentology. Elsevier, pp. 483–528. https://doi.org/10.1016/B978-0-444-63529-7.00014-6

Fernandes, A.M., Smith, V.B., Mason, K.G., 2018. Backwater Controls on the Sedimentology, Kinematics and Geometry of Bar Deposits in Coastal Rivers (preprint). EarthArXiv. https://doi.org/10.31223/osf.io/mpw2f

Fernandes, A.M., Törnqvist, T.E., Straub, K.M., Mohrig, D., 2016. Connecting the backwater hydraulics of coastal rivers to fluvio-deltaic sedimentology and stratigraphy. Geology 44, 979–982. https://doi.org/10.1130/G37965.1

Finotello, A., Lanzoni, S., Ghinassi, M., Marani, M., Rinaldo, A., D'Alpaos, A., 2018. Field migration rates of tidal meanders recapitulate fluvial morphodynamics. Proc. Natl. Acad. Sci. 115, 1463–1468. https://doi.org/10.1073/pnas.1711330115

Fisk, H.N., 1952. Geological investigation of the Atchafalaya Basin and problems of Mississippi River diversions. Mississippi River Commission, US Army Corps of Engineers, Vicksburg, Mississippi, USA.

Fisk, H.N., 1947. Fine-grained alluvial deposits and their effects on Mississippi River activity (Mississippi River Commission). USACE, Vicksburg, Mississippi.

Flood, R.P., Barr, I.D., Weltje, G.J., Roberson, S., Russell, M.I., Meneely, J., Orford, J.D., 2018. Provenance and depositional variability of the Thin Mud Facies in the lower Ganges-Brahmaputra delta, West Bengal Sundarbans, India. Mar. Geol. 395, 198–218. https://doi.org/10.1016/j.margeo.2017.09.001

Fourqurean, J.W., Duarte, C.M., Kennedy, H., Marbà, N., Holmer, M., Mateo, M.A., Apostolaki, E.T., Kendrick, G.A., Krause-Jensen, D., McGlathery, K.J., Serrano, O., 2012. Seagrass ecosystems as a globally significant carbon stock. Nat. Geosci. 5, 505–509. https://doi.org/10.1038/ngeo1477

Fredlund, M.D., Wilson, G.W., Fredlund, D.G., 2002. Use of the grain-size distribution for estimation of the soil-water characteristic curve. Can. Geotech. J. 39, 1103–1117. https://doi.org/10.1139/t02-049

Fu, H., Wang, W., Ma, W., Wang, M., 2018. Differential in surface elevation change across mangrove forests in the intertidal zone. Estuar. Coast. Shelf Sci. 207, 203–208. https://doi.org/10.1016/j.ecss.2018.03.025

Furukawa, K., Wolanski, E., 1996. Sedimentation in Mangrove Forests. Mangroves Salt Marshes 1, 3–10. https://doi.org/10.1023/A:1025973426404

Furukawa, K., Wolanski, E., Mueller, H., 1997. Currents and Sediment Transport in Mangrove Forests. Estuar. Coast. Shelf Sci. 44, 301–310. https://doi.org/10.1006/ecss.1996.0120

Gagliano, S.M., Meyer-Arendt, K.J., Wicker, K.M., 1981. Land Loss in the Mississippi River Deltaic Plain 31.

Galy, V., France-Lanord, C., Beyssac, O., Faure, P., Kudrass, H., Palhol, F., 2007. Efficient organic carbon burial in the Bengal fan sustained by the Himalayan erosional system. Nature 450, 407–410. https://doi.org/10.1038/nature06273

Ganti, V., Chadwick, A.J., Hassenruck-Gudipati, H.J., Fuller, B.M., Lamb, M.P., 2016. Experimental river delta size set by multiple floods and backwater hydrodynamics. Sci. Adv. 2, e1501768. https://doi.org/10.1126/sciadv.1501768

Ganti, V., Chu, Z., Lamb, M.P., Nittrouer, J.A., Parker, G., 2014. Testing morphodynamic controls on the location and frequency of river avulsions on fans versus deltas: Huanghe

(Yellow River), China: Avulsion drivers on fans versus deltas. Geophys. Res. Lett. 41, 7882–7890. https://doi.org/10.1002/2014GL061918

Gesch, D.B., 2009. Analysis of Lidar Elevation Data for Improved Identification and Delineation of Lands Vulnerable to Sea-Level Rise. J. Coast. Res. 49–58. https://doi.org/10.2112/SI53-006.1

Ghinassi, M., D'alpaos, A., Gasparotto, A., Carniello, L., Brivio, L., Finotello, A., Roner, M., Franceschinis, E., Realdon, N., Howes, N., Cantelli, A., 2018. Morphodynamic evolution and stratal architecture of translating tidal point bars: Inferences from the northern Venice Lagoon (Italy). Sedimentology 65, 1354–1377. https://doi.org/10.1111/sed.12425

Ghosh, P.B., Singh, B.N., Chakrabarty, C., Saha, A., Das, R.L., Choudhury, A., 1990. Mangrove Litter Production In A Tidal Creek Of Lothian Island Of Sundarbans, India. IJMS Vol194 Dec. 1990.

Gilman, E.L., Ellison, J., Duke, N.C., Field, C., 2008. Threats to mangroves from climate change and adaptation options: A review. Aquat. Bot., Mangrove Ecology – Applications in Forestry and Costal Zone Management 89, 237–250. https://doi.org/10.1016/j.aquabot.2007.12.009

Gingras, M.K., MacEachern, J.A., Dashtgard, S.E., 2011. Process ichnology and the elucidation of physico-chemical stress. Sediment. Geol. 237, 115–134. https://doi.org/10.1016/j.sedgeo.2011.02.006

Giri, C., Pengra, B., Zhu, Z., Singh, A., Tieszen, L.L., 2007. Monitoring mangrove forest dynamics of the Sundarbans in Bangladesh and India using multi-temporal satellite data from 1973 to 2000. Estuar. Coast. Shelf Sci. 73, 91–100. https://doi.org/10.1016/j.ecss.2006.12.019

Giri, S., Mukhopadhyay, A., Hazra, S., Mukherjee, S., Roy, D., Ghosh, S., Ghosh, T., Mitra, D., 2014. A study on abundance and distribution of mangrove species in Indian Sundarban using remote sensing technique. J. Coast. Conserv. 18, 359–367. https://doi.org/10.1007/s11852-014-0322-3

Godin, G., 1999. The Propagation of Tides up Rivers With Special Considerations on the Upper Saint Lawrence River. Estuar. Coast. Shelf Sci. 48, 307–324. https://doi.org/10.1006/ecss.1998.0422

Goodbred Jr, S.L., Ayers, J.C., Baroud, H., Gilligan, J.M., Passalacqua, P., Overeem, I., Wilson, C.A., 2016. Multi-scale modeling and observations of landscape dynamics, mass balance, and network connectivity for a sustainable Ganges-Brahmaputra delta (NSF Coastal SEES Collaborative Research Proposal).

Goodbred, S.L., Kuehl, S.A., 2000. The significance of large sediment supply, active tectonism, and eustasy on margin sequence development: Late Quaternary stratigraphy and

evolution of the Ganges–Brahmaputra delta. Sediment. Geol. 133, 227–248. https://doi.org/10.1016/S0037-0738(00)00041-5

Goodbred, S.L., Paolo, P.M., Ullah, M.S., Pate, R.D., Khan, S.R., Kuehl, S.A., Singh, S.K., Rahaman, W., 2014. Piecing together the Ganges-Brahmaputra-Meghna River delta: Use of sediment provenance to reconstruct the history and interaction of multiple fluvial systems during Holocene delta evolution. Geol. Soc. Am. Bull. 126, 1495–1510. https://doi.org/10.1130/B30965.1

Goodbred, S.L., Saito, Y., 2012. Tide-Dominated Deltas, in: Davis Jr., R.A., Dalrymple, R.W. (Eds.), Principles of Tidal Sedimentology. Springer Netherlands, Dordrecht, pp. 129–149. https://doi.org/10.1007/978-94-007-0123-6_7

Grall, C., Steckler, M.S., Pickering, J.L., Goodbred, S., Sincavage, R., Paola, C., Akhter, S.H., Spiess, V., 2018. A base-level stratigraphic approach to determining Holocene subsidence of the Ganges–Meghna–Brahmaputra Delta plain. Earth Planet. Sci. Lett. 499, 23–36. https://doi.org/10.1016/j.epsl.2018.07.008

Gugliotta, M., Kurcinka, C.E., Dalrymple, R.W., Flint, S.S., Hodgson, D.M., 2016. Decoupling seasonal fluctuations in fluvial discharge from the tidal signature in ancient deltaic deposits: an example from the Neuquén Basin, Argentina. J. Geol. Soc. 173, 94–107. https://doi.org/10.1144/jgs2015-030

Gugliotta, M., Saito, Y., 2019. Matching trends in channel width, sinuosity, and depth along the fluvial to marine transition zone of tide-dominated river deltas: The need for a revision of depositional and hydraulic models. Earth-Sci. Rev. 191, 93–113. https://doi.org/10.1016/j.earscirev.2019.02.002

Gugliotta, M., Saito, Y., Nguyen, V.L., Ta, T.K.O., Nakashima, R., Tamura, T., Uehara, K., Katsuki, K., Yamamoto, S., 2017. Process regime, salinity, morphological, and sedimentary trends along the fluvial to marine transition zone of the mixed-energy Mekong River delta, Vietnam. Cont. Shelf Res. 147, 7–26. https://doi.org/10.1016/j.csr.2017.03.001

Guo, L., van der Wegen, M., Jay, D.A., Matte, P., Wang, Z.B., Roelvink, D., He, Q., 2015. River-tide dynamics: Exploration of nonstationary and nonlinear tidal behavior in the Yangtze River estuary: River tidal dynamics. J. Geophys. Res. Oceans 120, 3499–3521. https://doi.org/10.1002/2014JC010491

Gupta, S.C., Larson, W.E., 1979. Estimating soil water retention characteristics from particle size distribution, organic matter percent, and bulk density. Water Resour. Res. 15, 1633–1635. https://doi.org/10.1029/WR015i006p01633

Hale, R., Bain, R., Goodbred Jr., S., Best, J., 2019. Observations and scaling of tidal mass transport acrossthe lower Ganges-Brahmaputra delta plain:implications for delta

management and sustainability. Earth Surf. Dyn. Discuss. 1–23. https://doi.org/10.5194/esurf-2018-66

Hale, R.P., Wilson, C.A., Bomer, E.J., in press. Seasonal variability of forces controlling sedimentation in the Sundarbans National Forest, Bangladesh. Front. Earth Sci.

Hanebuth, T.J.J., Kudrass, H.R., Linstädter, J., Islam, B., Zander, A.M., 2013. Rapid coastal subsidence in the central Ganges-Brahmaputra Delta (Bangladesh) since the 17th century deduced from submerged salt-producing kilns. Geology 41, 987–990. https://doi.org/10.1130/G34646.1

Haque, C.E., Zaman, M.Q., 1989. Coping with Riverbank Erosion Hazard and Displacement in Bangladesh: Survival Strategies and Adjustments. Disasters 13, 300–314. https://doi.org/10.1111/j.1467-7717.1989.tb00724.x

Harris, D., Horwáth, W.R., van Kessel, C., 2001. Acid fumigation of soils to remove carbonates prior to total organic carbon or CARBON-13 isotopic analysis. Soil Sci. Soc. Am. J. 65, 1853–1856. https://doi.org/10.2136/sssaj2001.1853

Hasegawa, K., 1989. Studies on qualitative and quantitative prediction of meander channel shift, in: Ikeda, S., Parker, G. (Eds.), Water Resources Monograph. American Geophysical Union, Washington, D. C., pp. 215–235. https://doi.org/10.1029/WM012p0215

Heiri, O., Lotter, A.F., Lemcke, G., 2001. Loss on ignition as a method for estimating organic and carbonate content in sediments: reproducibility and comparability of results. J. Paleolimnol. 25, 101–110. https://doi.org/10.1023/A:1008119611481

Higgins, S., Overeem, I., Rogers, K., Kalina, E., 2018. River linking in India: Downstream impacts on water discharge and suspended sediment transport to deltas. Elem Sci Anth 6, 20. https://doi.org/10.1525/elementa.269

Higgins, S., Overeem, I., Tanaka, A., Syvitski, J.P.M., 2013. Land subsidence at aquaculture facilities in the Yellow River delta, China: SUBSIDENCE AT AQUACULTURE FACILITIES. Geophys. Res. Lett. 40, 3898–3902. https://doi.org/10.1002/grl.50758

Higgins, S.A., 2016. Review: Advances in delta-subsidence research using satellite methods. Hydrogeol. J. 24, 587–600. https://doi.org/10.1007/s10040-015-1330-6

Higgins, S.A., Overeem, I., Steckler, M.S., Syvitski, J.P.M., Seeber, L., Akhter, S.H., 2014. InSAR measurements of compaction and subsidence in the Ganges-Brahmaputra Delta, Bangladesh. J. Geophys. Res. Earth Surf. 119, 1768–1781. https://doi.org/10.1002/2014JF003117

Hoitink, A.J.F., Wang, Z.B., Vermeulen, B., Huismans, Y., Kästner, K., 2017. Tidal controls on river delta morphology. Nat. Geosci. 10, 637–645. https://doi.org/10.1038/ngeo3000

Hossain, F., Khan, Z.H., Shum, C.K., 2015. Tidal river management in Bangladesh. Nat. Clim. Change 5, 492–492. https://doi.org/10.1038/nclimate2618

Hossain, M., Siddique, M.R.H., Abdullah, S.M.R., Saha, S., Ghosh, D.C., Rahman, Md.S., Limon, S.H., 2014. Nutrient Dynamics Associated with Leaching and Microbial Decomposition of Four Abundant Mangrove Species Leaf Litter of the Sundarbans, Bangladesh. Wetlands 34, 439–448. https://doi.org/10.1007/s13157-013-0510-1

Houghton, J., 2005. Global warming. Rep. Prog. Phys. 68, 1343–1403.

Hoyal, D.C.J.D., Sheets, B.A., 2009. Morphodynamic evolution of experimental cohesive deltas. J. Geophys. Res. 114, F02009. https://doi.org/10.1029/2007JF000882

Hudson, P.F., Kesel, R.H., 2000. Channel migration and meander-bend curvature in the lower Mississippi River prior to major human modification. Geology 28, 531–534.

Hunter, L.M., 2005. Migration and Environmental Hazards. Popul. Environ. 26, 273–302. https://doi.org/10.1007/s11111-005-3343-x

Hutchison, J., Manica, A., Swetnam, R., Balmford, A., Spalding, M., 2014. Predicting Global Patterns in Mangrove Forest Biomass. Conserv. Lett. 7, 233–240. https://doi.org/10.1111/conl.12060

Ichaso, A.A., Dalrymple, R.W., 2014. Eustatic, tectonic and climatic controls on an early syn-rift mixed-energy delta, Tilje Formation (Early Jurassic, Smørbukk field, offshore mid-Norway), in: From Depositional Systems to Sedimentary Successions on the Norwegian Continental Margin., International Association of Sedimentologists. pp. 339–388.

Iftekhar, M.S., Saenger, P., 2008. Vegetation dynamics in the Bangladesh Sundarbans mangroves: a review of forest inventories. Wetl. Ecol. Manag. 16, 291–312. https://doi.org/10.1007/s11273-007-9063-5

Ikeda, H., 1989. Sedimentary controls on channel migration and origin of point bars in sand-bedded meandering rivers, in: Ikeda, S., Parker, G. (Eds.), Water Resources Monograph. American Geophysical Union, Washington, D. C., pp. 51–68. https://doi.org/10.1029/WM012p0051

Ikeda, S., Parker, G., Sawai, K., 1981. Bend theory of river meanders. Part 1. Linear development. J. Fluid Mech. 112, 363. https://doi.org/10.1017/S0022112081000451

IPCC - International Panel on Climate Change, 2013. Climate change 2013: Projections of sea level rise.

Islam, M.R., 2006. Managing diverse land uses in coastal Bangladesh, in: Environment and Livelihoods in Tropical Coastal Zones. pp. 237–248.

Jablonski, B.V.J., Dalrymple, R.W., 2016. Recognition of strong seasonality and climatic cyclicity in an ancient, fluvially dominated, tidally influenced point bar: Middle McMurray Formation, Lower Steepbank River, north-eastern Alberta, Canada. Sedimentology 63, 552–585. https://doi.org/10.1111/sed.12228

Jadhav, R.S., Chen, Q., Smith, J.M., 2013. Spectral distribution of wave energy dissipation by salt marsh vegetation. Coast. Eng. 77, 99–107. https://doi.org/10.1016/j.coastaleng.2013.02.013

Jankowski, K.L., Törnqvist, T.E., Fernandes, A.M., 2017. Vulnerability of Louisiana's coastal wetlands to present-day rates of relative sea-level rise. Nat. Commun. 8, 14792. https://doi.org/10.1038/ncomms14792

Jennerjahn, T.C., Ittekkot, V., 2002. Relevance of mangroves for the production and deposition of organic matter along tropical continental margins. Naturwissenschaften 89, 23–30. https://doi.org/10.1007/s00114-001-0283-x

Jerolmack, D.J., Swenson, J.B., 2007. Scaling relationships and evolution of distributary networks on wave-influenced deltas: NETWORKS ON WAVE-INFLUENCED DELTAS. Geophys. Res. Lett. 34, n/a-n/a. https://doi.org/10.1029/2007GL031823

Jevrejeva, S., Moore, J.C., Grinsted, A., Woodworth, P.L., 2008. Recent global sea level acceleration started over 200 years ago? Geophys. Res. Lett. 35. https://doi.org/10.1029/2008GL033611

Johnson, S.M., Dashtgard, S.E., 2014. Inclined heterolithic stratification in a mixed tidal–fluvial channel: Differentiating tidal versus fluvial controls on sedimentation. Sediment. Geol. 301, 41–53. https://doi.org/10.1016/j.sedgeo.2013.12.004

Karathanasis, A.D., Hajek, B.F., 1985. Shrink-Swell Potential of Montmorillonitic Soils in Udic Moisture Regimes 1. Soil Sci. Soc. Am. J. 49, 159–166. https://doi.org/10.2136/sssaj1985.03615995004900010033x

Kauffman, J.B., Heider, C., Cole, T.G., Dwire, K.A., Donato, D.C., 2011. Ecosystem Carbon Stocks of Micronesian Mangrove Forests. Wetlands 31, 343–352. https://doi.org/10.1007/s13157-011-0148-9

Khan, S.R., Islam, B., 2008. Holocene stratigraphy of the lower Ganges-Brahmaputra river delta in Bangladesh. Front. Earth Sci. China 2, 393–399. https://doi.org/10.1007/s11707-008-0051-8

Kirwan, M.L., Guntenspergen, G.R., 2010. Influence of tidal range on the stability of coastal marshland: TIDAL RANGE AND MARSH STABILITY. J. Geophys. Res. Earth Surf. 115. https://doi.org/10.1029/2009JF001400

Kirwan, M.L., Megonigal, J.P., 2013. Tidal wetland stability in the face of human impacts and sea-level rise. Nature 504, 53–60. https://doi.org/10.1038/nature12856

Kirwan, M.L., Temmerman, S., Skeehan, E.E., Guntenspergen, G.R., Fagherazzi, S., 2016. Overestimation of marsh vulnerability to sea level rise. Nat. Clim. Change 6, 253–260. https://doi.org/10.1038/nclimate2909

Knott, J.F., Nuttle, W.K., Hemond, H.F., 1987. Hydrologic parameters of salt marsh peat. Hydrol. Process. 1, 211–220. https://doi.org/10.1002/hyp.3360010208

Kobayashi, N., Raichle, A.W., Asano, T., 1993. Wave Attenuation by Vegetation. J. Waterw. Port Coast. Ocean Eng. 119, 30–48. https://doi.org/10.1061/(ASCE)0733-950X(1993)119:1(30)

Kolb, C.R., 1963. SEDIMENTS FORMING THE BED AND BANKS OF THE LOWER MISSISSIPPI RIVER AND THEIR EFFECT ON RIVER MIGRATION. Sedimentology 2, 227–234. https://doi.org/10.1111/j.1365-3091.1963.tb01216.x

Krauss, K.W., Cahoon, D.R., Allen, J.A., Ewel, K.C., Lynch, J.C., Cormier, N., 2010. Surface Elevation Change and Susceptibility of Different Mangrove Zones to Sea-Level Rise on Pacific High Islands of Micronesia. Ecosystems 13, 129–143. https://doi.org/10.1007/s10021-009-9307-8

Krauss, K.W., McKee, K.L., Lovelock, C.E., Cahoon, D.R., Saintilan, N., Reef, R., Chen, L., 2014. How mangrove forests adjust to rising sea level. New Phytol. 202, 19–34. https://doi.org/10.1111/nph.12605

Kristensen, E., Bouillon, S., Dittmar, T., Marchand, C., 2008. Organic carbon dynamics in mangrove ecosystems: A review. Aquat. Bot., Mangrove Ecology – Applications in Forestry and Coastal Zone Management 89, 201–219. https://doi.org/10.1016/j.aquabot.2007.12.005

Kuehl, S.A., Allison, M.A., Goodbred, S.L., 2005. The Ganges-Brahmaputra Delta. SEPM Special Publication 83, 413-434.

Kvale, E.P., 2012. Tidal Constituents of Modern and Ancient Tidal Rhythmites: Criteria for Recognition and Analyses, in: Davis, R.A., Dalrymple, R.W. (Eds.), Principles of Tidal Sedimentology. Springer Netherlands, Dordrecht, pp. 1–17. https://doi.org/10.1007/978-94-007-0123-6_1

La Croix, A.D., Dashtgard, S.E., 2015. A Synthesis of Depositional Trends In Intertidal and Upper Subtidal Sediments Across the Tidal–Fluvial Transition In the Fraser River, Canada. J. Sediment. Res. 85, 683–698. https://doi.org/10.2110/jsr.2015.47

Lamb, M.P., Nittrouer, J.A., Mohrig, D., Shaw, J., 2012. Backwater and river plume controls on scour upstream of river mouths: Implications for fluvio-deltaic morphodynamics:

BACKWATER AND RIVER PLUME CONTROLS. J. Geophys. Res. Earth Surf. 117, n/a-n/a. https://doi.org/10.1029/2011JF002079

Langley, J.A., McKee, K.L., Cahoon, D.R., Cherry, J.A., Megonigal, J.P., 2009. Elevated CO2 stimulates marsh elevation gain, counterbalancing sea-level rise. Proc. Natl. Acad. Sci. 106, 6182–6186. https://doi.org/10.1073/pnas.0807695106

Largasse, 2004. Handbook for Predicting Stream Meander Migration and Supporting Software. Transportation Research Board, Washington, D.C. https://doi.org/10.17226/23346

Lentsch, N., Finotello, A., Paola, C., 2018. Reduction of deltaic channel mobility by tidal action under rising relative sea level. Geology 46, 599–602. https://doi.org/10.1130/G45087.1

Li, Q., Matthew Benson, W., Harlan, M., Robichaux, P., Sha, X., Xu, K., Straub, K.M., 2017. Influence of Sediment Cohesion on Deltaic Morphodynamics and Stratigraphy Over Basin-Filling Time Scales: Influence of Sediment Cohesion on Deltas. J. Geophys. Res. Earth Surf. 122, 1808–1826. https://doi.org/10.1002/2017JF004216

Loucks, C., Barber-Meyer, S., Hossain, Md.A.A., Barlow, A., Chowdhury, R.M., 2010. Sea level rise and tigers: predicted impacts to Bangladesh's Sundarbans mangroves: A letter. Clim. Change 98, 291–298. https://doi.org/10.1007/s10584-009-9761-5

Lovelock, C.E., Adame, M.F., Bennion, V., Hayes, M., O'Mara, J., Reef, R., Santini, N.S., 2014. Contemporary Rates of Carbon Sequestration Through Vertical Accretion of Sediments in Mangrove Forests and Saltmarshes of South East Queensland, Australia. Estuaries Coasts 37, 763–771. https://doi.org/10.1007/s12237-013-9702-4

Lovelock, C.E., Bennion, V., Grinham, A., Cahoon, D.R., 2011. The Role of Surface and Subsurface Processes in Keeping Pace with Sea Level Rise in Intertidal Wetlands of Moreton Bay, Queensland, Australia. Ecosystems 14, 745–757. https://doi.org/10.1007/s10021-011-9443-9

Lovelock, C.E., Cahoon, D.R., Friess, D.A., Guntenspergen, G.R., Krauss, K.W., Reef, R., Rogers, K., Saunders, M.L., Sidik, F., Swales, A., Saintilan, N., Thuyen, L.X., Triet, T., 2015. The vulnerability of Indo-Pacific mangrove forests to sea-level rise. Nature 526, 559–563. https://doi.org/10.1038/nature15538

Lützow, M. v, Kögel‐Knabner, I., Ekschmitt, K., Matzner, E., Guggenberger, G., Marschner, B., Flessa, H., 2006. Stabilization of organic matter in temperate soils: mechanisms and their relevance under different soil conditions – a review. Eur. J. Soil Sci. 57, 426–445. https://doi.org/10.1111/j.1365-2389.2006.00809.x

Madsen, O.S., Poon, Y.-K., Graber, H.C., 1989. Spectral Wave Attenuation by Bottom Friction: Theory, in: Coastal Engineering 1988. Presented at the 21st International Conference on Coastal Engineering, American Society of Civil Engineers, Costa del Sol-Malaga, Spain, pp. 492–504. https://doi.org/10.1061/9780872626874.035

Marion, C., Anthony, E.J., Trentesaux, A., 2009. Short-term (≤2 yrs) estuarine mudflat and saltmarsh sedimentation: High-resolution data from ultrasonic altimetery, rod surface-elevation table, and filter traps. Estuar. Coast. Shelf Sci. 83, 475–484. https://doi.org/10.1016/j.ecss.2009.03.039

Martin, J., Fernandes, A.M., Pickering, J., Howes, N., Mann, S., McNeil, K., 2018. The Stratigraphically Preserved Signature of Persistent Backwater Dynamics in a Large Paleodelta System: The Mungaroo Formation, North West Shelf, Australia. J. Sediment. Res. 88, 850–872. https://doi.org/10.2110/jsr.2018.38

McGranahan, G., Balk, D., Anderson, B., 2007. The rising tide: assessing the risks of climate change and human settlements in low elevation coastal zones. Environ. Urban. 19, 17–37. https://doi.org/10.1177/0956247807076960

McIvor, A.L., Spencer, T., Möller, I., Spalding, M., 2013. The response of mangrove soil surface elevation to sea level rise (No. 42), Natural Coastal Protection Series: Report 3. Cambridge Coastal Research Unit.

McKee, K.L., 2011. Biophysical controls on accretion and elevation change in Caribbean mangrove ecosystems. Estuar. Coast. Shelf Sci. 91, 475–483. https://doi.org/10.1016/j.ecss.2010.05.001

McKee, K.L., Cahoon, D.R., Feller, I.C., 2007. Caribbean mangroves adjust to rising sea level through biotic controls on change in soil elevation. Glob. Ecol. Biogeogr. 16, 545–556. https://doi.org/10.1111/j.1466-8238.2007.00317.x

Mcleod, E., Chmura, G.L., Bouillon, S., Salm, R., Björk, M., Duarte, C.M., Lovelock, C.E., Schlesinger, W.H., Silliman, B.R., 2011. A blueprint for blue carbon: toward an improved understanding of the role of vegetated coastal habitats in sequestering CO2. Front. Ecol. Environ. 9, 552–560. https://doi.org/10.1890/110004

McManus, J., 2002. Deltaic responses to changes in river regimes. Mar. Chem. 79, 155–170. https://doi.org/10.1016/S0304-4203(02)00061-0

Meade, R.H., Moody, J.A., 2009. Causes for the decline of suspended-sediment discharge in the Mississippi River system, 1940-2007. Hydrol. Process. n/a-n/a. https://doi.org/10.1002/hyp.7477

Meckel, T.A., Brink, U.S. ten, Williams, S.J., 2006. Current subsidence rates due to compaction of Holocene sediments in southern Louisiana. Geophys. Res. Lett. 33. https://doi.org/10.1029/2006GL026300

Meckel, T.A., Brink, U.S.T., Williams, S.J., 2007. Sediment compaction rates and subsidence in deltaic plains: numerical constraints and stratigraphic influences. Basin Res. 19, 19–31. https://doi.org/10.1111/j.1365-2117.2006.00310.x

Mehta, A.J., 1991. Review notes on cohesive sediment erosion, in: Coastal Sediments. Presented at the ASCE, pp. 40–53.

Mehta, A.J., 1989. On estuarine cohesive sediment suspension behavior. J. Geophys. Res. Oceans 94, 14303–14314.

Meinshausen, M., Smith, S.J., Calvin, K., Daniel, J.S., Kainuma, M.L.T., Lamarque, J.-F., Matsumoto, K., Montzka, S.A., Raper, S.C.B., Riahi, K., Thomson, A., Velders, G.J.M., van Vuuren, D.P.P., 2011. The RCP greenhouse gas concentrations and their extensions from 1765 to 2300. Clim. Change 109, 213. https://doi.org/10.1007/s10584-011-0156-z

Michael, H.A., Voss, C.I., 2009. Controls on groundwater flow in the Bengal Basin of India and Bangladesh: regional modeling analysis. Hydrogeol. J. 17, 1561–1577. https://doi.org/10.1007/s10040-008-0429-4

Middleton, B.A., McKee, K.L., 2001. Degradation of mangrove tissues and implications for peat formation in Belizean island forests. J. Ecol. 89, 818–828. https://doi.org/10.1046/j.0022-0477.2001.00602.x

Milliman, J.D., Farnsworth, K.L., 2011. River Discharge to the Coastal Ocean: A Global Synthesis. Cambridge University Press, Cambridge. https://doi.org/10.1017/CBO9780511781247

Milliman, J.D., Meade, R.H., 1983. World-Wide Delivery of River Sediment to the Oceans. J. Geol. 91, 1–21. https://doi.org/10.1086/628741

Milliman, J.D., Syvitski, J.P.M., 1992. Geomorphic/Tectonic Control of Sediment Discharge to the Ocean: The Importance of Small Mountainous Rivers. J. Geol. 100, 525–544. https://doi.org/10.1086/629606

Mirza, M.M.Q., 1998. Diversion of the Ganges Water at Farakka and Its Effects on Salinity in Bangladesh. Environ. Manage. 22, 711–722. https://doi.org/10.1007/s002679900141

Mitchell, J.K., Soga, K., 2005. Fundamentals of soil behavior, 3rd ed. ed. John Wiley & Sons, Hoboken, N.J.

Möller, I., 2006. Quantifying saltmarsh vegetation and its effect on wave height dissipation: Results from a UK East coast saltmarsh. Estuar. Coast. Shelf Sci. 69, 337–351. https://doi.org/10.1016/j.ecss.2006.05.003

Morris, J.T., Sundareshwar, P.V., Nietch, C.T., Kjerfve, B., Cahoon, D.R., 2002. Responses of Coastal Wetlands to Rising Sea Level. Ecology 83, 2869–2877. https://doi.org/10.1890/0012-9658(2002)083[2869:ROCWTR]2.0.CO;2

Murdiyarso, D., Donato, D., Kauffman, J.B., Kurnianto, S., Stidham, M., Kanninen, M., 2009. Carbon storage in mangrove and peatland ecosystems: A preliminary account from plots in Indonesia. Work. Pap. 48 Bogor Banat Indones. Cent. Int. For. Res. 35 P 1–35.

Murray, N.J., Clemens, R.S., Phinn, S.R., Possingham, H.P., Fuller, R.A., 2014. Tracking the rapid loss of tidal wetlands in the Yellow Sea. Front. Ecol. Environ. 12, 267–272. https://doi.org/10.1890/130260

Musial, G., Reynaud, J.-Y., Gingras, M.K., Féniès, H., Labourdette, R., Parize, O., 2012. Subsurface and outcrop characterization of large tidally influenced point bars of the Cretaceous McMurray Formation (Alberta, Canada). Sediment. Geol. 279, 156–172. https://doi.org/10.1016/j.sedgeo.2011.04.020

Mutton, D., Haque, C.E., 2004. Human Vulnerability, Dislocation and Resettlement: Adaptation Processes of River-bank Erosion-induced Displacees in Bangladesh. Disasters 28, 41–62. https://doi.org/10.1111/j.0361-3666.2004.00242.x

Nayak, B., Zaman, S., Gadi, S.D., Raha, A.K., Mitra, A., 2014. Dominant gastropods of Indian Sundarbans: A major sink of carbon 3, 9.

Nelson, J.D., Miller, D.J., 1997. Expansive soils: problems and practice in foundation and pavement engineering. John Wiley, New York; Chichester.

Neubauer, S.C., 2008. Contributions of mineral and organic components to tidal freshwater marsh accretion. Estuar. Coast. Shelf Sci. 78, 78–88. https://doi.org/10.1016/j.ecss.2007.11.011

Nicholls, R.J., Cazenave, A., 2010. Sea-Level Rise and Its Impact on Coastal Zones. Science 328, 1517–1520. https://doi.org/10.1126/science.1185782

Nicholls, R.J., Wong, P.P., Burkett, V., Codignotto, J., Hay, J., 2007. Coastal systems and low-lying areas, in: Climate Change 2007: Impacts, Adaptation, and Vulnerability, Contribution of Working Group II to the Fourth Assessment Report of the Intergovernmental Panel on Climate Change. Cambridge University Press, Cambridge, UK, pp. 315–357.

Nittrouer, J.A., 2013. Backwater hydrodynamics and sediment transport in the lowermost Mississippi River Delta: Implications for development of fluvial-deltaic landforms in a large lowland river, in: IAHS Publication 358. Presented at the Deltas: Landforms, Ecosystems, and Human Activities, Gothenburg, Sweden, pp. 48–61.

Nittrouer, J.A., Mohrig, D., Allison, M., 2011. Punctuated sand transport in the lowermost Mississippi River. J. Geophys. Res. 116, F04025. https://doi.org/10.1029/2011JF002026

Nittrouer, J.A., Shaw, J., Lamb, M.P., Mohrig, D., 2012. Spatial and temporal trends for water-flow velocity and bed-material sediment transport in the lower Mississippi River. Geol. Soc. Am. Bull. 124, 400–414. https://doi.org/10.1130/B30497.1

Nuttle, W.K., Hemand, H.F., 1988. Salt marsh hydrology: Implications for biogeochemical fluxes to the atmosphere and estuaries. Glob. Biogeochem. Cycles 2, 91–114. https://doi.org/10.1029/GB002i002p00091

Nuttle, W.K., Hemond, H.F., Stolzenbach, K.D., 1990. Mechanisms of water storage in salt marsh sediments: The importance of dilation. Hydrol. Process. 4, 1–13. https://doi.org/10.1002/hyp.3360040102

Nyman, J.A., Walters, R.J., Delaune, R.D., Patrick, W.H., 2006. Marsh vertical accretion via vegetative growth. Estuar. Coast. Shelf Sci. 69, 370–380. https://doi.org/10.1016/j.ecss.2006.05.041

Olariu, C., Steel, R.J., Olariu, M.I., Choi, K., 2015. Facies and architecture of unusual fluvial–tidal channels with inclined heterolithic strata, in: Developments in Sedimentology. Elsevier, pp. 353–394. https://doi.org/10.1016/B978-0-444-63529-7.00011-0

Orton, G.J., Reading, H.G., 1993. Variability of deltaic processes in terms of sediment supply, with particular emphasis on grain size. Sedimentology 40, 475–512. https://doi.org/10.1111/j.1365-3091.1993.tb01347.x

Paola, C., Mohrig, D., 1996. Palaeohydraulics revisited: palaeoslope estimation in coarse-grained braided rivers. Basin Res. 8, 243–254. https://doi.org/10.1046/j.1365-2117.1996.00253.x

Pearson, N.J., Gingras, M.K., 2006. An Ichnological and Sedimentological Facies Model for Muddy Point-Bar Deposits. J. Sediment. Res. 76, 771–782. https://doi.org/10.2110/jsr.2006.070

Pethick, J., 2012. Assessing changes in the landform and geomorphology due to sea level rise in the Bangladesh Sundarbans (Unpublished report to World Bank).

Pethick, J., Orford, J.D., 2013. Rapid rise in effective sea-level in southwest Bangladesh: Its causes and contemporary rates. Glob. Planet. Change 111, 237–245. https://doi.org/10.1016/j.gloplacha.2013.09.019

Peyronnin, N., Green, M., Richards, C.P., Owens, A., Reed, D., Chamberlain, J., Groves, D.G., Rhinehart, W.K., Belhadjali, K., 2013. Louisiana's 2012 Coastal Master Plan: Overview of a Science-Based and Publicly Informed Decision-Making Process. J. Coast. Res. 67, 1–15. https://doi.org/10.2112/SI_67_1.1

Pickering, J.L., Goodbred, S.L., Reitz, M.D., Hartzog, T.R., Mondal, D.R., Hossain, Md.S., 2014. Late Quaternary sedimentary record and Holocene channel avulsions of the Jamuna

and Old Brahmaputra River valleys in the upper Bengal delta plain. Geomorphology 227, 123–136. https://doi.org/10.1016/j.geomorph.2013.09.021

Polidoro, B.A., Carpenter, K.E., Collins, L., Duke, N.C., Ellison, A.M., Ellison, J.C., Farnsworth, E.J., Fernando, E.S., Kathiresan, K., Koedam, N.E., Livingstone, S.R., Miyagi, T., Moore, G.E., Nam, V.N., Ong, J.E., Primavera, J.H., Iii, S.G.S., Sanciangco, J.C., Sukardjo, S., Wang, Y., Yong, J.W.H., 2010. The Loss of Species: Mangrove Extinction Risk and Geographic Areas of Global Concern. PLOS ONE 5, e10095. https://doi.org/10.1371/journal.pone.0010095

Prokocki, E.W., Best, J.L., Ashworth, P.J., Parsons, D.R., Smith, G.H.S., Nicholas, A.P., Simpson, C.J., Wang, H., Sandbach, S.D., Keevil, C.E., 2015. Mid to late Holocene geomorphological and sedimentological evolution of the fluvial–tidal zone, in: Developments in Sedimentology. Elsevier, pp. 193–226. https://doi.org/10.1016/B978-0-444-63529-7.00022-5

Rahman, A., 2018. Personal communication (interview with local villagers).

Rahman, L.M., 2000. The Sundarbans: a unique wilderness of the world. McCool Stephen F Cole David N Borrie William T O'Loughlin Jennifer Comps 2000 Wilderness Sci. Time Change Conf. 2 Wilderness Context Larg. Syst. 1999 May 23–27 Missoula MT Proc. RMRS-P-15-VOL-2 Ogden UT US Dep. Agric. For. Serv. Rocky Mt. Res. Stn. P 143-148 015.

Renschler, C.S., Flanagan, D.C., Engel, B.A., Kramer, L.A., Sudduth, K.A., 2002. Site-specific decision-making based on RTK GPS survey and six alternative elevation data sources: watershed topography and delineation. Trans. ASAE 45, 15.

RMMRU, R. and M.M.R.U., 2007. Coping with riverbank erosion induced displacement.

Robertson, A.I., 1988. Decomposition of mangrove leaf litter in tropical Australia. J. Exp. Mar. Biol. Ecol. 116, 235–247. https://doi.org/10.1016/0022-0981(88)90029-9

Rogers, K., Carrico, A., Donato, K., Wilson, C., Gilligan, J., 2017. Socioeconomic system dynamics related to livelihood, human migration, and landscape evolution in the Ganges-Brahmaputra-Meghna Delta (NSF Coupled Human-Natural Systems Proposal).

Rogers, K., Overeem, I., 2017. Doomed to Drown? Sediment Dynamics in the Human-controlled Floodplains of the Active Bengal Delta. Elem. Sci. Anthr. https://doi.org/10.1525/elementa.250

Rogers, K., Saintilan, N., 2008. Relationships between Surface Elevation and Groundwater in Mangrove Forests of Southeast Australia. J. Coast. Res. 24, 63–69. https://doi.org/10.2112/05-0519.1

Rogers, K., Saintilan, N., Cahoon, D., 2005. Surface Elevation Dynamics in a Regenerating Mangrove Forest at Homebush Bay, Australia. Wetl. Ecol. Manag. 13, 587–598. https://doi.org/10.1007/s11273-004-0003-3

Rogers, K., Wilton, K.M., Saintilan, N., 2006. Vegetation change and surface elevation dynamics in estuarine wetlands of southeast Australia. Estuar. Coast. Shelf Sci. 66, 559–569. https://doi.org/10.1016/j.ecss.2005.11.004

Rogers, K.G., Goodbred, S.L., 2014. The Sundarbans and Bengal Delta: The World's Largest Tidal Mangrove and Delta System, in: Kale, V.S. (Ed.), Landscapes and Landforms of India, World Geomorphological Landscapes. Springer Netherlands, Dordrecht, pp. 181–187. https://doi.org/10.1007/978-94-017-8029-2_18

Rogers, K.G., Goodbred, S.L., Mondal, D.R., 2013. Monsoon sedimentation on the 'abandoned' tide-influenced Ganges–Brahmaputra delta plain. Estuar. Coast. Shelf Sci. 131, 297–309. https://doi.org/10.1016/j.ecss.2013.07.014

Roscoe G. Jackson II, 1976. Depositional Model of Point Bars in the Lower Wabash River. SEPM J. Sediment. Res. Vol. 46. https://doi.org/10.1306/212F6FF5-2B24-11D7-8648000102C1865D

Rovai, A.S., Twilley, R.R., Castañeda-Moya, E., Riul, P., Cifuentes-Jara, M., Manrow-Villalobos, M., Horta, P.A., Simonassi, J.C., Fonseca, A.L., Pagliosa, P.R., 2018. Global controls on carbon storage in mangrove soils. Nat. Clim. Change 8, 534. https://doi.org/10.1038/s41558-018-0162-5

Sambrook Smith, G.H., Nicholas, A.P., Best, J.L., Bull, J.M., Dixon, S.J., Goodbred, S., Sarker, M.H., Vardy, M.E., 2019. The sedimentology of river confluences. Sedimentology 66, 391–407. https://doi.org/10.1111/sed.12504

Sasmito, S.D., Murdiyarso, D., Friess, D.A., Kurnianto, S., 2016. Can mangroves keep pace with contemporary sea level rise? A global data review. Wetl. Ecol. Manag. 24, 263–278. https://doi.org/10.1007/s11273-015-9466-7

Schafer, W.M., Singer, M.J., 1976. Influence of Physical and Mineralogical Properties on Swelling of Soils in Yolo County, California 1. Soil Sci. Soc. Am. J. 40, 557–562. https://doi.org/10.2136/sssaj1976.03615995004000040029x

Schumacher, B.A., 2002. Methods for the determination of total organic carbon (TOC) in soils and sediments (No. NCEA-C-1282). U.S. Environmental Protection Agency, National Exposure Research Laboratory, Washington D.C.

Seto, K.C., 2011. Exploring the dynamics of migration to mega-delta cities in Asia and Africa: Contemporary drivers and future scenarios. Glob. Environ. Change, Migration and Global Environmental Change – Review of Drivers of Migration 21, S94–S107. https://doi.org/10.1016/j.gloenvcha.2011.08.005

Shaha, D.C., Cho, Y.-K., 2016. Salt Plug Formation Caused by Decreased River Discharge in a Multi-channel Estuary. Sci. Rep. 6, 27176. https://doi.org/10.1038/srep27176

Sidi, F.H., Nummedal, D., Imbert, P., Darman, H., Posamentier, H.W. (Eds.), 2003. Tropical Deltas of Southeast Asia. SEPM (Society for Sedimentary Geology). https://doi.org/10.2110/pec.03.76

Sisulak, C.F., Dashtgard, S.E., 2012. Seasonal Controls On the Development And Character of Inclined Heterolithic Stratification In A Tide-Influenced, Fluvially Dominated Channel: Fraser River, Canada. J. Sediment. Res. 82, 244–257. https://doi.org/10.2110/jsr.2012.21

Small, C., Nicholls, R.J., 2003. A Global Analysis of Human Settlement in Coastal Zones. J. Coast. Res. 19, 584–599.

Small, C., Sousa, D., Yetman, G., Elvidge, C., MacManus, K., 2018a. Decades of urban growth and development on the Asian megadeltas. Glob. Planet. Change 165, 62–89. https://doi.org/10.1016/j.gloplacha.2018.03.005

Small, C., Sousa, D., Yetman, G., Elvidge, C., MacManus, K., 2018b. Decades of urban growth and development on the Asian megadeltas. Glob. Planet. Change 165, 62–89. https://doi.org/10.1016/j.gloplacha.2018.03.005

Smith, V.B., 2012. Geomorphology of a coastal sand-bed river: Lower Trinity River, Texas. University of Texas, Austin, Texas.

Soulsby, R.L., Whitehouse, R.J.S., 1997. Threshold of sediment motion in coastal environments, in: Pacific Coasts and Ports' 97: Proceedings of the 13th Australasian Coastal and Ocean Engineering Conference and the 6th Australasian Port and Harbour Conference. Centre of Advanced Engineering, Univeristy of Canterbury, p. 145.

Stanley, D.J., 1996. Nile delta: extreme case of sediment entrapment on a delta plain and consequent coastal land loss. Mar. Geol. 129, 189–195. https://doi.org/10.1016/0025-3227(96)83344-5

Steckler, M.S., Nooner, S.L., Akhter, S.H., Chowdhury, S.K., Bettadpur, S., Seeber, L., Kogan, M.G., 2010. Modeling Earth deformation from monsoonal flooding in Bangladesh using hydrographic, GPS, and Gravity Recovery and Climate Experiment (GRACE) data. J. Geophys. Res. Solid Earth 115. https://doi.org/10.1029/2009JB007018

Steiger, J., Gurnell, A.M., Goodson, J.M., 2003. Quantifying and characterizing contemporary riparian sedimentation. River Res. Appl. 19, 335–352. https://doi.org/10.1002/rra.708

Swales, A., Bentley, S.J., Lovelock, C.E., 2015. Mangrove-forest evolution in a sediment-rich estuarine system: opportunists or agents of geomorphic change? Earth Surf. Process. Landf. 40, 1672–1687. https://doi.org/10.1002/esp.3759

Syvitski, J.P.M., Kettner, A.J., Overeem, I., Hutton, E.W.H., Hannon, M.T., Brakenridge, G.R., Day, J., Vörösmarty, C., Saito, Y., Giosan, L., Nicholls, R.J., 2009. Sinking deltas due to human activities. Nat. Geosci. 2, 681–686. https://doi.org/10.1038/ngeo629

Syvitski, J.P.M., Saito, Y., 2007. Morphodynamics of deltas under the influence of humans. Glob. Planet. Change 57, 261–282. https://doi.org/10.1016/j.gloplacha.2006.12.001

Taylor, A., Goldring, R., Gowland, S., 2003. Analysis and application of ichnofabrics. Earth-Sci. Rev. 60, 227–259. https://doi.org/10.1016/S0012-8252(02)00105-8

Taylor, A.M., Goldring, R., 1993. Description and analysis of bioturbation and ichnofabric. J. Geol. Soc. 150, 141–148. https://doi.org/10.1144/gsjgs.150.1.0141

Tessler, Z.D., Vörösmarty, C.J., Grossberg, M., Gladkova, I., Aizenman, H., Syvitski, J.P.M., Foufoula-Georgiou, E., 2015. Profiling risk and sustainability in coastal deltas of the world. Science 349, 638–643. https://doi.org/10.1126/science.aab3574

Torbjorn E. Tornqvist, 1993. Holocene Alternation of Meandering and Anastomosing Fluvial Systems in the Rhine-Meuse Delta (Central Netherlands) Controlled by Sea-Level Rise and Subsoil Erodibility. SEPM J. Sediment. Res. Vol. 63. https://doi.org/10.1306/D4267BB8-2B26-11D7-8648000102C1865D

Tornqvist, T.E., Bridge, J.S., 2002. Spatial variation of overbank aggradation rate and its influence on avulsion frequency. Sedimentology 49, 891–905. https://doi.org/10.1046/j.1365-3091.2002.00478.x

Törnqvist, T.E., Wallace, D.J., Storms, J.E.A., Wallinga, J., van Dam, R.L., Blaauw, M., Derksen, M.S., Klerks, C.J.W., Meijneken, C., Snijders, E.M.A., 2008. Mississippi Delta subsidence primarily caused by compaction of Holocene strata. Nat. Geosci. 1, 173–176. https://doi.org/10.1038/ngeo129

Twilley, R.R., Chen, R.H., Hargis, T., 1992. Carbon sinks in mangroves and their implications to carbon budget of tropical coastal ecosystems. Water. Air. Soil Pollut. 64, 265–288. https://doi.org/10.1007/BF00477106

van Asselen, S., Stouthamer, E., van Asch, Th.W.J., 2009. Effects of peat compaction on delta evolution: A review on processes, responses, measuring and modeling. Earth-Sci. Rev. 92, 35–51. https://doi.org/10.1016/j.earscirev.2008.11.001

Van Coppenolle, R., Schwarz, C., Temmerman, S., 2018. Contribution of Mangroves and Salt Marshes to Nature-Based Mitigation of Coastal Flood Risks in Major Deltas of the World. Estuaries Coasts 41, 1699–1711. https://doi.org/10.1007/s12237-018-0394-7

van den Berg, J.H., Boersma, J.R., van Gelder, A., 2007. Diagnostic sedimentary structures of the fluvial-tidal transition zone – Evidence from deposits of the Rhine and Meuse. Neth. J. Geosci. 86, 287–306. https://doi.org/10.1017/S0016774600077866

Vegas-Vilarrúbia, T., Baritto, F., López, P., Meleán, G., Ponce, M.E., Mora, L., Gómez, O., 2010. Tropical Histosols of the lower Orinoco Delta, features and preliminary quantification of their carbon storage. Geoderma 155, 280–288. https://doi.org/10.1016/j.geoderma.2009.12.011

Victor, S., Golbuu, Y., Wolanski, E., Richmond, R.H., 2004. Fine sediment trapping in two mangrove-fringed estuaries exposed to contrasting land-use intensity, Palau, Micronesia. Wetl. Ecol. Manag. 12, 277–283. https://doi.org/10.1007/s11273-005-8319-1

Victor, S., Neth, L., Golbuu, Y., Wolanski, E., Richmond, R.H., 2006. Sedimentation in mangroves and coral reefs in a wet tropical island, Pohnpei, Micronesia. Estuar. Coast. Shelf Sci. 66, 409–416. https://doi.org/10.1016/j.ecss.2005.07.025

Vörösmarty, C.J., Syvitski, J., Day, J., Sherbinin, A. de, Giosan, L., Paola, C., 2009. Battling to Save the World's River Deltas. Bull. At. Sci. 65, 31–43. https://doi.org/10.2968/065002005

Wang, H., Yang, Z., Saito, Y., Liu, J.P., Sun, X., Wang, Y., 2007. Stepwise decreases of the Huanghe (Yellow River) sediment load (1950–2005): Impacts of climate change and human activities. Glob. Planet. Change 57, 331–354. https://doi.org/10.1016/j.gloplacha.2007.01.003

Webb, E.L., Friess, D.A., Krauss, K.W., Cahoon, D.R., Guntenspergen, G.R., Phelps, J., 2013. A global standard for monitoring coastal wetland vulnerability to accelerated sea-level rise. Nat. Clim. Change 3, 458–465. https://doi.org/10.1038/nclimate1756

Webb, N.D., Seyler, B., Grube, J.P., 2015. Geologic reservoir characterization of Carboniferous fluvio-tidal deposits of the Illinois Basin, USA, in: Developments in Sedimentology. Elsevier, pp. 395–443. https://doi.org/10.1016/B978-0-444-63529-7.00013-4

Webster, J.R., Benfield, E.F., 1986. Vascular Plant Breakdown in Freshwater Ecosystems. Annu. Rev. Ecol. Syst. 17, 567–594. https://doi.org/10.1146/annurev.es.17.110186.003031

Whelan, K.R.T., Smith, T.J., Cahoon, D.R., Lynch, J.C., Anderson, G.H., 2005. Groundwater control of mangrove surface elevation: Shrink and swell varies with soil depth. Estuaries 28, 833–843. https://doi.org/10.1007/BF02696013

Wilson, C., Goodbred, S., Small, C., Gilligan, J., Sams, S., Mallick, B., Hale, R., 2017. Widespread infilling of tidal channels and navigable waterways in human-modified tidal deltaplain of southwest Bangladesh. Elem Sci Anth 5, 78. https://doi.org/10.1525/elementa.263

Wilson, C.A., Goodbred, S.L., 2015. Construction and Maintenance of the Ganges-Brahmaputra-Meghna Delta: Linking Process, Morphology, and Stratigraphy. Annu. Rev. Mar. Sci. 7, 67–88. https://doi.org/10.1146/annurev-marine-010213-135032

Wilson, C.A., Sincavage, R., Goodbred, S.L., Patrick, M., Hale, R.P., Bain, R., Steckler, M., 2017. Coupling mass extraction of sediment, topography, and backwater effects in the Ganges-Brahmaputra delta.

Wilson, C.A., Valentine, L., 2018. Personal communication (unpublished data).

Winterwerp, J.C., Giardino, A., 2012. Assessment of increasing freshwater input on salinity and sedimentation in the Gorai River system (No. 1206292– 000). World Bank Project.

Winterwerp, J.C., Kesteren, W.G.M. van, 2004. Introduction to the physics of cohesive sediment in the marine environment, Developments in sedimentology. Elsevier, Amsterdam ; Boston.

Wolanski, E., Moore, K., Spagnol, S., D'Adamo, N., Pattiaratchi, C., 2001. Rapid, Human-Induced Siltation of the Macro-Tidal Ord River Estuary, Western Australia. Estuar. Coast. Shelf Sci. 53, 717–732. https://doi.org/10.1006/ecss.2001.0799

Woodroffe, C.D., Nicholls, R.J., Saito, Y., Chen, Z., Goodbred, S.L., 2006a. Landscape Variability and the Response of Asian Megadeltas to Environmental Change, in: Harvey, N. (Ed.), Global Change and Integrated Coastal Management: The Asia-Pacific Region, Coastal Systems and Continental Margins. Springer Netherlands, Dordrecht, pp. 277–314. https://doi.org/10.1007/1-4020-3628-0_10

Woodroffe, C.D., Nicholls, R.J., Saito, Y., Chen, Z., Goodbred, S.L., 2006b. Landscape Variability and the Response of Asian Megadeltas to Environmental Change, in: Harvey, N. (Ed.), Global Change and Integrated Coastal Management. Springer Netherlands, Dordrecht, pp. 277–314. https://doi.org/10.1007/1-4020-3628-0_10

Woodroffe, C.D., Rogers, K., McKee, K.L., Lovelock, C.E., Mendelssohn, I.A., Saintilan, N., 2016. Mangrove Sedimentation and Response to Relative Sea-Level Rise. Annu. Rev. Mar. Sci. 8, 243–266. https://doi.org/10.1146/annurev-marine-122414-034025

World Bank, 2015. Bangladesh morphology and climate adaptation, Coastal Embankment Improvment Project, Phase-I (CEIP-I): Long term monitoring, research and analysis of Bangladesh coastal zone (sustainable polders adapted to coastal dynamics) (Technical Proposal to Bangladesh Water Development Board (BWDB)).

Zaman, M.Q., 1991. The Displaced Poor and Resettlement Policies in Bangladesh. Disasters 15, 117–125. https://doi.org/10.1111/j.1467-7717.1991.tb00440.x

Zhang, M., Townend, I., Zhou, Y., Cai, H., 2016. Seasonal variation of river and tide energy in the Yangtze estuary, China: Seasonal energy in Yangtze. Earth Surf. Process. Landf. 41, 98–116. https://doi.org/10.1002/esp.3790

VITA

Edwin Jefferson “Jeff” Bomer was born and raised in Corpus Christi, Texas. After completing high school, he enrolled at Washington University in St. Louis, Missouri, where he earned a Bachelors of Arts in Geophysics in 2014. Following his undergraduate studies, Jeff earned a Master of Science in Geology at Louisiana State University under the supervision of Dr. Sam Bentley. Here, he conducted research on the shallow subsurface sedimentology and stratigraphy of Middle Barataria Bay and Middle Breton Sound receiving basins in southeast Louisiana, and its significance for the implementation of future river sediment diversions. Following graduation in 2016, he began pursuing his doctoral degree at LSU focused on sediment and landscape dynamics in the Ganges-Brahmaputra Delta of Bangladesh. Upon completion of his PhD program, Jeff will join Shell Exploration Company in Houston, Texas as a geoscientist.